Direct and Large-Eddy Simulations of Turbulent Boundary Layers with Heat Transfer

by

Qiang Li

October 2011 Technical Reports Royal Institute of Technology Department of Mechanics SE-100 44 Stockholm, Sweden

Akademisk avhandling som med tillstånd av Kungliga Tekniska Högskolan i Stockholm framlägges till offentlig granskning för avläggande av teknologie licentiatsexamen torsdagen den 10 oktober 2011 kl 10.15 i sal F3, Kungliga Tekniska Högskolan, Lindstedsv. 26, Stockholm.

©Qiang Li 2011
Universitetsservice US-AB, Stockholm 2011

Direct and Large-Eddy Simulations of Turbulent Boundary Layers with Heat Transfer

Qiang Li

Linné Flow Centre, KTH Mechanics, Royal Institute of Technology SE-100 44 Stockholm, Sweden

Abstract

A new parallelisation of the existing fully spectral research code has been implemented and validated, and is used to perform simulations on massively parallel computer architectures with $\mathcal{O}(1000)$ cores. Using the parallelised code, direct numerical simulations (DNS) and large-eddy simulations (LES) of a spatially developing turbulent boundary layer with and without passive scalars over a flat plate under zero-pressure gradient (ZPG) have been carried out. The Navier-Stokes equations are solved employing a spectral method with up to 7 billion grid points. The Reynolds numbers obtained are the highest for a turbulent boundary layer obtained to date for the various setups considered. An extensive number of turbulence statistics for both flow and scalar fields are computed and compared to the well-established experimental/numerical database. In general, good agreement for all considered quantities with existing literature results, both experimentally and numerically is found. Premultiplied spanwise and temporal spectra are also used to identify the large-scale motions in the outer part of the boundary layer. The similarities shared by the streamwise velocity and the scalar with Pr = 0.71 indicate that they might be generated by the same mechanism. The effects from the different Prandtl numbers and wall boundary conditions are also discussed in detail. Furthermore, the effects of the free-stream turbulence (FST) on the heat transfer on the wall are examined. This problem is of great interest in industrial applications as such boundary layers are rarely developing below clean ambient free streams. The momentum and heat transfer on the wall is compared with those obtained with a clean free stream and augmentations of both momentum and heat transfer in the turbulent region are found. In addition, the boundary layer structures are studied and a change of the structures in the outer region are found due to the presence of the free-stream turbulence. By examining the one-dimensional spanwise spectrum, it is speculated that the increase of the momentum and heat transfer are associated with the large-scale motions in the outer layer. In addition, rare events occurring in the viscous sublayer, i.e. isolated regions of flow reversal and high intermittent values of the wall-normal velocity fluctuations leading to high flatness values, are studied, and an attempt to quantify their occurance and origin is given. In a similar spirit, a recent DNS database has been postprocessed in an effort to educe the dominant vortical structures found in the near-wall region. It is found that hairpin vortices are reminiscent of the transition process and tend to disappear in the fully turbulent region. Finally, statistics of a turbulent boundary layer have also been studied with the concept of SED (structural ensemble dynamics), and comparisons to channel flows are made. Furthermore, closure models are proposed for both mean velocity profile and also energy budget terms.

Descriptors: direct numerical simulation (DNS), large-eddy simulation (LES), turbulent boundary layer, passive scalar, coherent structures, free-stream turbulence (FST), structure ensemble dynamics (SED), massively parallel simulations

Preface

This thesis can be considered as a review of my PhD project which deals with turbulence in spatially evolving flat-plate boundary-layer flows including heat transfer. I feel very lucky to have such a research project concerning fundemental problems since nowadays, many projects tend to be more application-oriented. On the other hand, being such a well-developed subject which has been studied for more than a hundred years, any groud-breaking results are not likely to happen, not like those in the newly-born fields. But thrilling moments do exist when something new is discovered since one small step towards our understanding of turbulence will results in a big step in technology in the future¹.

The present thesis contains two parts: a brief introduction on the basic concepts and methods together with few selected results are presented in the first part; the second part is a collection of the following articles. All the papers included in this their are recompiled according to the thesis format used at the Department of Mechanics at KTH for consistency. The PDF file of the present thesis is also available at KTH library or from me directly. Here the selected papers are listed:

Paper 1. Q. LI, P. SCHLATTER, L. BRANDT, & D. S. HENNINGSON, Direct numerical simulation of a spatially developing turbulent boundary layer with passive scalar transport. Published in Int. J. Heat Fluid Flow, 30(5), pp. 916-929, 2009

Paper 2. Q. LI & P. SCHLATTER,

Large-eddy simulation of a spatially developing turbulent boundary layer with passive scalar transport: Part I-flow statistics. Submitted to Int. J. Heat Fluid Flow

Paper 3. Q. LI & P. SCHLATTER,

Large-eddy simulation of a spatially developing turbulent boundary layer with passive scalar transport: Part II-turbulence structures. Submitted to Int. J. Heat Fluid Flow

Paper 4. Q. LI, P. SCHLATTER & D. S. HENNINGSON,

Simulations of heat transfer in a boundary layer subject to free-stream turbulence. Published in J. Turbulence, 11(45), pp. 1-33, 2010

Paper 5. Q. Li, P. Schlatter & D. S. Henningson,

Comparison of SGS models for passive scalar mixing in turbulent channel flows. Proc. of Direct and Large-Eddy Simulation VIII (DLES8), Eindhoven, The Netherlands, 2010

V

¹No matter you believe it or not, I do.

- **Paper 6.** P. Schlatter, R. Örlü, Q. Li, G. Brethouwer, J. H. M. Fransson, A. V. Johansson, P. H. Alfredsson & D. S. Henningson, Turbulent boundary layers up to $Re_{\theta} = 2500$ studied through numerical simulation and experiments. Published in Phys. Fluids **21**, 051702 (2009)
- **Paper 7.** P. Schlatter, Q. Li, G. Brethouwer, A. V. Johansson & D. S. Henningson,

Simulations of spatially evolving turbulent boundary layers up to $Re_{\theta} = 4300$. Published in Int. J. Heat Fluid Flow, **31**(3), pp. 251-261, 2010

Paper 8. P. Lenaers, Q. Li, G. Brethouwer, P. Schlatter, & R. Örlü,

Negative streamwise velocities and other rare events near the wall in turbulent channel flow. Proc. of 13th European Turbulence Conference (ETC13), Warsaw, Poland, 2011

Paper 9. P. Schlatter, Q. Li, F. Hussain & D. S. Henningson, On the vortical structures of a turbulent boundary layer at high Reynolds number. Technical Report, 2011

Paper 10. Q. Li, X. Chen, Y. Wu, Z-S. She, P. Schlatter, D. S. Henningson, & F. Hussain,

Understanding wall turbulence, Part II: analysis of turbulent boundary layer. Technical Report, 2011

Due to various reasons, the following papers are not included in the present thesis:

Paper 11. Q. LI, P. SCHLATTER & D. S. HENNINGSON,

Spectral simulations of wall-bounded flows on massively-parallel computers. Internal report, included in Licentiate thesis, 2008

Paper 12. P. Schlatter, Q. Li, G. Brethouwer, A. V. Johansson, & D. S. Henningson,

Structure of a turbulent boundary layer studied by DNS. Proc. of Direct and Large-Eddy Simulation VIII (DLES8), Eindhoven, The Netherlands, 2010

Paper 13. P. Schlatter, R. Örlü, Q. Li, G. Brethouwer, A. V. Johansson, P. H. Alfredsson & D. S. Henningson,

Progress in simulations of turbulent boundary layers. Proc. of Seventh International Symposium on Turbulence and Shear Flow Phenomena (TSFP-7), invited lecture, Ottawa, Canada, 2011

 $\bf Paper~14.~$ A. Rasam, G. Brethouwer, P. Schlatter, Q. Li & A. V. Johansson,

Effects of modelling, resolution and anisotropy of subgrid-scales on large eddy simulations of channel flow. Published in J. Turbulence 12(10), pp. 1-20, 2011

Summary of the papers

Paper 1

DNS of a spatially developing turbulent boundary layer with passive scalar transport.

A turbulent boundary layer is simulated as a direct numerical simulation (DNS) together with five different passive scalars upto $Re_{\theta} = 830$. The focus is on the outer region behaviour of the scalar statistics which is distinct from channel flows. The influences of the different boundary conditions and Prandtl numbers are also discussed. In some sense, this paper and the corresponding implementation of scalars and their statistics can be considered as the basis of most following papers in this thesis. Note that the new parallelisation developed in conjunction with this paper is further discussed in the technical report by Li et al. (2008).

Paper 2

LES of a spatially developing turbulent boundary layer with passive scalar transport: Part I-flow statistics.

This paper is a continuation of the previous work of a flat-plate turbulent boundary layer with passive scalar transport presented in Paper 1 using LES technique reaching the high $Re_{\theta}=2500$. This part (Part I) is focused on the basic statistics pertaining to scalar field. Comparisions of various statistics with the previous DNS are satisfactory at all Reynolds numbers. The influences of the different Prandtl numbers are also discussed. With such a variety of scalars, the Reynolds number reached in this study is the highest in the current literature.

Paper 3

LES of a spatially developing turbulent boundary layer with passive scalar transport: Part II-turbulence structures.

This paper is a continuation of the previous work of a flat-plate turbulent boundary layer with passive scalar transport presented in Paper 1 using LES technique reaching the high $Re_{\theta} = 2500$. This part (Part II) is mainly focused on the structures pertaining to scalar field, and the influences of the Prandtl numbers are also highlighted.

Paper 4

Simulations of heat transfer in a boundary layer subject to free-stream turbulence.

In this paper, a flat-plate boundary layer is studied under the influence of a turbulent free stream. It has been long time that researchers have observed that in the presence of free-stream turbulence, the heat transfer on solid walls increases dramatically. Since there are difficulties in experiments to measure

very close to the wall, numerical simulations become a good alternative to shed light on the physical mechanisms. The present study summarises the previous experimental and simulation results, and furthermore attributes the increase of the heat transfer on the wall to the large-scale structures residing in the outer region of the boundary layer. Due to the requirements of large simulation domains, large-eddy simulation techniques have been used.

Paper 5

Comparison of SGS models for passive scalar mixing in turbulent channel flows. This conference paper is a extension of the previous work by Winckelmans et al. (2002). It is well known that for instance to compare the Reynolds stress obtained by LES with DNS or experimental data, the SGS contribution needs to be added. However, if only traceless SGS models are used, e.g. dynamic Smagorinsky model, then the comparison should be restricted to only the deviatoric part. The present contribution extends several existing SGS models to also include their corresponding models for the scalar field, and compares the statistics with the previous DNS data, demonstrating the weakness of the eddy-diffusivity assumption. Moreover, the present contribution also discussed how to compare the energy budget terms.

Paper 6

Turbulent boundary layers up to $Re_{\theta} = 2500$ studied through simulation and experiment.

Twenty years passed since the first numerical simulation of turbulent boundary layer was done. However, the Reynolds number achieved then is still among the highest despite the rapid development of super computers and algorithms. This article is about a joint experimental/DNS work of a flat-plate turbulent boundary layer aiming at providing the research community with reliable data for a truly spatially developing flow. It is the fist time that the Reynolds number is high enough to compare DNS to carefully obtained experimental data. On the other hand, it is also a big challenge for the experimentalists to conduct an experiment at such a low Reynolds number with good quality. The excellent match of the data obtained from both simulation and experiments indicates that quantities of interest are not sensitive to the experimental and numerical limitations.

Paper 7

Simulations of spatially evolving turbulent boundary layers up to $Re_{\theta} = 4300$. This paper is a continuation of the previous work of a flat-plate turbulent boundary layer by Schlatter et al. (2009) using LES technique reaching the high $Re_{\theta} = 4300$. A promising LES model is used with comparably good resolution and the results obtained at lower Reynolds number $Re_{\theta} = 2500$ compare very well with the previous DNS data. With the high Reynolds number reached in this study, the scale separation is much more clearer and the outer structures

are studied through one-dimensional spanwise and temporal premultiplied spectra. The coherent structures observed in the simulation compare very well with previous experimental studies at similar Reynolds number. One of the major conclusions of this paper is that one indeed can perform high-fidelity simulations of turbulent wall-bounded flows using LES techniques. This is used in the ongoing new simulations presented in Section 3.7.

Paper 8

Negative streamwise velocities and other rare events near the wall in turbulent channel flow.

This conference paper focusses on two separate rare events in wall turbulence, namely the negative streamwise velocity and the high kurtosis values of the wall-normal velocity fluctuation close to the wall. Data from fully resolved turbulent channel flow simulations are used to investigate the problem. It is observed that the negative streamwise velocity exists at all Reynolds number and such events only happens in the viscous sublayer, under an oblique vortex. The results concerning the high kurtosis values of the wall-normal velocity fluctuation are consistent with the previous studies. The region where the extremely high kurtosis values appears are always below certain spanwise vorticies and may be caused by sweep-type motions. It is further found that these two rare events are not correlated at all.

Paper 9

On the vortical structures of a turbulent boundary layer at high Reynolds number

This paper is discussing the vortical structures in the near-wall region in wall-bounded flows using the newly performed DNS data at high Reynolds number $Re_{\theta} = 4000$. Dominance of hairpin like structures is reported by the previous DNS study by Wu & Moin (2009). However, from the present simulation at much higher Reynolds number, hairpin vortices are rarely observable. It is shown that the dominance of the hairpin structures observed in Wu's simulation is mainly due to the post-transitional effects. Using the eduction scheme based on ensumble averaged velocity field, the educed structure is only a quasi-streamwise vortex which is similar to the previous turbulent channel flow results.

Paper 10

Understanding wall turbulence, Part II: analysis of turbulent boundary layer. This paper is dedicated to analysing the turbulent boundary layer results through the newly introduced statistical measures, i.e. order functions, which are defined in terms of mean strain rate, turbulent Reynolds stress, kinetic energy, and dissipation, etc. It is shown that these order functions are effective in quantifying statistical structures in turbulent boundary layers. In the end, using the order functions as a bridge, a closure description of turbulent boundary layer of the mean flow and energy budget terms are proposed.

x

Division of work between authors

The research project was initiated by Dr. Philipp Schlatter (PS) who has acted as the main advisor together with Prof. Dan S. Henningson (DH).

Paper 1

The simulations and the implementation of the statistics, correlations and time series, the two-dimensional parallelisation of the SIMSON code, and the data analysis were performed by Qiang Li (QL) and the paper has been written by QL with input from PS, Dr. Luca Brandt and DH.

Paper 2 & 3

The simulation setup, model implementations, calculations and data analysis were performed by QL and the paper was written by QL with input from PS.

Paper 4

The code adaptation, simulation setup, computations and data analysis were performed by QL and the paper was written by QL with input from PS and DH.

Paper 5

The SGS model implementation, computations and data analysis were performed by QL and the paper was written by QL with input from PS and DH.

Paper 6

The simulation code validation, problem setup and the performance and optimisation tuning was performed by QL and PS. The simulations were performed by PS and the paper was written by PS with input from the co-authors.

Paper 7

The simulation code validation, problem setup and the performance and optimisation was performed by PS and QL. The computations were performed by PS and the paper was written by PS with input from QL, Dr. Geert Brethouwer (GB), Prof. Arne V. Johansson and DH.

Paper 8

The computations and post-processing implementations were performed by Peter Lenaers (PL) and QL, and the paper was written by PL and QL with input from PS, GB and Dr. Ramis Örlü.

Paper 9

The computations used as database were originally performed by PS. The new post-processing implementations were performed by QL, and the paper was written by PS and QL with input from Prof. Fazle Hussain and DH.

Paper 10

The computations used as database were originally performed by PS, and the new evaluations were performed by QL. The paper was written by QL and X. Chen with inputs from the other authors.

Disclaimers and warnings

- I intend to write the thesis in a way that it is readable, but it turns out to be unreadable. For those who has to read this thesis, I offer my greatest sympathy.
- For those who want to find the ultimate answers to turbulence problem, you can close the thesis and go back to work now.
- About the references in the introduction part of the thesis, I must appologies to those papers which I have either not read, forgotten, ignored, used without citation or cited without realising the origin. Because: i) I do not have time to read everything since there are many other important things than reading. ii) For some of the papers I read, I do not understanding anything or I misunderstood everything. Sometimes it is my fault, while on other occasions, some authors write the paper in such a way as the Italians say "tutto fumo e niente arrosto". iii) I forget the origins of some papers that I read which is due to the fact that I am getting older and older.
- No doubt, this thesis contains certain amount of mistakes and typos which are unavoidable. I would greatly appreciate your criticism.
- It is very difficult to describe something completely "chaotic" with complete logical order.
- For the quotations appeared in the thesis, one should read the original source to fully understand what they mean. Intentional misuse by deliberately concentrating contents can be misleading, harmful or fatal, and it is the reader's responsibility NOT to do that.
- For the quotation in Chinese, even a Chinese guy will not understand it unless he/she knows where it comes from.
- Any resemblance of the text to other sources without citation is purely a coincidence.
- This is a curse. If you do NOT recommend this thesis to your friends within ten days after obtaining this thesis, you will NOT suffer any misfortune or other nasty things.
- You should stop reading this part and jump to the Acknowledgement or go back to work.

李强 5 7 2011年9月

斯德哥尔摩



Contents

Abstra	iii	
Prefac	v	
Chapte	er 1. Introduction	1
1.1.	Basic concepts	1
1.2.	Reynolds number effects	6
1.3.	Scalar transport	8
1.4.	Analysis methods	10
1.5.	Scope of the thesis	13
Chapt	er 2. Numerical issues	15
2.1.	Governing equations	15
2.2.	Sub-grid scale (SGS) modelling	17
2.3.	Resolution requirements	18
2.4.	Spatial & temporal discretisation	21
2.5.	Inflow & outflow condition	23
2.6.	Boundary condition	24
2.7.	Statistical convergence	27
2.8.	Validation & verification	28
2.9.	Summary of the employed numerical method	29
Chapt	33	
3.1.	Boundary layer equations	33
3.2.	Scalings for mean velocity field	35
3.3.	Scalings for mean scalar field	39
3.4.	Turbulence intensities	41
3.5.	High-order statistics	45
3.6.	Coherent structures	49
3.7.	Ongoing work	60
Chapt	63	

Acknowledgements	66			
Bibliography	68			
Direct numerical simulation of a spatiall boundary layer with passive	v 1 0			
Large-eddy simulation of a spatially development layer with passive scalar translations.	· ·			
Large-eddy simulation of a spatially development layer with passive scalar transtructures	1 0			
Simulations of heat transfer in a bounda stream turbulence	ry layer subject to free- 183			
Comparison of SGS models for passive sc channel flows	alar mixing in turbulent 221			
Turbulent Boundary Layers up to Re_{θ} = simulation and experiment	= 2500 studied through 231			
Simulations of spatially evolving turbulent boundary layers up to $Re_{\theta} = 4300 \hspace{1cm} 245$				
Negative streamwise velocities and othe wall in turbulent channel flo				
On the vortical structures of a turbulent Reynolds number	boundary layer at high 287			
Understanding wall turbulence, Part II: boundary layer	analysis of turbulent 321			

Part I Introduction

"不是什么也没有,不是什么也不是"

CHAPTER 1

Introduction

"Are you sitting comfortably, let's start"

- anonymous

"If you are going to make a mistake, make a big one"

- anonymous

1.1. Basic concepts

The place on Earth's surface where life dwells is surrounded by gases and liquids. A substance in the liquid or gas phase is referred as a fluid¹. Therefore, everyone must have some experiences of observing the fluid motions in everyday activities, e.g. mixing the coffee/tea with milk, water running out of the plumbing systems in household, the smoke from a chimney or a cigarettes, etc. Some other fluid motions are not directly observable but also common in daily life, e.g. the blood is pumped to all parts of the human body through veins and arteries, various gas/oil pipe-lines are buried underground, mixing of fuel and air happens in the combustion and they are purged in exhaust pipes, various flows in nature, such as meandering clouds, etc. The scientific discipline concerns about the fluid motion is called fluid dynamics. Usually, the fluid motion can be defined as laminar or turbulent. A laminar² flow has ordered, predictable, and layered characteristics while a turbulent one is exhibiting properties on the opposite. Since the flow motion can not change from laminar to turbulent abruptly, usually a laminar-turbulent transitional phase exists.

The most famous experiment, showing different flow regimes, namely laminar, transitional and turbulent status, is carried out by Osborne Reynolds in 1883. The experimental apparatus is still standing at the University of Manchester. Reynolds studied the flow of water in a glass tube, rendering the flow motions visible by means of colour bands, i.e. injecting a dye. For low flow rates, a steady stream was observed to follow a straight path through the tube. As the flow rate was increased, at some point, the colour band would all at once

 $^{^{1}}$ Recall that under normal conditions, there are three primary phases of a substance: solid, liquid and gas.

²From Latin word "lamina": layer, sheet, leaf.

mix up with the surrounding water, and fill the rest of the tube with a mass of coloured water, see also Figure 1.1. In order to quantify these experimental results, he introduced a non-dimensional number $Re = UL/\nu$, now known as the Reynolds number, in his classic paper published later (Reynolds 1883). Here U denotes the velocity scale (e.g. the mean flow velocity), L the length scale (e.g. the pipe diameter) and ν is the kinematic viscosity. The flow will become turbulent if the Reynolds number exceeds a critical value $\mathcal{O}(2000)$. The Reynolds number is by far one of the most important dimensionless numbers in fluid mechanics.

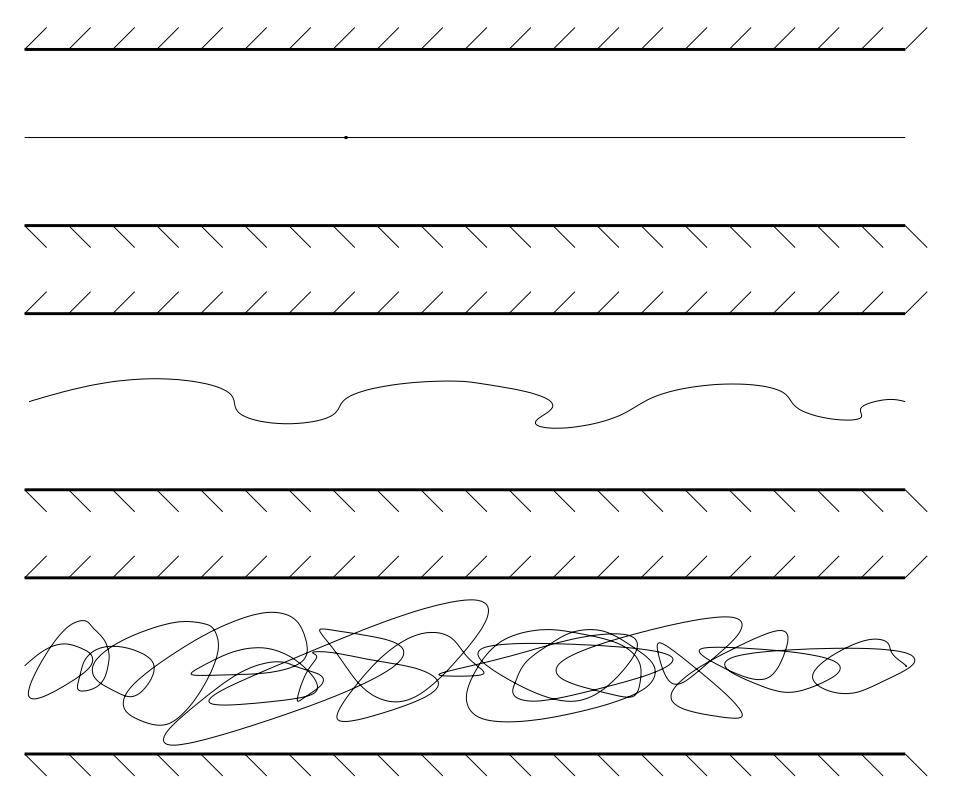


FIGURE 1.1. Sketch of Osborne Reynolds (1883) famous dye experiment. From top to bottom: laminar, transitional and turbulent flows.

Most of the fluid motions in nature and practical applications of primary interest are actually turbulent, which means by definition occuring at large Reynolds numbers. A strong argument is made by Moin & Kim (1997) :"Turbulence is the rule, not the exception, in fluid dynamics". In addition, the

³Such a statement does not imply that the laminar flow and transitional flow are not interesting. But one can think in this way, "All the flows are interesting, but some flows are more interesting than the others".

turbulent flows in most situations belong to the family of shear layers which are strongly inhomogeneous, i.e. variant under translations of the reference frame, and with the presence of velocity gradient. Shear layers can be divided into two categories: free shear flow⁴ (such as jets, wakes and mixing layers) and wall-bounded (shear) flow (such as pipe, channel and flat-plate boundary layer⁵). The inhomogeneity in the former category comes from the spreading of turbulent fluids into the ambient non-turbulent fluids, while in the latter case it is caused by the restriction of the solid boundary (Townsend 1976). The differences between free shear flows and wall-bounded flows are clearly due to the presence of the wall in the latter case. In free shear flows, as the Reynolds number increases sufficiently, the flow is nearly inviscid (free from viscous effects) which implies that the flow is Reynolds number independent. However, in wall-bounded flows, no matter how large the Reynolds number is, there is always a layer (no matter how thin it is) above the solid wall in which viscous effects must be taken into account. Such a thin layer above the solid surface where effects of viscosity of the fluid need to be considered is called boundary layer which is first postulated by Prandtl (1904). Prandtl proposed that an effect of friction is to retard the fluids immediately above the solid surface⁶ and such frictional effects are only experienced in the so-called boundary layer. Outside the boundary layer, the flow is essentially inviscid, see also the article by Anderson (2005). Though geometrically not important, many interesting parameters of the aerodynamic property of the body are determined in the viscous boundary layer, e.g. the drag coefficient, thus it is of great engineering significance in many applications.

Among the three wall-bounded flow types, i.e. pipe, channel, flat-plate boundary layer, the flat-plate boundary layer is different from the other two due to its semi-confinement of the wall. In fact, the near wall region is qualitatively similar to those of the channel and pipe flows, while the outer region of the flat-plate boundary layer is similar to those observed in the free shear flows (Gad-el Hak and Bandyopadhyay 1994). Usually pipe and channel flows are classified as internal flows while the flat-plate boundary layer is an external flow

Despite that the phenomena of turbulent flows vary from one case to the other, the governing equations describing the motion are always the same. These equations are the so-called Navier-Stokes (NS) equations, named after Claude-Louis Navier and George Gabriel Stokes who first formulated them in the 19th century (Navier 1823; Stokes 1845). The equations express the principle of conservation of momentum for a continuum fluid⁷ with viscous stress directly proportional to the rate of strain (velocity gradient), that is to say, only

⁴Here "free" means free from walls not from the shear!

 $^{^5\}mathrm{These}$ three types of flows are considered as the canonical wall-bounded flows.

⁶This is the so-called "no-slip" condition.

⁷One should not think of turbulence as molecular motions, e.g. in dilute gases, where the momentum is transferred via collisions between molecules and one solves the so-called Boltzmann equation.

Newtonian fluids is considered⁸. "The governing equations are the simplest that can be imagined, however the solutions, even for simple flow geometries, are too complicated to be comprehended by human mind" (Bradshaw 1976), and partially it is due to its "Nonlinear, Nonlocal, Nonequilibrium" characteristics in turbulence⁹.

Many attempts are made to define what turbulence is, but none of them is succeeded in the sense that there is no such a definition the whole community agrees on¹⁰. I am inclined to the definition favoured by Prof. Bradshaw: "Turbulence is the general solution of the Navier-Stokes equation." Due to a lack of satisfactory definition, usually turbulence is described by its characteristics or "syndromes" a word borrowed from pathology¹². Usual syndromes of turbulent flows are chaotic (irregularity), diffusive, non-local, consisting of three-dimensional vorticities, dissipative, continuum. Some of these syndromes need a little bit more discussions here.

1.1.1. Cascade

One of the most important characteristic of turbulence is the energy cascade. Turbulent flows involve eddies¹³ which are of various sizes, containing energy and additionally the larger eddy contains also smaller ones. The largest eddies are generated by forces driving the flow and they are unstable and produce eddies of a smaller size. Meanwhile the kinetic energy are transferred to the smaller eddies. These smaller eddies then undergo a similar breaking-up process and generate even smaller eddies together with the energy transferred to these even smaller eddies. This process continues successively until the eddies are so small that they are "killed" by molecular viscosity¹⁴. Such a process is known as (energy) cascade, the concept which probably owes its origin to Lewis Richardson (1922), who obtained the idea of cascade by observation of the clouds and summarised the idea in the often-cited verse¹⁵:

So, naturalists observe, a flea
Has smaller fleas that on him prey;
And these have smaller still to bite 'em,
And so proceed ad infinitum.

 $^{^8\}mathrm{The}$ consideration of non-Newtonian fluids is out of the scope of the thesis.

 $^{^9{\}rm These}$ words come from a seminar entitled "Some 'Non's in Turbulence - Nonlinear, Nonlocal, Nonequilibrium" given by Prof. Kaneda.

¹⁰One thing about turbulence that people agreed on is that it is the most complicated kind of fluid motion.

 $^{^{11}}$ "It is brief, it is entirely true, and it adds nothing to what was known already." – Prof. Bradshaw

¹²The word is actually borrowed from Prof. Stewart who borrowed it from pathology.

¹³There is no definition for "eddy", but it is conceived to be a region of correlated swirling motion. One can think it as a typical swirling flow pattern identifiable in a flow visualisation (Bradshaw 1996).

¹⁴Scientifically speaking, the viscous shear stress performs deformation work which converts the turbulent kinetic energy into heat, i.e. internal energy of the fluid. Therefore, a continuous energy supply is needed to account for the viscous dissipation.

¹⁵The verse written by Richardson is inspired by the verse written by Jonathan Swift (1733):

Big whorls have little whorls, Which feed on their velocity; And little whorls have lesser whorls, And so on to viscosity.

Note that occasionally the energy could transfer from smaller eddies to larger ones, i.e. the so-called "back-scatter". However, the net transfer is always from larger eddies to smaller ones.

The physical mechanism of cascade can be understood via "vortex stretching"¹⁶. One of the character of turbulence is rotational, i.e. containing a great number of three-dimensional vorticities. The flow can be thought as composed of vortex lines analogous to magnetic lines of forces. Due to the presence of the shear, the vortex tubes (a finite-thickness version of vortex lines) can be stretched which leads to an increasing of both rate of rotation (vorticity) and rotational kinetic energy but a decreasing of diameter of the vortex tube which is implied by conservation of angular momentum. On the other hand, vortex tubes can also be contracted/squeezed such that the opposite occurs, i.e. an decrease of both vorticity and rotational kinetic energy but an increase of diameter of the vortex. The vortex stretching implies that kinetic energy transfers from large scales (i.e. large vortex tube diameters) to small scales which is nothing but "energy cascade". The "back-scatter" is a consequence of vortex contraction since the vortex lines are not stretched monotonically (Tennekes & Lumley 1972; Bradshaw 1997).

1.1.2. Nonlocality

Another characteristic of turbulence is its nonlocality. The cause of the nonlocal behaviour can be understood via the pressure field which is a global quantity. The pressure field is governed by the Poisson equation¹⁷, whose right-hand-side (RHS) is a combination of squares of velocity gradients, with appropriate boundary conditions (Bradshaw & Koh 1981; Adrian 1982). That is to say, the pressure in each point in space is calculated based on the whole velocity field. Nonlocality does not only exist in space, but also in time which is closely related to the "memory effects" of turbulence, e.g. the sensitivity of the results to the initial/inlet/inflow conditions (Bevilagua & Lykoudis 1978; Zhou & Antonia 1995; George & Davidson 2004; Dimotakis 2005; Schlatter et al. 2010c; Cimbala et al. 1988)¹⁸. Such memory effects are present largely in

 $^{^{16}}$ There is no accepted definition about "vortex", and I am inclined to the definition by Lugt (1979): "A vortex is the rotating motion of a multitude of material particles around a common centre."

 $^{^{17}}$ For incompressible flows, it reads $\frac{\partial^2 p}{\partial x_k^2} = -\rho \frac{\partial u_i}{\partial x_j} \frac{\partial u_j}{\partial x_i}$ where ρ is the density. 18 Note that the reference Cimbala et~al.~(1988) shows that the memory effects also exist in passive tracers

free shear flows (e.g. jets, mixing layers, wakes) and flat-plate boundary layer flows¹⁹, but much weaker in internal flows, e.g. channels and pipes.

1.1.3. Diffusivity

The third feature of turbulence discussed here is the diffusivity which has great importance in engineering applications. Turbulence causes enhanced mixing and therefore increased rates of momentum transfer. This can be described with the help of the so-called "eddy viscosity", the concept of which is first introduced by Boussinesq (1877) and later developed by Prandtl. The eddy viscosity assumption is based on an analogy with molecular viscosity. "By the late 19th century, it is understood that molecular motion has macroscopic consequences. The existance of transport coefficients, which relate the transport coefficient, or flux, of some quantity such as heat to the gradient of the mean value of that quantity, is an example of the macroscopic manifestation of molecular motion. [...] the principal effects of the molecular motions on the large hydrodynamic scales is to cause the dynamics to be diffusive. An example is the momentum diffusion, which smooths velocity gradients on the hydrodynamic scales" (Frisch & Orszag 1990). Later, inspired by the molecular motion, Prandtl came up with idea that the small-scale eddies could act on the large eddies in a diffusive manner and introduced the idea of "eddy viscosity" ²⁰. Therefore, a much more rapidly smoothed mean velocity in a turbulent flow than that in a laminar flow is a consequence due to the enhanced momentum transport in the former. Furthermore, the ratio of the eddy viscosity over the molecular viscosity can be estimated and is on the order of the Reynolds number (Frisch & Orszag 1990). The eddy viscosity concept has a huge impact on many of the turbulence models used in engineering applications and even some analytical theories.

1.2. Reynolds number effects

Though the definition of the Reynolds number is simple, i.e. $Re = \frac{UL}{\nu}$, it contains important properties. Firstly, no matter how U, L, ν or their combination changes, as long as the Reynolds number stays invariant, the flow solution remains the same given similar geometry and boundary conditions²¹. This property e.g. allows to compare data generated by different methods (either experimental or numerical), from different groups and from different time. Another property is that the effects of changing any one or combination of U, L, ν only reflects in the change of the Reynolds number alone.

¹⁹A common feature of these flows (i.e. free shear flow and flat-plate boundary layer) is that there is a coexistence of both irrotational and rotational fluids, and the transition from potential flow to turbulent one is via the entrainment process (Tsinober 2009). Does this cause the much more influence of the results on the initial conditions?

²⁰One has to be careful, since such a concept tends to treat turbulence as a property of the fluid rather than a property of the flow, and this is conceptually/fundamentally wrong (Tennekes & Lumley 1972).

²¹This is the concept of dynamic similarity, see e.g. Gad-el Hak and Bandyopadhyay (1994).

Note that the first property requires strict similarities in geometry and boundary conditions. If some of the assumptions are violated, the similarity will break. This may explain the differences observed among pipe, channel and zero-pressure-gradient flat-plate boundary layer flows from various experimental/numerical data at the same Reynolds number (Buschmann & Gad-el Hak 2010), simply because the geometrical similarity is not achieved.

One always hopes that at sufficiently high Reynolds number, the effects of the viscosity can be neglected, therefore, the flow characteristics are Reynolds number independent. However, the results obtained from laboratory or computers show clearly Reynolds number effects on e.g. velocities profiles, turbulence structures, etc. So if the Reynolds number obtained will never be high enough to meet the requirement for the flow characteristics to be invariant, it is very important to understand the Reynolds number effects on the results within the Reynolds number range one can obtain.

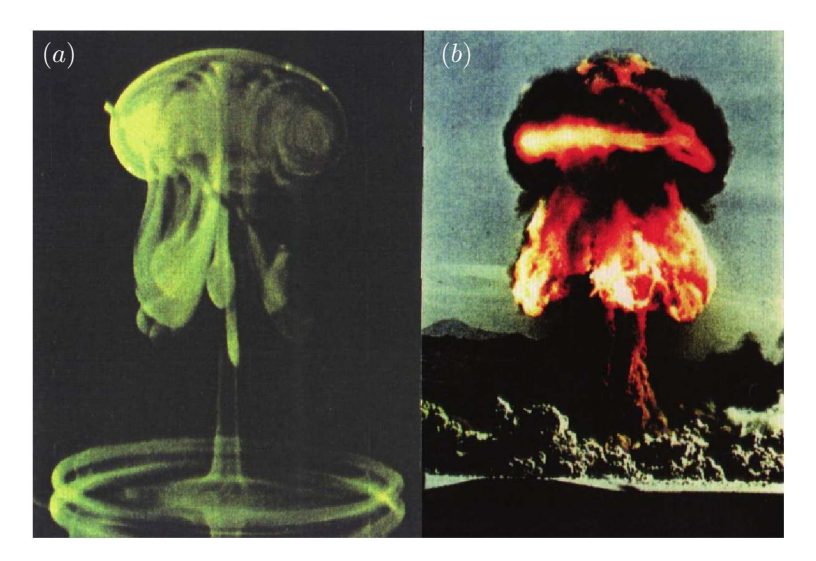


FIGURE 1.2. (a) A water drop falling into a pool of water. The Reynolds number is on the order of several hundred. (b) A nuclear test in Nevada in 1957 by US department of energy. The Reynolds number is LARGE! These pictures are taken from the book by Samimy *et al.* (2003). Fore more information about the picture (a), one can refer to the original paper by Peck & Sigurdson (1994).

The effects of the Reynolds number on the scales of turbulence are easily understood with the help of energy spectrum. As the Reynolds number increases, more and more smaller scales are excited while the size of the larger scales stays approximately constant. In addition, the separation between the large and small scales is much more clear. It is not difficult to imagine that

the size of the large eddies are strongly influenced by the geometry of the flow, e.g. the diameter of the pipe, the width of the channel or the boundary layer thickness, and the boundary conditions. Furthermore, in shear flows, the orientation of the large eddies is determined by the direction of the shear and usually they are anisotropic²². Indeed, the large scale motions are weakly dependent on Reynolds number (Townsend 1976), and this feature is further illustrated in Figure 1.2. The Reynolds number difference in the two cases is on the order of $\mathcal{O}(10^X)$, however, as long as the large-scale motions are concerned, the Reynolds number effects (effects of the viscosity) are of very little importance. This feature is widely used in the movie industry, e.g. especially in the films with explosions of buildings, cars, etc, where usually small-scale-models are used instead of destroying the real things. When the audience watches the movie, he/she barely observes the difference and this is because the very weak influences of Reynolds number on large-scale motions. Of course, if one watches in details (the small scales), one will definitely find subtle differences, therefore, in some cases, real explosions of buildings or cars are made to achieve a correct representation 23 .

A natural question is what are influences of Reynolds number on the smallest eddies? This leads to the introduction of one of the greatest theories about turbulence in the twentieth century by Kolmogorov (1941) (hereafter named K41). Here it is summarised in short: At sufficiently high Reynolds number, the small-scale turbulent motions ($\ell \ll \ell_0$) are statistically isotropic. The statistics of such small-scale motions ($\ell \ll \ell_{EI}$) have a universal form that is uniquely determined by the kinematic viscosity ν and dissipation rate ε . The statistics of the motions of scales with medium size have a universal form that is uniquely determined by dissipation rate, independent of the kinematic viscosity ν^{24} .

Note that the smallest scales in a flow are usually called Kolmogorov scales η , and simple dimensional analysis gives that $\eta = (\nu^3 \varepsilon)^{1/4}$. One important conclusion made from the K41 theory is that in the so-called inertial subrange (where the motions are of medium size and only determined by the dissipation rate), the energy spectrum has a power-law behaviour, i.e. $E(\kappa) \sim \kappa^{-5/3}$ where κ is the wavenumber. It took almost 20 years to test this theory convincingly by a field experiment, i.e. a tidal channel in the wake of an island, by Grant et al. (1962) in which the energy spectrum shows $\kappa^{-5/3}$ law for more than three decades of wavenumber.

1.3. Scalar transport

If examining all those engineering applications mentioned in the previous sections more carefully, soon one will realise that apart from the momentum transport, there are other transport phenomena happening at the same time, the

 $^{^{22}\}mathrm{Variant}$ under rotation of the framework.

 $^{^{23} \}mathrm{Unfortunately},$ the correct representation usually comes with a higher cost.

²⁴Here ℓ is the eddy size, ℓ_0 represents the energy containing range, $\ell < \ell_{EI}$ is referred to as the universal equilibrium range.

most common ones are e.g. heat transfer and mass transfer. "In fact, the occurrence of any single transport process by itself is the exception rather than the rule" (Bird et al. 2002). If the concentration of the heat or the mass is so small that they do not have influence on the fluid motion, then they could be considered as a passive scalar²⁵. Recall the famous Reynolds' experiments discussed in Section 1.1, it is actually a very nice example of transport of passive scalar (i.e. the colour band). Due to its passive nature, the colour band was used to represent the flow motion (which itself is transparent). An understanding and prediction of the passive scalar behaviour in a turbulent flow is crucial (apart from being used as a "tracer" for the flow motion) since the turbulent scalar transport play a key role in many engineering applications: meteorology, biology, chemistry, material and especially in global environmental problems (Kasagi & Iida 1999). For example, in the gas turbine industry, it is necessary to predict the turbine blade temperature accurately which is crucial to the engine efficiency, safety and hardware designs. Another example is the prediction of the composition of combustion products which is essential in meeting environmental regulations (Bradshaw 1996).

1.3.1. Prandtl and Schmidt number

The introduction of scalar transport leads to the new critical dimensionless parameter: Prandtl number (Pr) for heat transfer problems or Schmidt number (Sc) for mass transfer (e.g. molecular species) problems. Sometimes, the Péclet number (Pe) is recognised as the product of Reynolds number and Prandtl (Schmidt) number. The Prandtl/Schmidt number is a material property and defined by the ratio between the viscous diffusion and the thermal/molecular diffusion coefficients. Typical values of Pr are 0.71 for air and many other gases, around 7 for water, between 100 and 40,000 for engine oil and around 0.025 for liquid metal like mercury (White 2006). A superficial conclusion can be made that for low Prandtl/Schmidt numbers, i.e. $Pr \ll 1, Sc \ll 1$, the scalar transfer is mainly via conduction and in this case the scalar boundary layer grows much faster than the momentum boundary layer. On the other hand, for large Prandtl/Schmidt numbers, i.e. $Pr \gg 1, Sc \gg 1$, the scalar transfer is mainly dominated by convection. In this case, the scalar boundary layer formed on the solid surface becomes extremely thin, in which the conductive effects are important since conduction is the only mechanism for the near wall scalar transfer (Leal 2007). From now on, no difference between a heat transfer and mass transfer problem will be made and only Prandtl number will be used to denote the scalar property.

A direct effect of the Prandtl number is to alter the smallest scales in the scalar fluctuations, i.e. the so-called Batchelor scale $\eta_{\theta} = \eta/Pr^{1/2}$ (Batchelor 1959) where η is the Kolmogorov scale. The Batchelor scale decreases with

²⁵The counterpart is the active scalar, in which case interactions exist between the velocity field and scalar field. The consideration of an active scalar is out of the scope of the thesis.

increasing Pr. For large Pr numbers, i.e. $Pr \gg 1$, this makes the representation of these small scales on the numerical grid much more expansive.

1.3.2. Reynolds analogy

The reason to discuss the scalar transport after the flow field is not because the scalar transport is less important than the momentum transport, but because i) one need the information of the flow field to calculate the scalar field 26 , ii) the transport phenomenon due to turbulence between the momentum and scalar field is roughly the same (Bradshaw 1996). Therefore, the scalar transfer problem is usually studied in analogous way as the velocity field, based on the idea of the so-called Reynolds analogy. The basic equations that govern the transport of a passive scalar are indeed closely related to those govern the momentum transport. If assuming similar boundary conditions, the similarity of the governing equations provides the basis for solving the scalar transport "by analogy" (Bird et al. 2002).

The first study about the analogy between momentum and heat transfer is reported in a short and farsighted paper 27 by Reynolds (1874). Almost half a century later, these ideas were taken up and extended by authors such as Prandtl, Taylor and von Kármán (Prandtl 1910; Taylor 1919; von Kármán 1939). In most industry applications, the Reynolds analogy is extremely useful, e.g. a first approximation for heat transfer on the solid surface quantified by the so-called Stanton number St can be obtained via the skin-friction c_f . It should be noted that the Reynolds analogy is only a tool based on a hypothesis about the mechanism of scalar transfer and momentum transfer but not a physical law. For Pr = 1 with certain simple boundary conditions²⁸, the Reynolds analogy is exact which leads to the relation $St = \frac{c_f}{2}$ (Kays & Crawford 1993). In practice, when the Prandtl number differs from unity, the analogy usually does not hold any more and other correlations accounting Prandtl number effects need to be used, e.g. the analogy correlation by Colbrun (1933), which is based on experimental data of both laminar and turbulent flow. The Reynolds analogy also breaks for non-canonical flow cases, e.g. in the presence of pressure gradient or free-stream turbulence.

1.4. Analysis methods

Methods that can be used to study turbulent flows are usually divided into theoretical and experimental ones, within which the latter are further divided into laboratory/field experiments and numerical simulations²⁹. However, being such an extremely intricate problem involving non-local interactions, there is no analytical solutions to the governing equations so far. All the early goals

 $^{^{26}}$ This is also why this thesis is so long, since I cannot directly describe the scalar fields without introducing the velocity field.

²⁷Nowadays, such a paper is termed a fast-track paper in JFM or letter in PoF.

²⁸For instance, constant velocity in the free stream and constant scalar concentration difference between the free stream and the wall (Kays & Crawford 1993).

 $^{^{29}}$ Some authors prefer to name numerical simulation to be numerical experiments.

of the statistical theory to obtain a finite, closed set of equations for average quantities, including the mean velocity and the energy spectrum turns out to be unrealistic (Frisch & Orszag 1990). In spite of the distinct physical and mathematical approaches advocated by different researchers, none of the existing theories³⁰ are completely satisfactory (Buschmann & Gad-el Hak 2007). One possible reason for the absence of an analytical solution is associated with the fact that adequate tools to handle both the mathematical problem and the phenomenon of turbulence are not mature (Tsinober 2009). Therefore, most work has been performed in physical experiments and since last 30 years also in numerical experiments.

In a physical experiment, the flow can be traced either in a Lagrangian way, i.e. one follows the history of the individual fluid particle, consequently, a flow variable f (e.g. velocity) at time t can be expressed as $f(\vec{x}_0, t_0, t)$ where \vec{x}_0 is the reference position at $t = t_0$; or in an Eulerian way, i.e. in which what happens at a position \vec{x} is focused on, so a flow variable f at this position at time t is expressed as $f = f(\vec{x}, t)$. In practice, measurements of Lagrangian flow quantities are extremely difficult and Eulerian framework is often used³¹.

1.4.1. Averaging and Reynolds' decomposition

Usually the time signals of certain instantaneous flow quantities are obtained in experiments e.g. from hot-wires measurements. Due to the chaotic nature of turbulence, usually certain (spatial, time or ensemble) average is performed on the measured instantaneous flow variable $f(\vec{x},t)$ (which is a function of space and time). On the other hand, one does not need to know every detail of the instantaneous signal. The simplest kind of average is a time average at a given point in space. For example, the time average of a flow variable $f(\vec{x},t)$ is defined as

$$\langle f \rangle(\vec{x}) = \lim_{T \to \infty} \frac{1}{T} \int_{t_0}^{t_0 + T} f(\vec{x}, t) dt , \qquad (1.1)$$

where $\langle \cdot \rangle$ denotes the averaged quantity, T is the averaging time and t_0 is the time when averaging is started. In principle the averaging depends on t_0 , but usually the influence of t_0 on the final averaged quantity is negligible assuming long enough averaging and a statistically stationary process. Moreover, $T \to \infty$ means the averaging time should be large enough so that the averaged quantity converges to acceptable accuracy. In practice, $f(\vec{x}, t)$ is usually a digital output either from experiment or computation at discrete times $t_n, n = 1, 2, 3 \cdots N$, so equation (1.1) is replaced by

$$\langle f \rangle(\vec{x}) = \lim_{N \to \infty} \frac{1}{N} \sum_{n=1}^{N} f(\vec{x}, t_n) . \tag{1.2}$$

 $^{^{30}}$ Moreover, they are by far too complicated to be understood, at least for me, therefore they will not be mentioned and discussed here.

³¹With the advances of experimental techniques, more and more studies are performed in Lagrangian framework.

Note that t_n does not necessarily have to be equally spaced and $N \to \infty$ only means certain large number of samples is required for given accuracy of the averaged quantity. If the samples are "independent", e.g. if the time is widely spaced between two successive measurements, that is to say, there is no correlation of the behaviour of $f(\vec{x}, t)$ between time instance at t_{n-1} and t_n . In such a case, the number of samples needed to reach certain given convergence is minimum (Bradshaw 1996).

Another average is the so-called ensemble average, defined as,

$$\langle f \rangle(\vec{x}, t_0) = \lim_{N \to \infty} \frac{1}{N} \sum_{n=1}^{N} f(\vec{x}, t_0) , \qquad (1.3)$$

here consider N as the number of realizations, e.g. runs of an experiment, and the sample is taken at the same time t_0 after the start of each run of an experiment. Note the averaged quantity is a function of both space and time when the measurements are taken, i.e. t_0 .

The majority of flows studies in a laboratory are statistically stationary with respect to time, which implies that the time average is identical with the ensemble average according to the ergodic hypothesis. In addition, the spatial average can be performed on homogeneous directions, however in real world complex flows, usually none of the three spatial directions is homogeneous, hence this leads to a very long averaging time to get acceptable convergence.

Already in the early 16th century, the Italian genius Leonardo da Vinci sketched the famous "Old Man with Water Studies" and the following observations are made (Piomelli 2001): "The water has eddying motions, one part of which is due to the principal current, the other to the random and reverse motion." These pure observations may be seen as a precursor to the Reynolds' decomposition which is a sophisticated way to study turbulence. In 1890s, Osborne Reynolds for the first time in his paper Reynolds (1895) introduced a decomposition of the instantaneous velocity fields into a averaged (mean) part and a fluctuating part, i.e. $f(\vec{x},t) = \langle f(\vec{x},t) \rangle + f'(\vec{x},t)$, nowadays known as the Reynolds decomposition. The Reynolds decomposition has very important status since almost all the statistical results (either experimental or numerical) concerning turbulence rely on it.

1.4.2. Experiments & simulations

Being a long established technique, experiments have been used in fundamental research but also practical problems. Though large parallel computer systems develop fast during the last years, the Reynolds numbers reached by simulations are still low compared to those obtained in experiments. Moreover, many flows in complex geometries or with complex flow phenomena are still only accessible to experiments (Tsinober 2009). Apart from these, the most important advantage of experiments is that they are dealing with physically "correct" flows. A lot of elaborate methods used/developed to study turbulent flows are e.g. hot/cold-wire anemometry, laser Doppler anemometry, particle

image velocimetry, particle tracking velocimetry³². The main drawback for experimental measurements is that sometimes accurate measurements are impossible especially close to the solid surface due to the instrumental problems³³ and the methods/probes for measuring certain quantities are not born yet.

As opposed to the experiments, numerical simulations are relatively young. Most of the simulations are limited at moderate Reynolds numbers and simple geometries compared to the experiments. However, by its nature, simulations can be "designed" to accurately measure quantities, at any positions in the flow which are not accessible in experiments or flows that are not reproducible in the laboratory. Sometimes, even unphysical situations due to the choice of unrealistic parameters can be simulated. One can perform the so-called "thought experiments"³⁴ using simulations tools. However, there are many doubts on the simulation results due to the sensitivity on the initial/boundary conditions together with issues of resolutions, computational box dimensions, etc. Nevertheless, it is very difficult to overestimate the importance of numerical simulations and a carefully designed simulation should be given as much credibility as a carefully conducted experiment. The most commonly used methods for simulations are direct numerical simulation (DNS), large-eddy simulation (LES) and Reynolds-averaged Navier-Stokes (RANS), among which only the DNS gives the correct answer to the governing equations. The other two, i.e. LES and RANS, involve certain extent of modelling³⁵ which might lead to inexact solutions and therefore they are not as trustful as DNS or experimental results.

1.5. Scope of the thesis

The present thesis is mainly concerned with the canonical flat-plate boundary layer including passive scalar transport. Here the word "canonical" means the following simplified situations as opposed to the more complicated real situations:

- Nominal zero-pressure-gradient. Neither adverse nor favourite pressure gradient is considered along the streamwise direction far away from the wall.
- The wall is perfectly smooth and flat. Neither wall roughness nor wall curvature is considered.
- Incompressibility. Any compressible effects are not considered, i.e. flow is at low Mach number ($Ma \le 0.3$).
 - Two-dimensional mean flow with homogeneous spanwise direction.
- Constant fluid property, e.g. viscosity and density do not vary with temperature.

Some of the simplifications are justified here:

 $^{^{32}}$ There are definitely more methods than these.

³³As a student doing numerical simulations, I even doubt my ability to judge numerical techniques. It is certain that I am not qualified to judge on experimental techniques.

³⁴The words probably comes from Ernst Mach in the science community.

 $^{^{35}\}mbox{``that}$ is to say, a cheap answer to an expensive problem." – Prof. Bradshaw

- Turbulence (fluctuation) is always three-dimensional, therefore even with a two-dimensional mean flow, one will not observe qualitative differences in the turbulence structures.
- Compressibility has no direct influence on turbulence if the density fluctuations are small compared to the absolute density, i.e. Morkovin's hypothesis (Morkovin 1964). However, the density variation or extra velocity gradient resulting from pressure gradients do affect turbulence.
- Viscosity's dependence on the temperature should not directly influence the flow except in the conductive sublayer where most temperature difference occurs (Rannie 1956). Especially for high Prandtl number fluids, the conductive sublayer becomes so thin that the outer part is approximately isothermal. In general, an understanding of variable viscosity is always desirable.

The reason to conduct the thesis on such a simple setup is obvious, i.e. the problem should be as simple as possible to exclude influences from other complex/unknown factors. However, as suggested by Clauser (1956), the physical understanding of a canonical turbulent boundary layer can be improved by observing the its response to different outside influences³⁶. For the present thesis, as an extension to more complex situations, the effects of free-stream turbulence are considered in some cases in the hope that these "external disturbances" could shed some light on the canonical flow case.

The thesis is arranged in such an order: Chapter 2 will provide the numerical issues concerning the present study. Chapter 3 includes some of the results pertaining to both velocity and scalar fields. Chapter 4 summarises and the conclusions are drawn and outlooks are made.

 $^{^{36}}$ For more details about the behaviours of a perturbed boundary layer, one could refer to the review by Smits & Wood (1985) and references therein.

Numerical issues

"You don't get what you don't pay for"

- Peter Bradshaw

"You shouldn't get what you don't pay for"

- anonymous

This section gives a general view of different aspects of numerical simulations. Starting from the governing equation, follows a discussion of the resolution requirement for the various simulation methods. In addition, both the spatial and temporal discretization schemes are discussed, followed by how to specify proper inflow/outflow conditions and boundary conditions. In the end, some general rules about code validation are given.

2.1. Governing equations

2.1.1. Direct numerical simulation (DNS)

The governing equations for the direct numerical simulation (DNS) of an incompressible (laminar, transitional or turbulent) flow with passive scalars are the Navier-Stokes equations and the scalar transport equation, here written in non-dimensional form and tensor notation as

$$\begin{split} \frac{\partial u_i}{\partial t} + u_j \frac{\partial u_i}{\partial x_j} &= -\frac{\partial p}{\partial x_i} + \frac{1}{Re} \frac{\partial^2 u_i}{\partial x_j \partial x_j} ,\\ \frac{\partial u_i}{\partial x_i} &= 0 , \\ \frac{\partial \theta}{\partial t} + u_i \frac{\partial \theta}{\partial x_i} &= \frac{1}{RePr} \frac{\partial^2 \theta}{\partial x_i \partial x_i} , \end{split} \tag{2.1}$$

where $(x_1, x_2, x_3) = (x, y, z)$ are the Cartesian coordinates in the streamwise, wall-normal and spanwise direction, respectively. $(u_1, u_2, u_3) = (u, v, w)$ are the corresponding instantaneous velocity fields, p is the pressure and θ the scalar concentration. The Reynolds number Re is defined as

$$Re = \frac{U_{\rm ref}L_{\rm ref}}{\nu} \ ,$$

where $U_{\rm ref}$, $L_{\rm ref}$ and ν are the dimensional reference velocity and length and kinematic viscosity, respectively, which are also used for non-dimensionalisation. Pr is the Prandtl number defined by

$$Pr = \frac{\nu}{\alpha}$$
,

where α is the scalar diffusivity.

The summation convention is implied over repeated indices throughout this thesis unless stated otherwise. The streamwise and spanwise directions will be alternatively termed as the horizontal/wall-parallel directions.

2.1.2. Large-eddy simulation (LES)

The governing equations for large-eddy simulation (LES) are the spatially filtered Navier-Stokes equations and the scalar transport equation which in dimensionless form read

$$\frac{\partial \widetilde{u}_{i}}{\partial t} + \widetilde{u}_{j} \frac{\partial \widetilde{u}_{i}}{\partial x_{j}} = -\frac{\partial \widetilde{p}}{\partial x_{i}} + \frac{1}{Re} \frac{\partial^{2} \widetilde{u}_{i}}{\partial x_{j} \partial x_{j}} - \frac{\partial \tau_{ij}}{\partial x_{j}} ,
\frac{\partial \widetilde{u}_{i}}{\partial x_{i}} = 0 ,
\frac{\partial \widetilde{\theta}}{\partial t} + \widetilde{u}_{i} \frac{\partial \widetilde{\theta}}{\partial x_{i}} = \frac{1}{RePr} \frac{\partial^{2} \widetilde{\theta}}{\partial x_{i} \partial x_{i}} - \frac{\partial \sigma_{i}}{\partial x_{i}} ,$$
(2.2)

where the so-called sub-grid scale (SGS) stresses $\tau_{ij} = \widetilde{u_i u_j} - \widetilde{u}_i \widetilde{u}_j$ and $\sigma_i = \widetilde{u_i \theta} - \widetilde{u}_i \widetilde{\theta}$ represent the impact of the unresolved velocities/scalar on the resolved ones and have to be modelled. Mathematically, they arise from the nonlinearity of the convection term which does not commute with the linear filtering operation.

A filtered quantity $\widetilde{f}(x)$ in one dimension is defined by

$$\widetilde{f}(x) = G^P * f = \int_{\Omega} G^P(x, x', \Delta) f(x') dx'$$
,

where Ω is the computational domain, G^P is the primary filter with Δ being the filter width. A three-dimensional filter can be easily formulated and the common filters are the sharp cut-off filter, Gaussian filter and top-hat filter. For more mathematical properties of these filters, one could refer to e.g. Pope (2000). The filtering operation separates the large and small scales and the filter function G^P determines the size and structures of the large scales. For the differentiation and the filtering operation to commute, G^P has to be a function of x-x' only (Leonard 1974). A rough classification of the LES models can be made depending on the primary filter G^P : implicitly filtered models if the primary filter G^P is the grid filter, e.g. the ones used in the classical eddy-viscosity models; explicitly filtered models where an explicit filter operation is taken, e.g. the graded primary filter used in the approximate deconvolution model (ADM) (Stolz & Adams 1999).

2.2. Sub-grid scale (SGS) modelling

In LES, the effects of the unresolved scales on the resolved ones have to be provided via the sub-grid scale (SGS) model. Therefore, a good SGS model is generally desirable. Here the following SGS models, namely Smagorinsky model (SM), high-pass filtered Smagorinsky model (HPF-SM) and relaxation-term (RT) model are considered. Their counterpart account for passive scalar transport are discussed in the following subsection. For the models presented in the thesis, the formulations are taken from the thesis by Schlatter (2005). For more detailed formulation/derivation, please refer to the original thesis or papers therein. For other models, one could refer to the textbook by e.g. Sagaut (2005).

2.2.1. SGS model for velocity field

For the Smagorinsky model, the SGS stresses are modelled by

$$\tau_{ij} - \frac{\delta_{ij}}{3} \tau_{kk} = -2\nu_t S_{ij}(\widetilde{u}) ,$$

$$S_{ij}(\widetilde{u}) = \frac{1}{2} \left(\frac{\partial \widetilde{u}_i}{\partial x_j} + \frac{\partial \widetilde{u}_j}{\partial x_i} \right) ,$$

$$\nu_t = (C_s \Delta)^2 |S(\widetilde{u})| ,$$

$$|S(\widetilde{u})| = \sqrt{2S_{ij}(\widetilde{u})S_{ij}(\widetilde{u})} ,$$

where Δ is a typical length scale of the primary filter usually computed from the grid size as $\Delta = (\Delta x \Delta y \Delta z)^{\frac{1}{3}}$ (Deardorff 1970). The model coefficient C_s known as the Smagorinsky constant is actually not a constant and has to be determined a priori based on the flow case.

For HPF-SM model, the formulation is similar to that of the SM model, and the only difference is that the SGS stresses are evaluated based on the filtered velocity field instead of the resolved velocity field. The moldelled SGS stress are given by

$$\begin{split} \tau_{ij} &- \frac{\delta_{ij}}{3} \tau_{kk} &= -2 \nu_t^{HPF} S_{ij} (H * \widetilde{u}) \;, \\ S_{ij} (H * \widetilde{u}) &= \frac{1}{2} \left(\frac{\partial H * \widetilde{u}_i}{\partial x_j} + \frac{\partial H * \widetilde{u}_j}{\partial x_i} \right) \;, \\ \nu_t^{HPF} &= (C_s^{HPF} \Delta)^2 |S(H * \widetilde{u})| \;, \\ |S(H * \widetilde{u})| &= \sqrt{2 S_{ij} (H * \widetilde{u}) S_{ij} (H * \widetilde{u})} \;, \end{split}$$

where H is a high-pass filter, and C_s^{HPF} being the model coefficient.

Note that for both SM and HPF-SM models, the model coefficient can be also computed dynamically. The same recipe will not be repeated here and one may refer to Germano *et al.* (1991); Lilly (1992); Schlatter *et al.* (2006) for more details.

For RT model, the SGS forcing terms $\frac{\partial \tau_{ij}}{\partial x_j}$ are modelled by

$$\frac{\partial \tau_{ij}}{\partial x_j} = \chi H_N * \widetilde{u}_i ,$$

where H_N is a high-pass filter and χ is the model constant usually set to 0.2. The constant χ can be determined dynamically, however, tests showed that the results are rather insensitive to it (Stolz *et al.* 2001; Schlatter *et al.* 2006).

The sub-grid scale (SGS) model for the passive scalar corresponding to eddy-viscosity models is the so-called eddy-diffusivity model. The SGS stress σ_i is obtained by

$$\sigma_i = -\frac{\nu_t}{Pr_t} \frac{\partial \widetilde{\theta}}{\partial x_i}$$

or

$$\sigma_i = -\frac{\nu_t^{HPF}}{Pr_t} \frac{\partial H * \widetilde{\theta}}{\partial x_i}$$

for classic or high-pass filtered eddy-viscosity models and

$$\sigma_i = -\frac{\chi}{Pr_t} \frac{\partial H_N * \widetilde{\theta}}{\partial x_i}$$

for RT model. A constant turbulent Prandtl number $Pr_t = 0.6$ is usually assumed. Note that all the drawbacks of the models for the velocity are present in the scalar models as well. It should be noted that the literature on SGS modelling of passive scalars is much less extensive than that for the velocities. In particular high Péclet numbers (high Re or Pr) are seldomly addressed.

2.3. Resolution requirements

With the advances of the large-scales parallel computers, numerical simulations are getting more and more involved in our understanding of turbulence. In principle, the Navier-Stokes equations are discretised on the numerical grid and integrated over time with appropriate boundary condition and initial condition. There should be no doubt that a carefully designed numerical simulation is just an experiment equipped with "ghost sensing probes", i.e. a sensing probe without instrumental defects. Furthermore, there is no reason to expect the numerical data to be less accurate than those obtained by experiments, see e.g. a recent study of comparison of both simulation and experimental results in a turbulent boundary layer by Schlatter $et\ al.\ (2009)$. "When people regret that we do not 'understand' turbulence they are really regretting that we are not able to integrate the Navier-Stokes equations in our heads: for that, one would need a Cray in the cranium." (Bradshaw 1996). Unfortunately, even one could put the most powerful Cray in the cranium, one could not solve the "mysterious" problem, simply because the Reynolds number reached by large-scale

 $^{^1\}mathrm{For}$ those who do not like Cray, one could think of another vender as you like.

computers nowadays is still too low even compared to the Reynolds number range obtainable by wind-tunnel experiments, let alone those in industry applications or in nature. This is a major disadvantage of all the simulations. One could always push the Reynolds number higher at the expense of accuracy, but even in those cases, the obtained Reynolds number is still not high enough.

2.3.1. DNS

DNS provides the most accurate three-dimensional, time-dependent numerical solutions to the governing equations, i.e. the NS equations and the scalar transport equation if passive scalar transport is considered. These equations are solved without employing any turbulence models, i.e. no assumption for the physics, hence the errors come only from the numerical approximations and domain truncation. Due to its requirement to accurately represent the flow field, the most smallest eddies with the Kolmogorov/Batchelor length scales need to be resolved on the numerical grid which then leads to billions of grid points or spectral modes to be used for even a low laboratory Reynolds number.

Considering wall-bounded flows², the number of grid points (resolution) required can be estimated from the ratio L/η where L is the integral lengthscale (characterising the large eddies, e.g. the pipe radius, channel height or the boundary layer thickness) and η is the Kolmogorov scale. Usually at least two grid points are needed for each smallest scale η (Jiménez 2003), the necessary number of grid N in each dimension is on the order of Re_{τ} , which is a certain measure of Reynolds number. The number of time steps needed for a fluid particle to go through the computational box once, is on the order of N(Jiménez 2003). A rule of thumb is that the fluid particles need to go through at least 10 times the computational box to get converged low-order statistics, e.g. the mean and second-order statistics. The total computational cost which depends on the product of number of points by the number of time steps is then on the order of Re_{τ}^4 (Jiménez 2003) for a three-dimensional problem. It is clear the high cost with increasing Reynolds number is restricting DNS only as a research tool. A rule of thumb about the required resolutions in wall-parallel directions for a DNS are of the order $\Delta x^+ = 8, \Delta z^+ = 4$ (Kim et al. 1987)³. Usually in the wall-normal direction, a non-equal distance grid is adopted, e.g. Chebyshev polynomials used in the psedospectral simulations, or grid stretching in finite difference codes. So a general guideline is at least 10 grid points are needed in the region $y^+ < 10$ and three points below $y^+ = 1$. In the outer region e.g. near the boundary layer edge or channel/pipe centre line, $\Delta y^+ = 10$ can be used. Note that if considering also the scalar transport at Pr > 1, due to a smaller Batchelor scale $\eta_{\theta} = \eta/Pr^{1/2}$ needs to be resolved, the resolution

 $^{^2}$ For flows without walls, the estimation for the computational cost is a little bit less and one could find more detailed derivations/discussions in e.g. Pope (2000).

³Here grid spacing is scaled in wall (inner) units, i.e. $\Delta x^+ = \frac{u_\tau \Delta x}{\nu}$ with $u_\tau = \sqrt{\nu \frac{\partial \langle u \rangle}{\partial y}}\Big|_{y=0}$, since the viscous wall unit is the wall equivalent of the Kolmogorov scale (Jiménez 2003).

requirement is more severe and which usually leads to an over-resolved velocity field.

2.3.2. LES

LES take advantage of the idea from K41 theory (see Section 1.2) that the small eddies are statistically more isotropic⁴ at high enough Reynolds number and the inertial range is independent of the dissipation mechanism. So the large anisotropic eddies need to be resolved on the numerical grid while the effects of the unresolved smaller eddies are modelled by the so-called sub-grid scales (SGS) models which is working like an energy drain and in the hope that the dynamics of the large scales would not be disturbed.

However, for wall-bounded flows as opposed to the free shear flows, all the eddies are anisotropic as long as they have a size larger than something on the order of the wall distance y and this trend continues until y is of the order of the viscous wall unit which is equivalent to the Kolmogorov scales (Jiménez 2003). Moreover, truncating the spectrum at certain chosen wavelength according to the filter width (related to the grid resolution for implicit LES) will make e.g. some part of an eddy in the resolved motion while the other part in the SGS motion, since a turbulent eddy is not as simple as an Fourier mode (Bradshaw 1997). The overall performance of a LES calculation thus to a large extent depends on the chosen SGS model assuming sufficient grid points to resolve the relevant physics. The resolution requirement of a usual wall-resolved LES calculation is that the number of grid points has to be sufficient to resolve the wall layer (Piomelli 2001), i.e. to capture the energy-producing structures, e.g. the so-called streaks. The cost of such LES calculations also depends on the Reynolds number. An estimation of the total number of points (grid resolution) is proportional to Re_{τ}^2 (Jiménez 2003) which is indeed lower (but not that much lower) than the case for DNS which is proportional to Re_{τ}^3 . This means that using LES one can obtain results at higher Reynolds number than DNS for equivalent cost, but the Reynolds number reached is still not high enough for practical engineering flows. Recent studies have shown especially for wall-bounded turbulent flows, that a good LES is almost as expensive as a DNS, e.g. see the discussion in Fröhlich & Rodi (2002). Therefore, one way to reduce the computational cost in LES is to use the so-called wall models⁵ which enables the calculations to be finished in an acceptable time for practical engineering applications. The idea of the wall model is to only resolve the outer part of the boundary layer leaving the wall region being completely modelled by specifying a correlation between the velocity in the outer region and the shear stress at the wall. For more details about wall modelling, one can refer to the review by Piomelli & Balaras (2002) and references therein. In general, the resolution guidelines for LES are $\Delta x^+ \approx 50-150$, $\Delta z^+ \approx 15-40$ and the first

⁴Or put it differently as done by Prof. Stewart: "They don't know which way is up".

⁵Other alternatives include using hybrid LES/RANS or detached eddy simulation (DES) (Spalart 2009), however, these methods in turn require a good RANS model.

point is at $y^+ < 1$. With the help of wall models, the resolution requirement can be relaxed to $\Delta x^+ \approx 100 - 600$, $\Delta z^+ \approx 100 - 300$ and the first point in wall-normal direction can be located at $y^+ \approx 30 - 150$ (Piomelli 2001).

2.3.3. RANS

The cheapest solution to the NS equations is obtainable via a solution to the Reynolds averaged Navier-Stokes (RANS) equations but with the lowest accuracy. However, it is favoured by the industry since most of the cases only the very basic mean statistics are needed⁶. Hybrid LES/RANS or LES with wall models begin to be appreciated in the companies but only confined to a small part for development. Due to the averaging, much information is lost and therefore one or more equations with empirical coefficients (usually obtained from experimental/simulation data) must be solved for compensation. For those who are interested, one may refer to e.g. Pope (2000) for more detailed discussions about RANS models and references therein.

2.4. Spatial & temporal discretisation

Due to the large resolution requirement, i.e. high computational cost, DNS and LES are not used as a design tool in the industry where RANS simulations are still dominant. Therefore, DNS and LES are still mainly dominant in the research community for addressing basic questions regarding physics and modelling. Regarding these issues, the numerical errors must be monitored and controlled which is important for the successfully reproducing all the scales present in the turbulent flows (Coleman & Sandberg 2010).

2.4.1. Spatial discretisation

So far, the solvers for turbulent flows in research community are dominated by spectral and finite-difference schemes depending on the flow case at hand. For canonical geometries, such as channel or flat-plate boundary layer, usually highly accurate and efficient algorithms, i.e. spectral methods (Canuto et al. 1988) which have barely no dissipation and dispersion errors, can be employed. Due to the global basis functions used in the spectral methods⁷, to compute each single quantity at one grid point, information from all the other points in the entire direction is needed. On the other hand, the disadvantages of spectral methods contains the inability to be applied in complex flow geometries and special treatments are required to enforce the inflow/outflow boundary conditions⁸, see also discussions in Section 2.5. These shortcomings lead some researchers to choose the high-order finite-difference schemes for non-canonical cases, see e.g. discussions in Sandham (2002). Nowadays, simulations are usually performed on large memory-distributed systems, i.e. data is distributed on

^{6&}quot;One does not pay for what one does not need, no matter how good it is."

⁷Usually high-order polynomials or Fourier series are chosen.

⁸Using spectral methods, the solid boundaries tend to give rise to stability problems which are poorly understood and further restrict the time step (Trefethen 1996).

different processors and at any given time, there is no single processor which has access to all the data in the entire domain. To access the data belonging to other processors, communication between different processors is needed. Such communication intensive applications in general have lower performance since the communication is not fully overlapping computation.

Compared to spectral methods, finite difference schemes are easier to implement, and suitable for more complex geometry and parallelization since only local information (information from neighbouring points) is needed for computing quantity at each grid point. However, a shortcoming for finite difference schemes is its low order accuracy compared to the spectral method. This in turn leads to an enormous amount of grid points to be spent to achieve the same accuracy compared to the spectral method. Moreover, the dispersion errors present in the finite difference method e.g. introduce unphysical behaviour in acoustic field or evolution of the vortical structure of the turbulence (Coleman & Sandberg 2010). In the end, one always need to compromise between the accuracy and complexity of the flow case.

One way to overcome this drawback is to use the so-called spectral-element method first introduced by Patera (1984) and later developed by many others, see e.g. Maday & Patera (1989); Karniadakis & Sherwin (2005). This method combines the geometric generality/flexibility of the finite element method with the accuracy of spectral methods, and is suitable for simulations in complex geometries⁹.

2.4.2. Temporal discretisation

Since turbulence contains various spatial scales, there is a need to resolve their associated parts in temporal space, i.e. accurate temporal discretisation is necessary. The time integration schemes can be in general divided into two categories: i) explicit schemes: the state of a system at a later time is calculated from the state of the system at the current time; ii) implicit schemes: the state of a system at a later time is obtained by solving an equation involving both the current state and the later state of the system. The explicit scheme can be designed to have high order of accuracy, however, the restriction of explicit scheme comes from the numerical instability. It is often the case that the maximum time step ensuring the scheme to be stable is well below the accuracy threshold required to resolve all the relevant temporal scales. On the other hand, implicit schemes are usually stable, but difficult to be designed to have high order of accuracy and furthermore, they require extra computations.

Based on a one-dimensional linear model problem, i.e. convection-diffusion equation: $\frac{\partial \theta}{\partial t} + c \frac{\partial \theta}{\partial x} = \nu \frac{\partial^2 \theta}{\partial x^2}$ where c and ν are constant convection velocity and viscosity coefficient. Following the derivation in Coleman & Sandberg (2010), one can show that for a spectral method, the maximum time step Δt has to

⁹For more details about the turbulence simulation using spectral-element methods, one could refer to e.g. the very nice work performed on my neighbour's desk (Ohlsson *et al.* 2010).

fulfil the following condition¹⁰:

$$(1 - \pi^2 \frac{\nu \Delta t}{\Delta x^2})^2 + (\pi \frac{c \Delta t}{\Delta x}) \le 1.$$
 (2.3)

It is clear from this condition that the viscosity is extremely important to keep the scheme stable. Moreover, the first term is usually called the viscous condition which indicates that $\Delta t_{\nu} \sim \frac{\Delta x^2}{\nu}$; The other one is the so-called Courant-Friederichs-Lewy (CFL) condition (Courant et al. 1928) which requires $\Delta t_c \sim \frac{\Delta x}{c}$. For turbulence in wall-bounded flows, e.g. channel, pipe and boundary layer flows, the near wall resolution usually is very fine (especially in the wall-normal direction due to the Gauss-Lobatto distribution in spectral method or grid stretching in finite difference schemes) which then leads to a prohibitively small viscous condition. Consequently, a combination of both explicit and implicit schemes is usually adopted in most solvers for incompressible wall-bounded flows: an explicit scheme (usually Runge-Kutta scheme) is applied for non-linear (convective) terms and an implicit scheme (usually Crank-Nicolson scheme (Crank & Nicolson 1947)) for linear (viscous) terms.

2.5. Inflow & outflow condition

For spatially developing flows, e.g. boundary layer flows, it is extremely challenging to impose the appropriate inflow/outflow which is the best model for a boundary layer which grows in the downstream direction rather than in time. The most "straight-forward" way to generate turbulent inflow would be through laminar-turbulent transition as what is done in the laboratory. Usually in the experiments, the flow is disturbed by tripping devices mounted near the leading edge of the flat plate such that it becomes turbulent downstream. To mimic these tripping wires effects, one could add a volume forcing close to the inlet of the numerical domain which induces laminar-turbulent transition (Chevalier et al. 2007). Another way to generate turbulence through laminar-turbulent transition is to use free-stream turbulence. In this case, the disturbances in the free steam penetrate the boundary layer and cause the so-called "bypass" transition, see e.g. Brandt et al. (2004). It is obvious that one disadvantage of these two methods is that the flow in the initial part of the computational domain are during transition and thus can not be used to study turbulence. To avoid simulating laminar-turbulent transition, one could resort to the so-called "recycling method" originally proposed by Lund et al. (1998). Using this method, the turbulent inflow is synthesised by rescaling a reference downstream plane of the simulation at each time step. However, one issue about the "recycling method" is how to choose the rescaling parameters which are not clear. Furthermore, appropriate turbulent inflow generally requires complete, physically realistic, correct history for each variable at each grid point (Coleman & Sandberg 2010), therefore, though the synthesised inflow is turbulent, it still needs

 $^{^{10}}$ "Though the stability criteria is derived from one-dimensional linear model problem, in practise, it usually provides reasonable estimate for nonlinear and three-dimensional problems" (Coleman & Sandberg 2010).

certain downstream distance for the flow to evolve and adjust itself to have the correct dynamics (Jiménez et al. 2008). Moreover, there are e.g. streamwise correlations in the fluctuations when employed recycling method which is not for the case using trip forcing. Another way of generating turbulent inflow data is to run an auxiliary DNS and take the data from there, but again this auxiliary DNS does have similar problems in its own setup and is thus not a perfect solution.

For spectral methods, since it is required to have periodic boundary condition in the streamwise, therefore some special treatments have to be done to enforce the periodicity. The most common trick is to add the so-called "fringe region" (Spalart 1988; Bertolotti et al. 1992; Nordström et al. 1999; Chevalier et al. 2007), i.e. an extra region is added at the downstream end of the physical domain. Within this region, to fulfil the periodic boundary conditions in the streamwise direction, a volume force is added to the Navier–Stokes equations and the boundary layer is brought back to the exact inflow condition, e.g. a laminar Blasius profile. Note that the fringe forcing is also applied to the scalar field in a similar fashion.

2.6. Boundary condition

Imposing approporiate boundary conditions is not at all trivial and correct boundary conditions can easily make the computation successful, stable and fast (Trefethen 1996)¹¹.

The velocity and scalar fields are periodic in the horizontal directions whereas specified boundary conditions at the wall and in the free-stream are needed to solve the governing equations. For the boundary conditions on the solid wall¹², the most common one being used is the so-called no-slip boundary condition, i.e. the velocity of the fluid at a solid surface must be equal to the velocity of the surface. Another type of wall boundary condition is usually used for scalar field which is a constant scalar flux condition at the wall.

Concerning the boundary condition in the free stream, physically the flow is assumed to extend to an infinite distance perpendicular to the wall. However, in practise, the computational domain is always finite, so is the size of the wind tunnel. Therefore, the flow domain is always truncated and an artificial boundary condition needs to be applied in the free stream at a height of the computational box y_L . The requirement of such a free stream boundary condition is that the solutions to the governing equations in the truncated domain should approximate the correct solutions in an unbounded domain, i.e. whatever condition employed in the free stream should not propagate back into the computational domain and contaminate the solutions (Trefethen 1996). The most common idea is to use a so-called "sponge region" in which the same governing equations are solved but with extra dissipative terms added to absorb

 $^{^{11}\}mathrm{Usually}$ the problem is that correct boundary conditions are unknown.

¹²Here no blowing nor suction on the wall is considered.

 $^{^{13}}$ Similar to the idea of "fringe region" which forces the flow to a desired flow condition.

energy or damp disturbances, and thus avoiding disturbances to reflect back into the physical interesting domain. One drawback similar to the concept of "fringe region" is that the "sponge region" is only used to prevent reflections of fluctuations, and the disturbances should be "killed" smoothly, i.e. the extra dissipative term should not have large amplitude. As a consequence, the region must be thick, and thus computationally expensive especially in three-dimensional calculations.

Another way of imposing free stream boundary condition is to match the solutions of the physical problem at the free stream. Apparently, imposing such a boundary condition requires the knowledge of the physical problem at far field. For the present simulations, both wall boundary condition and the free stream boundary condition are implemented in the following way, see the original report by Chevalier *et al.* (2007) for more detailed discussions.

2.6.1. Boundary conditions for flow field

At the wall, the no-slip boundary conditions are applied,

$$u\big|_{u=0} = 0, \ v\big|_{u=0} = 0, \ w\big|_{u=0} = 0$$
 (2.4)

and

$$\left. \frac{\partial v}{\partial y} \right|_{y=0} = 0 , \qquad (2.5)$$

which is derived from the continuity equation.

In the free stream, the simplest possible boundary condition is a Dirichlet condition which is defined as

$$u_i\big|_{y=y_L} = \mathcal{U}_i\big|_{y=y_L} , \qquad (2.6)$$

where y_L is the height of the solution domain in the wall-normal direction. $\mathcal{U}_i(x,y)$ is a laminar base flow that is usually chosen as the Blasius flow for a canonical zero-pressure-gradient turbulent boundary layer¹⁴. However, the desired flow solution generally contains small disturbances which will be forced to zero by the Dirichlet condition resulting in increased damping of disturbances in the boundary layer. This introduces errors compared to the exact solution for which the boundary condition is applied at an infinite distance from the wall. Some improvement can be made by imposing a Neumann condition which is defined as

$$\frac{\partial u_i}{\partial y}\Big|_{y=y_L} = \frac{\partial \mathcal{U}_i}{\partial y}\Big|_{y=y_L} \ . \tag{2.7}$$
 The Neumann condition can be shown to be stable if the upper boundary is

The Neumann condition can be shown to be stable if the upper boundary is placed on a sufficiently large distance from the wall¹⁵, so that the disturbance velocity is small.

 $^{^{14}}$ For boundary layers with pressure gradient, one could choose Falkner-Skan-Cooke (FSC) flow as the base flow.

¹⁵In the present simulations, the domain height is usually chosen at least twice as high as the boundary layer thickness at the highest Reynolds number. A generalisation of the boundary condition used by Malik *et al.* (1985) can be employed to place the upper boundary closer to the wall.

2.6.2. Boundary conditions for scalar field

In the present implementation for the scalar field, two types of wall boundary conditions are available: an isoscalar wall or an isoflux wall which are given by

$$\theta\big|_{y=0}=0$$
 , $% \left| \theta\right| =0$ for the isoscalar boundary condition

$$\frac{\partial \theta}{\partial y}\Big|_{y=0} = 1$$
, for the isoflux boundary condition (2.8)

These two kinds of wall boundary conditions are actually two limiting cases of the physical configuration. Considering θ to be the temperature concentration, the isoscalar wall boundary condition corresponds to a situation where the fluid with negligible density ρ , heat capacity c_p and thermal conductivity k is heated by an infinitely thick wall with large density ρ_w , heat capacity c_{pw} and thermal conductivity k_w . Hence the thermal activity ratio $K = \sqrt{\frac{\rho c_p k}{\rho_w c_{pw} k_w}}$ is vanishing in this case. The isoflux wall boundary condition, however, is an opposite case. It signifies an extremely thin wall with small density, heat capacity and thermal conductivity while the corresponding fluid properties are quite large. This leads to a thermal activity ratio K of ∞ (Tiselj et al. 2001). In order to reveal the details of the heat transfer near the wall for a more general case, one has to solve the conjugate heat transfer problem with a given thickness, material properties of the solid wall and the properties of the fluid. For more details about conjugate heat transfer, see e.g. Kasagi et al. (1989).

The boundary condition in the free-stream is of Dirichlet type, i.e.

$$\theta\big|_{y=y_L} = 1 \ . \tag{2.9}$$

A Neumann condition was also tested, and the results turned out to be indistinguishable to those obtained with the Dirichlet condition.

2.6.3. Free-stream turbulence generation

In some occasions, the boundary layer is subject to external disturbances, for instance free-stream turbulence (FST) which can be either isotropic/homogeneous or anisotropic/inhomogeneous. To generate isotropic and homogeneous free-stream turbulence, usually it is done by using a turbulence grid in experiments. To synthesise free-stream turbulence in a simulation, Jacobs & Durbin (2001) followed the methodology proposed by Grosch & Salwen (1978), i.e. superimposing Fourier modes and the Orr-Sommerfeld modes from the continuous spectrum. Later, Brandt et al. (2004) used a similar way to generate FST by summing up both Orr-Sommerfeld modes and Squire modes. It can be shown that far above the boundary layer, these continuous Orr-Sommerfeld modes behave the same as the Fourier modes. Other possibilities, e.g. followed by Péneau et al. (2000), generate the inflow free-stream turbulence by composing random Oseen vortices. By using all these methods to generate FST, one could avoid the inclusion of the leading edge of the flat plate which saves considerable computational effort. On the other hand, possible history effects of the FST cannot be considered, i.e. the FST effects only depend on

the local turbulence intensity and the length scale, due to the lack of leading edge effects. To investigate such history effects of the FST and better compare with the experiments, one has to include the leading edge of the plate. Such simulations have been performed previously by some authors, e.g. see references by Péneau et al. (2000); Ovchinnikov et al. (2008). However, these studies are mainly in an effort to study transition to turbulence, rather than a fully turbulent boundary layer under FST. As opposed to the isotropic/homogeneous FST, anisotropic/inhomogeneous FST can also be generated, and such cases are more likely to happen in turbine industries. To generate these high intensity, anisotropic FST, one could use the e.g. a turbulent jet as in Maciejewski & Moffat (1992a,b). Apart from corresponding better to practical situations, the jet-generated FST has an intensity more or less constant along large distance downstream which is a nice property to distinguish the effects of free-stream intensity from other possible factors (Kondjoyan et al. 2002).

The FST is usually characterised by its intensity Tu and its lengthscale. The turbulence intensity Tu is defined by

$$Tu = \sqrt{\frac{u_{rms}^2 + v_{rms}^2 + w_{rms}^2}{3}} \ . \tag{2.10}$$

For the lengthscale, following Tennekes & Lumley (1972), an integral length scale L characterising the FST¹⁶ is defined as

$$L = \frac{1.8}{\kappa_{max}} \,, \tag{2.11}$$

where κ_{max} is the wavenumber where the maximum energy is located in the spectrum. Another length scale L_u , based on the streamwise velocity fluctuations usually employed in experiments, see e.g. Simonich & Bradshaw (1978), is defined by

$$L_u = \frac{\langle u'^2 \rangle^{3/2}}{-U_\infty \frac{\mathrm{d}\langle u'^2 \rangle}{\mathrm{d}x}} \,, \tag{2.12}$$

with $\langle \cdot \rangle$ denoting a spanwise/temporal average, and the prime denoting fluctuating quantities according to the Reynolds decomposition, $u = \langle u \rangle + u'$.

2.7. Statistical convergence

Another important issue is related to collecting statistics. The rate at which the statistics converge varies greatly, with low-order statistics (e.g. mean and RMS of fluctuations) converge fast while higher-order statistics (e.g. skewness and flatness factors) much slower. Moreover, statistics dominated by very large-scale structures, i.e. involving fewer "eddy samples" within a given finite domain, tend to converge slow, such as two-point correlations at large separation or spectra at low wavenumbers (Coleman & Sandberg 2010). A rule of thumb is that to obtain converged statistics, one needs about 10-20 flow

The length scale L_{11} defined by the longitudinal two-point correlation can be related to L via $L_{11} = \int_0^\infty \frac{\overline{u'(x)u'(x+r)}}{\overline{(u')^2}} dr = \frac{3\pi}{2q} \int_0^\infty \frac{E(\kappa)}{\kappa} d\kappa \approx 1.286L$ (Schlatter 2001).

though times. "From a practical point of view, an inadequate statistical sample is just as serious a problem as inadequate spatial or temporal resolution, and can seriously limit the utility of the DNS results. The only remedy for poorly converged statistics is to extend the computational resources needed to gather more samples, by either increasing the averaging period for a time average, or the number of experiments entering the ensemble average" (Coleman & Sandberg 2010). Last, one has to bear in mind that the averaged/mean quantity which only depends on the local position is not adequate since turbulence is non-local, i.e. the motion at any given point is influenced by other distant points (Townsend 1976).

2.8. Validation & verification

One unique feature of numerical simulations is that they are able to simulate "wrong" physics, such as spurious modes, wrong thresholds, incorrect reattachment points, underestimated/overestimated functions due to under-resolved simulations, irrelevant size of the computational box, not appropriate boundary conditions or unrealistic parameters, etc. Thus, to generate simulation data with good quality is not simple nor cheap at all. Therefore, the validation of the results becomes relatively important. Suggestions made in Sandham (2002) and Coleman & Sandberg (2010) for DNS calculations are summarised here:

- Validate the code against analytical solutions (if possible), asymptotic limits and well-established database;
- Carry out systematic studies by varying the resolutions, box sizes, time steps and numerical methods;
- The grid resolution Δx_i should be compared with the Kolmogorov/Batchelor length scale $\eta = (\nu^3 \varepsilon)^{1/4}$, $\eta_\theta = \eta/Pr^{1/2}$ and the time step Δt with the Kolmogorov time scale $t_\eta = (\nu/\varepsilon)^{1/2}$. The ratios of $\Delta x_i/\eta$ and $\Delta t/t_\eta$ should be on the order of unity;
 - Budgets of statistical quantities should be evaluated and balance.

For LES, Geurts (1999) interpreted it as a balancing between different sources of errors, i.e. modelling and numerical ones. This makes the validation of LES results even more complicated. Therefore, to assess the quality of an LES model, spectral methods are in general recommended. In addition to the guidelines suggested for DNS, one should also follow the rules (Geurts & Leonard 2002)

- Avoid dissipative numerical methods;
- Vary the filter width while fixing the resolution;
- Use dynamic modelling.

Moreover, to validate a given SGS model, one could conduct either a priori or a posteriori tests during which accurate data from either DNS or experiments are required. In a priori test, no actual simulations are carried out. The SGS model is evaluated based on the available DNS or experimental data and compared with the exact SGS stress. However, care has to be taken when

interpreting the results since a successful a priori test does not guarantee good results in an actual LES calculation; sometimes the simulations can be even unstable (Vreman et al. 1995). On the other hand, a poor a priori test does not necessarily lead to poor results in an actual run (Meneveau 1994). Therefore, to judge whether a SGS model performs well or not, one has to run a simulation with the correctly implemented model and then compare the results with DNS or experimental data. This approach is known as a posteriori test (Piomelli et al. 1988) in the LES community. To correctly compare the obtained LES results with DNS or experimental database, one should add the SGS contribution to the resolved part and then compare to DNS data, e.g. when comparing the RMS of the fluctuations. However, for certain SGS models, it is only possible to obtain partial SGS contribution, i.e. only the anisotropic part of SGS contribution. Thus in these cases, only the anisotropic part of the statistics should be compared (Winckelmans et al. 2002; Sagaut 2005).

2.9. Summary of the employed numerical method

The results presented in this thesis are obtained using the simulation code **SIMSON** (Chevalier *et al.* 2007) developed at KTH Mechanics over many years. The governing equations are discretised based on a standard spectral method (Canuto *et al.* 1988). The discretization in the horizontal directions uses Fourier expansions assuming periodic solutions. In the wall-normal direction, Chebyshev polynomials with the Chebyshev tau method (CTM) (Canuto *et al.* 1988) to discretise the solution and the boundary condition. The time advancement used is a third-order Runge-Kutta method for the non-linear terms and a second-order Crank-Nicolson method for the linear terms. Adaptive time stepping is adopted to exploit the maximum stable time step. The non-linear terms are calculated in physical space rather than spectral space (pseudospectral method). Aliasing errors from the evaluation of the non-linear terms are removed by the 3/2-rule (Canuto *et al.* 1988) when the horizontal FFTs are performed¹⁷.

A sketch of the computational box is shown in Figure 2.1. The periodicity in the wall parallel directions is fulfilled by adding a "fringe region" (Bertolotti et al. 1992; Nordström et al. 1999) at the downstream end of the domain. In addition, to trigger rapid (natural) laminar-turbulent transition, a random volume forcing directed normal to the wall is located at a short distance downstream of the inlet.

The generation of the FST is by a superposition of eigenmodes of the Orr-Sommerfeld/Squire operator with prescribed energy spectrum, i.e. the von Kármán spectrum. For more details about the generation of FST, one could refer to Brandt *et al.* (2004); Schlatter (2001); Jacobs & Durbin (2000). The generated FST is homogeneous and isotropic, and satisfies the continuity constraint as well.

 $^{^{17}}$ In the wall-normal direction, no dealiasing is performed since the wall-normal resolution is usually finer than required owing to the specific Gauss-Lobatto distribution.

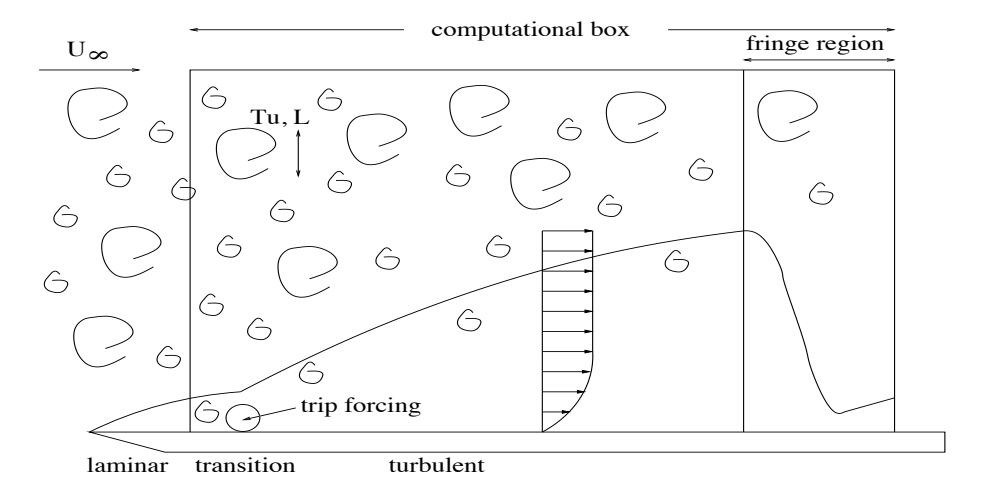


FIGURE 2.1. Sketch of the computational domain with free-stream turbulence.

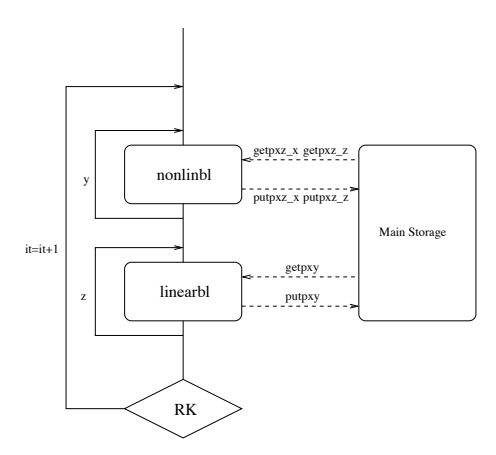


FIGURE 2.2. The main structure of the code. Note that there exist FFTs between calls to the subroutines getpxz_z and getpxz_x and inverse FFTs between calls to putpxz_z and putpxz_x.

The numerical code is written in FORTRAN 77/90 and consists of two major parts: one linear part where the equations are solved in spectral (Fourier/Chebyshev) space, and one non-linear part where the non-linear terms are computed in physical space, see Figure 2.2 for the general code structure. The main computational effort in these two parts is in the FFT which consumes more than 55% of the total execution time for a typical serial run. Thanks to the parallelisation, the expensive computation of the FFTs is not the main problem; the communication between processors being the bottle neck. For

the global communication needed in the subroutines getpxz and putpxz, two different ways are currently implemented. On one hand, a self-written version of the global transpose which is based on the explicit point to point communication using MPI commands MPI_ISEND, MPI_WAIT and MPI_RECV is available. For more details about this implementation, see e.g. Alvelius & Skote (2000). On the other hand, an alternative version is to adopt the standard collective communication command, i.e. MPI_ALLTOALL as illustrated in Figure 2.3. This standard MPI command transfers a subset of data from all

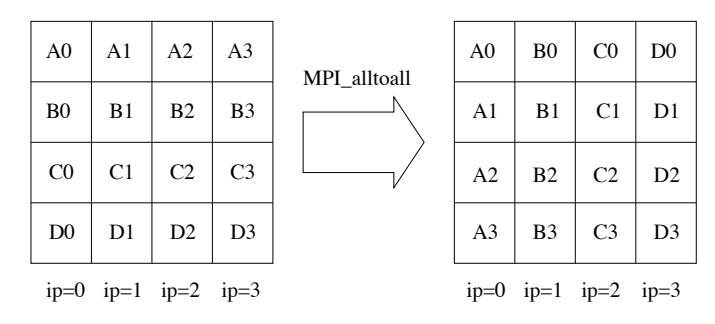


FIGURE 2.3. The MPI_ALLTOALL command illustrated for a group of four processors ip = 0, 1, 2, 3.

members to all members within a group. Each processor sends distinct data to each of the other processor. As seen from the figure, the MPI_ALLTOALL actually does a global transpose of the data among all the members in the group. Both versions of implementation for the global communication essentially perform approximately the same in terms of speed and memory requirement. However, if the collective communication version is used, the amount of data stored on each processors is slightly larger and thus the amount of communication compared to the hand-written version is marginally increased.

The present code has been highly parallelised either using OpenMP (Multi Processing) on shared memory machines or MPI (Message Passing Interface) on distributed memory machines. Recently, a new parallelisation has been implemented (Li et al. 2008) in which the data is distributed in a "pencilbased" 2D manner instead of the previous "slice-based" 1D manner, see also Figure 2.4. The advantages are clear, for instance, in the present example, with the 2D data decomposition, each processor only save one quarter of the data as in the 1D case, so the requirement for the memory on each single processor is greatly reduced. Moreover, one could use 4 times more processors than the 1D case, which is more suitable for a modern clusters which are build on processors on the order of 50000. One obvious disadvantage is that the communication will become more severe in terms of performance. Figure 2.5 (a) shows a performance of the benchmark case $(512 \times 513 \times 512)$ and very good speedup of the code is obtained. In Figure 2.5 (b), the performance curves using the 2D data decomposition are shown. With the new 2D implementation,

the number of cores could be used is greatly increased as compared to the 1D implementation. For the largest case considered so far with **SIMSON** (being part of an ongoing PRACE¹⁸ project), a total of 60 billion grid points is considered, running on 16384 cores. It is amazing that a research code, having many subroutines similar to the ones originally written around 1990, can still be used on the latest computer architectures!

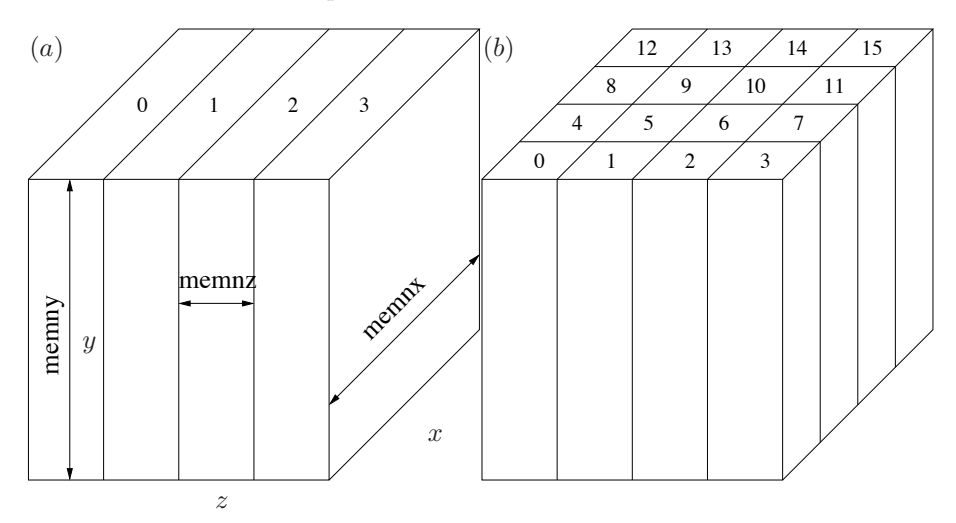


Figure 2.4. Data distribution among all the processors. (a) "Slice-based" data decomposition. (b) "Pencil-based" data decomposition.

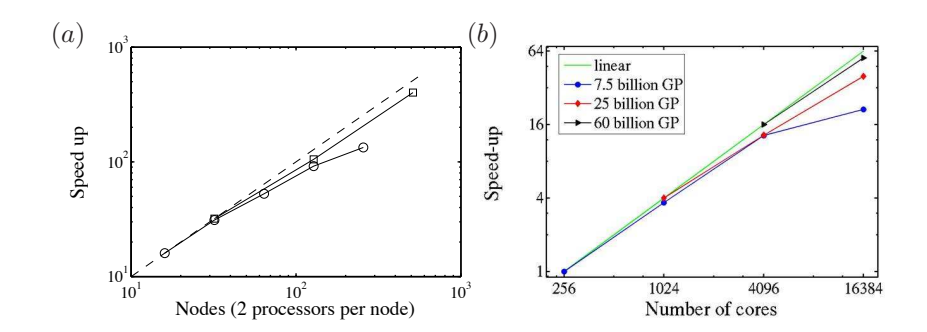


FIGURE 2.5. Speedup curve for the benchmark case. (a) \circ 1D parallelisation, -2D parallelisation, -- linear speedup. (b) Comparison among different cases.

 $^{^{18}\}mathrm{Partnership}$ for advanced computing in Europe.

CHAPTER 3

Turbulent boundary layer

- "Would you tell me, please, which law I ought to choose to fit my mean velocity profile?"
- "That depends a good deal on the accuracy you want to achieve", said the Cat
- "I don't much care what accuracy-"
- "Then it doesn't matter which law you choose" Said the Cat
- '-so long as it fits the profile SOMEWHERE,' I added as an explanation
- "Oh, you're sure to do that," Said the Cat, "if you simulate large Reynolds number enough"
 - A dialogue happened in my dream

"The wonderful thing about scaling is that you can get everything right without understanding anything"

- anonymous

3.1. Boundary layer equations

Due to its importance in applications, research has been focused on the structure and scaling of the wall turbulence, among which the flat-plate turbulent boundary layer is the most popular one being studied by experiments¹. If proper scaling of the experimental/numerical data can be obtained and this will provide prediction at those Reynolds number in the industrial application which is usually several orders of magnitude higher than those in the laboratory. Therefore one of the main research activities in fluid dynamics community is to find the coordinate transformation using different parameters (based on either physical argument or intuitive argument) to collapse the data for turbulence statistical quantities, e.g. mean velocity or fluctuations. However, none of the scalings seems to be completely satisfactory even for the mean velocity profile, and there seems to be no chance of finding such one even for the mean profile².

¹Which turns out to be relatively easy to be conducted in laboratory. However, it is the most difficult one to be simulated.

²"Even the Blasius solution is a numerical one" Buschmann & Gad-el Hak (2007).

In a statistically stationary and two-dimensional boundary layer, the governing equations for the mean flow can be obtained by taking the average of the governing equations and assuming boundary layer approximations (Schlichting

$$\frac{\partial \langle u \rangle}{\partial x} + \frac{\partial \langle v \rangle}{\partial y} = 0 , \qquad (3.1)$$

$$\langle u \rangle \frac{\partial \langle u \rangle}{\partial x} + \langle v \rangle \frac{\partial \langle u \rangle}{\partial y} = -\frac{\mathrm{d} \langle p_{\infty} \rangle}{\mathrm{d}x} + \frac{\partial}{\partial y} \left(\frac{1}{Re} \frac{\partial \langle u \rangle}{\partial y} - \langle u'v' \rangle \right) - \frac{\partial}{\partial x} (\langle u'u' \rangle - \langle u'v' \rangle) ,$$
(3.2)

$$\langle u \rangle \frac{\partial \langle \theta \rangle}{\partial x} + \langle v \rangle \frac{\partial \langle \theta \rangle}{\partial y} = \frac{\partial}{\partial y} \left(\frac{1}{RePr} \frac{\partial \langle \theta \rangle}{\partial y} - \langle v' \theta' \rangle \right) . \tag{3.3}$$

Note that p_{∞} is the pressure in the free stream and is a function of x only. Furthermore, this pressure term can be replaced by $U_{\infty} \frac{\mathrm{d}U_{\infty}}{\mathrm{d}x}$ according to Bernoulli's equation where U_{∞} is the free-stream velocity. Under the condition of zero-pressure gradient, the pressure term vanishes. The last term in equation (3.2), namely $\frac{\partial}{\partial x}(\langle u'u'\rangle - \langle u'v'\rangle)$ can be also omitted since its contribution is one order of magnitude smaller than the other leading terms, see e.g. Schlatter *et al.* (2010) where it is shown that $\frac{\partial}{\partial x}(\langle u'u'\rangle - \langle u'v'\rangle)$ is about $\mathcal{O}(50)$ times smaller than the leading order term in fully turbulent region. Integrating equation $(3.2)^3$ from the wall to the free stream yields the so-called von Kármán integral momentum equation which reads

$$\frac{\tau_w}{\rho} = \frac{\mathrm{d}}{\mathrm{d}x} \left[U_\infty^2 \int_0^\infty \frac{\langle u \rangle}{U_\infty} \left(1 - \frac{\langle u \rangle}{U_\infty} \right) \mathrm{d}y \right] + U_\infty \frac{\mathrm{d}U_\infty}{\mathrm{d}x} \int_0^\infty \left(1 - \frac{\langle u \rangle}{U_\infty} \right) \mathrm{d}y \quad (3.4)$$

where τ_w is the total shear stress⁴ at the wall. Introducing two commonly used measures for boundary layer thickness⁵, i.e. displacement thickness δ^* and momentum (loss) thickness θ (sometimes, they are also denoted as δ_1 and δ_2 , respectively) which are defined as

$$\delta^* = \int_0^\infty \left(1 - \frac{\langle u \rangle}{U_\infty} \right) dy \tag{3.5}$$

and

$$\theta = \int_0^\infty \frac{\langle u \rangle}{U_\infty} \left(1 - \frac{\langle u \rangle}{U_\infty} \right) dy . \tag{3.6}$$

³Note that the term $\frac{\partial}{\partial x}(\langle u'u'\rangle - \langle u'v'\rangle)$ is neglected and the pressure term $\frac{\mathrm{d}\langle p_{\infty}\rangle}{\mathrm{d}x}$ is expressed

in terms of free stream velocity as $U_{\infty} \frac{\mathrm{d}U_{\infty}}{\mathrm{d}x}$ as discussed.

⁴Total shear stress τ is defined as $\tau = \mu \frac{\partial \langle u \rangle}{\partial y} - \rho \langle u'v' \rangle$, where the kinematic viscosity ν is related to molecular viscosity μ by the relation $\nu = \frac{\mu}{\rho}$.

 $^{^5}$ The usual measure for boundary layer thickness is the 99% boundary layer thickness δ_{99} which is defined as the distance from the wall where the velocity reaches 99% the free stream velocity. However, this measure is an arbitrary measure and poorly conditioned (Örlü 2009). Therefore, other measures are preferably used, e.g. displacement thickness δ^* or momentum (loss) thickness θ .

Using the definition of displacement thickness δ^* and momentum thickness θ as well as the skin-friction coefficient c_f , the von Kármán integral momentum equation (3.4) can be rewritten as (see e.g. Örlü (2009))

$$c_f \equiv \frac{\tau_w}{\frac{1}{2}\rho U_\infty^2} = 2\frac{\mathrm{d}\theta}{\mathrm{d}x} + \frac{4\theta + 2\delta^*}{U_\infty} \frac{\mathrm{d}U_\infty}{\mathrm{d}x}$$
(3.7)

Note that the second term in equation (3.7) is identical to zero in the condition of zero-pressure gradient. In laboratory experiments, the skin-friction coefficient can be calculated according to the equation (3.7) based on the measured mean velocity profile alone, however, special care has to be paid to make sure a well resolved mean velocity profile is obtained (Örlü 2009)⁶.

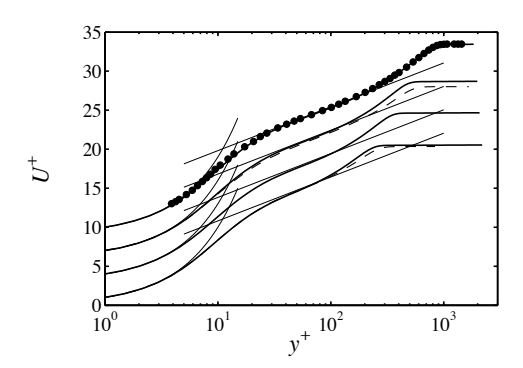


FIGURE 3.1. Mean streamwise velocity profiles U at $Re_{\theta} = 671,1000,1412,2512$. ——DNS by Schlatter *et al.* (2009), • experimental data by Schlatter *et al.* (2009), • – – DNS by Spalart (1988). The thin lines indicate the linear and logarithmic laws, using $\frac{1}{\kappa} \ln y^+ + 5.2$ with $\kappa = 0.41$. A detailed discussion of the figure is found in Paper 6.

3.2. Scalings for mean velocity field

A typical streamwise mean velocity profile from the present results at low Reynolds number⁷ is shown in Figure 3.1. According to the classic theory, the boundary layer is composed of two regions: a near-wall region (also called viscous region) where viscosity is important and the outer region where the viscous effects are negligible. Since is no sharp boundary between these two regions, a overlap region is existing as a transitional region. The boundary layer equations (3.2) can be further simplified in these regions.

⁶The only accurate way of measuring skin friction is to use the so-called oil-film interferometry (OFI) (Rüedi *et al.* 2003; Örlü 2009).

⁷Here "low" is relative to the experimental ones.

3.2.1. Inner region

The inner layer was first treated in the work by Ludwig Prandtl (Prandtl 1932). Within the inner region where the viscous effects are dominant, the boundary layer equation (3.2) reduces to

$$0 = \frac{1}{Re} \frac{\partial^2 \langle u \rangle}{\partial y^2} - \frac{\partial}{\partial y} \langle u'v' \rangle . \tag{3.8}$$

The governing law of the inner region is the so-called "law of the wall" which is considered to be the cornerstones of fluid dynamics (Bradshaw and Huang 1995). The law of the wall assumes that in the vicinity of the wall, the flow only depends on the distance of the wall y, the wall shear stress τ_w and the fluid properties (density ρ and molecular viscosity μ) (Bradshaw and Huang 1995) and these arguments lead to the "law of the wall" after some dimensional analysis:

$$\langle u \rangle^+ \equiv \frac{\langle u \rangle}{u_\tau} = \Phi_1(\frac{y}{\ell_*}) \equiv \Phi_1(y^+) ,$$
 (3.9)

and

$$\langle u'v'\rangle^+ \equiv \frac{\langle u'v'\rangle}{u_\tau^2} = \Phi_2(\frac{y}{\ell_*}) = \Phi_2(y^+) ,$$
 (3.10)

where u_{τ} (the so-called "friction velocity") and ℓ_* are a characteristic velocity scale and a viscous length scale respectively for the near wall region (viscous region). They are defined as

$$u_{\tau} \equiv \sqrt{\frac{\tau_w}{\rho}} = \sqrt{\nu \frac{\partial \langle u \rangle}{\partial y}}\Big|_{y=0} \quad \text{and} \quad \ell_* = \frac{\nu}{u_{\tau}} .$$

The superscript "+" denotes quantities in "viscous units"⁸, i.e. normalised by viscous velocity and length scales. Φ_1 and Φ_2 will be the same mathematical function for all flows at sufficiently high Reynolds number (Pope 2000).

Within the so-called viscous sub-layer, i.e. $y^+ \leq 5$ (Pope 2000), where the flow is mainly dominant by the viscous effects, i.e. the Reynolds stress $\langle u'v' \rangle$ due to turbulence is negligible, a linear relation can be obtained:

$$\langle u \rangle^+ = y^+ \ . \tag{3.11}$$

3.2.2. Outer region

As opposed to the inner region, the outer region is considered to be "inviscid", therefore the governing equation reduces to

$$\langle u \rangle \frac{\partial \langle u \rangle}{\partial x} + \langle v \rangle \frac{\partial \langle u \rangle}{\partial y} = -\frac{\partial \langle u'v' \rangle}{\partial y} .$$
 (3.12)

The large eddies transport turbulent energy from the outer part of the inner region and are assumed not strongly affected by the viscosity, i.e. the momentum transport is mainly due to turbulence. The appropriate characteristic length scale is chosen as the 99% boundary layer thickness δ_{99} (boundary

 $^{^8 \}mathrm{Some}$ authors prefer to use the word "wall units".

layer thickness at which the velocity reaches 99% of the free stream velocity), or pipe radius R or channel height h. Other outer length scales commonly used in boundary layer flows could be e.g. displacement thickness δ^* , or Rotta-Clauser length $\delta_{RC} \equiv \frac{U_\infty \delta^*}{u_\tau}$. The characteristic velocity scale is usually chosen as u_τ , since one can think of the inner layer as being a boundary condition for the outer flow. According to Townsend (1976), u_τ is regarded as a "slip" velocity seen by the motion in the outer part and hence appropriate velocity scale for the deviation of mean velocity from the free-steam velocity in boundary layer or centre line velocity as in pipe and channel flow. However, different velocity scales are proposed, e.g. see the previous work by George (2007), where it is suggested that the only appropriate velocity scale for the outer part of a zero-pressure-gradient turbulent boundary layer is the free-stream velocity U_∞ .

Once fixed the velocity (here the friction velocity is chosen) and length scales, the so-called velocity defect law can be formulated:

$$\frac{\langle u \rangle - U_{\infty}}{u_{\tau}} = \Psi_1(\frac{y}{\Delta}) , \qquad (3.13)$$

and

$$\frac{\langle u'v'\rangle}{u_{\tau}^2} = \Psi_2(\frac{y}{\Delta}) , \qquad (3.14)$$

where Δ is denoted as the outer length scale which can be δ^* , δ_{99} or δ_{RC} .

Note that the inner region for pipe/channel and boundary layer flows are similar, but the outer regions are different. For the internal flows, the flow is not intermittent and there is no free stream, but there are influences from the opposite wall in the channel and even more complicated in the case of the circular pipe. Intermittency and entrainment present in the boundary layer flow give rise to the wake region of the outer part of the flow, which is sensitive to pressure gradient and free stream turbulence (Gad-el Hak and Bandyopadhyay 1994). Moreover, the probability distribution of the interface between the turbulent and irrotational fluid in a boundary layer is roughly Gaussian with a mean value about $0.85 \, \delta_{99}$. Occasionally, the interface extends as deep as $0.4 \, \delta_{99}$ or as far out as $1.2 \, \delta_{99}$ (Klebanoff 1954; Kline et al. 1967; Bradshaw 1972), see also Figure 3.2.

3.2.3. Overlap region

Outside the buffer layer starting at about $y^+=100$ or so up to $\frac{y}{\delta_{99}}\approx 0.2$ is the so-called overlap region. This region is maybe one of the topic in turbulence research that has the most controversial debates. Most of the research is devoted to determine the scalings law of the mean profile and associated coefficients.



FIGURE 3.2. Instantaneous field of vorticity magnitude $|\omega|$ in the x-y section plane showing the intermittent characteristics in the outer region $Re_{\theta}=2300-2500$. The wall-normal cut only shows half of the domain in the wall-normal direction. The solid line indicate the 99% boundary layer thickness at $Re_{\theta}=2500$. The grey bar is from 0 (grey) to 0.1 (black). A detailed discussion of the figure is found in Paper 3.

3.2.3.1. Logarithmic law & power law

The velocity distribution in the overlap region is also called logarithmic law or log-law for short. There are various ways to derive the logarithmic law which reads

$$\langle u \rangle^{+} = \frac{1}{\kappa} \ln(y^{+}) + A , \qquad (3.15)$$

where κ is a universal constant and called von Kármán constant¹⁰. The constant $\kappa \approx 0.41$, and additive constant $A \approx 5.2$ can be determined from the experiments. For flat-plate zero-pressure-gradient turbulent boundary layer, Österlund *et al.* (2000) proposed a value for the Kármán constant of 0.38 for large Reynolds number. However, Spalart (1988) has shown that the traditional value of 0.41 gives good agreement for lower Reynolds numbers¹¹.

As an alternative to the logarithmic profile, the power law is favoured by some researchers, for more detailed discussion, one could refer to e.g. Barenblatt (1993); Barenblatt & Prostokishin (1993); Barenblatt $et\ al.\ (1997b,a)$; George & Castillo (1997).

The fundamental difference between the log-law and power law is choosing whether mean velocity $\langle u \rangle$ or its derivative $\frac{\partial \langle u \rangle}{\partial y}$ to enter the inner-outer matching process as commented by Millikan. In other word, it is a difference

 $^{^9}$ For the derivation, see e.g. Millikan (1938) or Landau (1944) or any modern text book about fluid dynamics.

¹⁰Experimental data shows that Kármán constant is actually not constant among different canonical wall-bounded flows (Nagib & Chauhan 2008).

¹¹This discrepancy of values can easily be understood by looking at the proposed composite profiles by Monkewitz *et al.* (2007), which show an initial dip in the log-law indicator function Ξ before settling to a lower κ for higher Reynolds numbers.

of position on Galilean invariance¹² as noted by Spalart (2011). For this reason, all modern turbulence models based on Galilean invariant equations prefer log-law over the power law.

3.3. Scalings for mean scalar field

3.3.1. Law of the wall for scalar field

By analogy, a law of the wall and log law are existing for the scalar field. By the same reasoning as above for the velocity, the law of the wall, the defect law and the log-law for scalar field read:

$$\langle \theta \rangle^{+} \equiv \frac{\theta_{w} - \langle \theta \rangle}{\theta_{\tau}} = \Phi_{\theta}(y^{+}, Pr) ,$$

$$\frac{\langle \theta \rangle - \theta_{\infty}}{\theta_{\tau}} = \Psi_{\theta}(\frac{y}{\Delta}, Pr) ,$$

$$\Phi_{\theta}(y^{+}, Pr) = \frac{\theta_{w} - \langle \theta \rangle}{\theta_{\tau}} = \frac{1}{\kappa_{\theta}} \ln(y^{+}) + A_{\theta}(Pr) ,$$
(3.16)

where κ_{θ} is the von Kármán constant for the scalar field, function Φ_{θ} is a universal function which is dependent on y^+ and the molecular Prandtl number Pr. A_{θ} and B_{θ} are addictive constants which are functions of Pr. θ_w is the scalar concentration at the wall and θ_{∞} the concentration in the free stream. θ_{τ} is called friction scalar or friction temperature for a heat transfer problem. According to Cebeci & Bradshaw (1984), the friction temperature is analogous to the friction velocity u_{τ} and defined by

$$\theta_{\tau} \equiv \frac{q_w}{\rho c_p u_{\tau}} \,, \tag{3.17}$$

where ρ is the density of the fluid, c_p is the scalar capacity of the fluid, u_{τ} is the friction velocity and q_w is the rate of the scalar transfer from the wall to the flow which is defined by

$$q_w = -k \frac{d\langle \theta \rangle}{dy} \Big|_{y=0} , \qquad (3.18)$$

where k is the scalar conductivity and this equation is referred as the Fourier's law for the heat transfer problem or Fick's law for a mass transfer problem.

Analogously, very close to the wall, a conductive sub-layer exists for the scalar field as a viscous sub-layer for the velocity field which is governed by

$$\langle \theta \rangle^+ = Pr \ y^+ \ . \tag{3.19}$$

This linear relation is found to be valid for $Pr y^+ < 3$ (Cebeci & Bradshaw 1984).

One should always bear in mind that to obtain equations (3.16), it is assumed that the diffusion term $\frac{1}{RePr}\frac{\partial^2\langle\theta\rangle}{\partial x_i\partial x_i}$ in equation (3.3) is dominant in the inner region while turbulence convection is dominant in the outer region.

 $^{^{12}}$ Galilean invariance stats that the fundamental laws of physics are the same in all inertial frames.

However this might not be true since $\frac{1}{RePr} \frac{\partial^2 \langle \theta \rangle}{\partial x_i \partial x_i}$ can vary tremendously with the molecular Prandtl number which depends on the particular fluid. Prandtl numbers for viscous fluids like oils can easily exceed 100, while those for liquid metals can be as low as 0.001. By choosing a different Prandtl number, the situation may be reversed. For the present study, it is restricted to $Pr = \mathcal{O}(1)$. The use of the Φ_{θ} in equation (3.16) which is a function of y^+ and Pr is a way of compensating for this effect (Kays & Crawford 1993).

3.3.2. Fragility of the log-law for scalar field

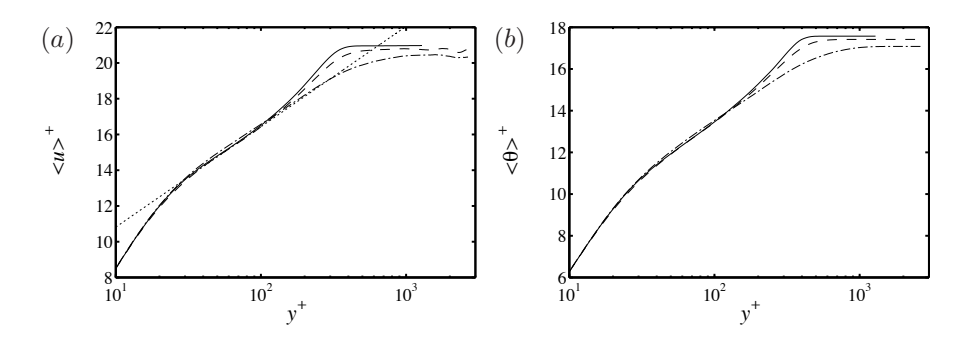


FIGURE 3.3. Mean velocity and temperature fields with FST at $Re_{\theta} \approx 850$. (a) $\langle u \rangle$, (b) $\langle \theta \rangle$ with Pr = 0.71. —no FST, --Tu = 4.7% at the inlet, --Tu = 40% at the inlet, log-law. A detailed discussion of the figure is found in Paper 4.

Due to the analogy to the velocity field, the law of the wall for the scalar field is supposed to have the same range of validity as for the law of the wall for the flow field under complex situations (Bradshaw and Huang 1995), e.g. in the presence of pressure gradient, or free-stream turbulence.

The influence of the free-stream turbulence on the mean flow is shown in Figure 3.3. It is clearly shown that the profiles below the logarithmic region are insensitive to the FST for both velocity and scalar fields whereas in the wake region significant depression of the boundary-layer wake starts appearing with increasing free stream intensity Tu. Especially for the highest intensity case of locally Tu = 7%, the wake region even vanishes for both fields. Consistent results are reported by the previous experimental work (Blair 1983a,b). The reason for the depressing wake region is due to that with increasing intensity of FST, the outer region becomes less and less intermittent, i.e. the outer region is more and more similar to the internal flows. However, the results from an LES simulation by Péneau et al. (2000) show that the slope of the logarithmic region varies significantly with Tu for the temperature profile but not for the velocity, which is similar to what was observed by Maciejewski & Moffat (1992a,b) in which they showed that the law-of-the-wall for the scalar field is also fragile in

the presence of anisotropic free-stream turbulence. Apart from the influence of the free-stream turbulence, the law-of-the-wall for the scalar field also fails in the presence of pressure gradient, e.g. see discussions in Bradshaw and Huang (1995). It is observed that different pressure gradient gave rise to different slope in the log region for the temperature profile but not for the velocity profile. Moreover, the sensitivity of the scalar profile to the pressure gradient is difficult to understand since the the governing equation of the scalar transport does not even have the pressure term (Bradshaw and Huang 1995).

3.4. Turbulence intensities

The intensity of the turbulent fluctuations is usually quantified via its root-mean-square (RMS) value. Most experiments only measure the streamwise component due to the fact that to measure the other two component requires two hot wires either in X-shape or V-shape. Very close to the wall, reliable measurements becomes extremely difficult and it is also very difficult to construct small X-shape or V-shape probes.

3.4.1. Turbulence intensities for velocity field

From the law of the wall, the turbulence intensities should have a constant value within the overlap region. However, experimental results from zero-pressure gradient turbulent boundary layer show that the streamwise intensity actually decreases in the log region. Furthermore, early experiments of a zero-pressure gradient boundary layer by Purtell et al. (1981) suggest that the Reynolds number effects penetrate much deeper into the boundary layer for the streamwise turbulent intensity than that for the mean velocity profile. A systematic decrease of the turbulence intensity is observed with decreasing Reynolds number and the authors attribute this to the stronger suppression of all but the largest scales in the turbulence at lower Reynolds number. Later the DNS by Spalart (1988) in a turbulent boundary layer confirmed the same trend in the streamwise component and spanwise component but not in the wall-normal and shear component. In channel flows, similar observations are also reported, see e.g. Jiménez & Hoyas (2008).

Even though, increasing peak value of u_{rms} in channel and boundary layers with increasing Reynolds number is shown convincingly in simulations, see e.g. Jiménez & Hoyas (2008); Schlatter & Örlü (2010) and experiments by De Graaff & Eaton (2000); Marusic & Kunkel (2003), surveys of experiments by Mochizuki & Nieuwstadt (1996); Fernholz & Finley (1996) based on earlier studies concluded that there was a weak/no Reynolds number dependence on the peak value of u_{rms} , and this is related to the insufficient spatial resolution of the measuring probe. Though the spatial averaging of the sensor probe is well-known, see e.g. Johansson & Alfredsson (1983); Ligrani & Bradshaw (1987), it is either ignored or is thought that the effects are limited. Until recently, Hutchins et al. (2009) showed explicitly that the near-wall peak of the streamwise velocity fluctuation is directly coupled to the effects of the spatial

resolution of the hot-wire. Later, Örlü & Alfredsson (2011) extend the work by Hutchins $et\ al.\ (2009)$ to the mean and higher-order moments. DNS/LES data can be used to "simulate" such instrumental errors by averaging in the spanwise direction, i.e. only consider scales which are larger than the sensor length, and the results are shown in Figure 3.4. It is clearly seen that with more spanwise averaging which is equivalent to a larger hot-wire resolution L^+ , the peak of u_{rms} decreases. Considering scales larger than 40 plus units, one can already observe a significant difference, while averaging scales smaller than 250 plus units, the outer peak becomes more dominant than the inner one (Hutchins $et\ al.\ 2009$). Recently, a method to evaluate the streamwise turbulence intensity was proposed by Segalini $et\ al.\ (2011)$. The new method is based on combining the measurements from two sensors with different wire lengths and a compensation scheme for probe resolution effects. Results showed that very good agreement with DNS data can be obtained (Segalini $et\ al.\ 2011$).

Once fully understanding the effects from the probe, the increasing peak value of the turbulence intensity can only come from the Reynolds number effects, indicating a growing outer-region influence on the near-wall motions. One possible explanation for the increasing of the peak value of u_{rms} with Reynolds number is that the motion near the solid wall though mainly influenced by eddies near the wall, but also affected by eddies from the outer part of the flow whose length scales are on the order of the boundary layer thickness or channel height. Such influences from the outer part of the flow are from pressure fluctuation which is the most obvious quantity which interact between the inner and outer regions (Townsend 1976; Bradshaw 1967). Equivalently, the so-called "splatting" mechanism also provides an explanation. When the large eddies move towards the solid surface from the outer region of the boundary layer, the wall-normal component is gradually reduced due to the "impermeability" condition at the wall. Especially close the wall, almost all the energy is transferred from the wall-normal component to the horizontal (streamwise and spanwise) components by pressure fluctuations. This phenomenon was observed by Daly & Harlow (1970) and later termed by Moin & Kim (1982) as the splatting or impingement effects¹³. The splatting effect is an important property of the flow in the vicinity of the wall and should be taken into account in the modelling of the near wall turbulence (Moin & Kim 1982). Since the influences come from the motions in the outer region where the length scales are much longer compared to those near the wall, the increase of the peak value of u_{rms} is mainly due to the large-wavelength components. This is confirmed in a recent study by Marusic et al. (2010a) where u_{rms} profile is filtered using certain spatial filter to separate large and small scales. It is shown that the increase of Reynolds number only influences the profile with large length scales while those with smaller length scales are essentially unchanged. However, inconsistent results for the behaviour of peak value of u_{rms} with Reynolds

 $^{^{13}}$ Some authors argue that the term is first introduced into literature by Wood (1980).

number are reported in pipe flow experiments by Hultmark et al. (2010) where no increase of the inner peak of u_{rms} with increasing Reynolds number is shown.

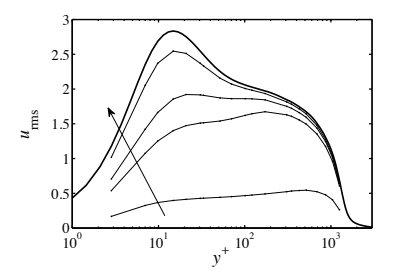


FIGURE 3.4. Dependence of resolved $u_{\rm rms}$ fluctuations on the range of spanwise scales included at $Re_{\theta}=4307$. — $u_{\rm rms}$ with full LES resolution $\Delta z^+=10.8$, — in direction of arrow: scales $\geq 2000^+$, $\geq 250^+$, $\geq 100^+$, $\geq 40^+$. A detailed discussion of the figure is found in Paper 7.

3.4.2. Turbulence intensities for scalar field

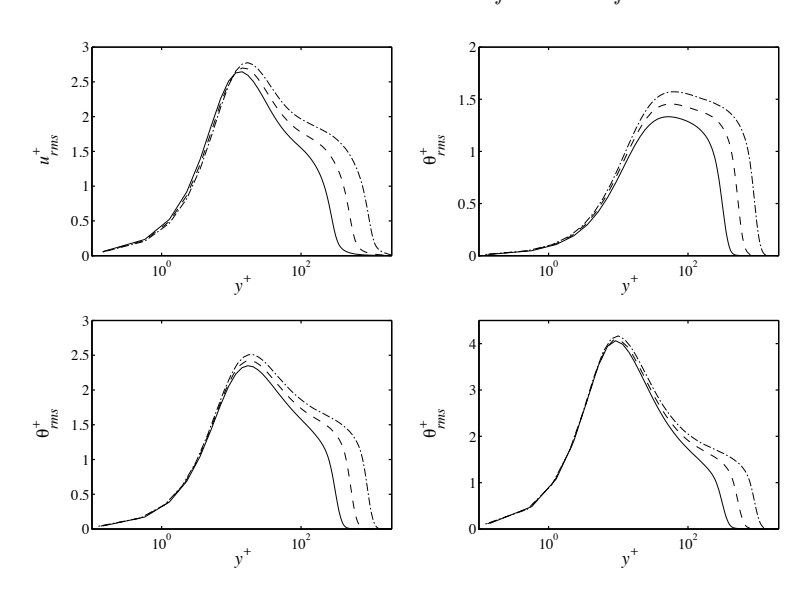


FIGURE 3.5. (a) u_{rms} , (b) θ_{rms} , Pr = 0.2, (c) θ_{rms} , Pr = 0.71, (d) θ_{rms} , Pr = 2.0. $Re_{\theta} = 670$, $--Re_{\theta} = 1410$, $--Re_{\theta} = 2526$. A detailed discussion of the figure is found in Paper 2.

In Figure 3.5, the RMS of scalars and streamwise velocity fluctuations are shown at three different Reynolds number $Re_{\theta}=800,1410,2526$. As expected,

the peak value of the intensity of the scalar fluctuation also increases with Reynolds number for Prandtl number being 0.71. However, large differences are observed when compared among the cases with different Prandtl numbers, i.e. Pr = 0.2 and Pr = 2.0. With increasing Pr, the RMS values increase and the peak positions move towards the wall. For the highest Prandtl number case (Pr = 2.0), the increase of the near-wall peak value is barely observable while for the lowest Prandtl number case (Pr = 0.2), a substantial increase is observed. Only the case with Pr = 0.71 has a similar behaviour as that of the streamwise velocity as shown in Figure 3.5 (a). These results indicate that for the lower Prandtl number case (Pr = 0.2), the structures in the outer region are somewhat much stronger (similar to what is observed in the high Reynolds number flow case) while the opposite for the higher Prandtl number case which leads to much weaker increase of the peak value. Furthermore, these results indirectly confirmed what is observed by Marusic et al. (2010a) that the increase of the near wall peak is due to the structures in the outer region. The Prandtl number effects on the scalar variance are surprising considering that 0.2 and 2.0 are both $\mathcal{O}(1)$.

In addition, the influences of different wall-boundary conditions, i.e. isoscalar and isoflux boundary conditions, are shown in Figure 3.6. Due to isoflux wall boundary condition, the RMS values remain constant near the wall while the ones with isoscalar wall boundary condition decrease to zero. Away from the wall, say $y^+ > 200$ or so, the influences from different boundary condition are negligible, which is consistent with the previous study by Kong et al. (2000).

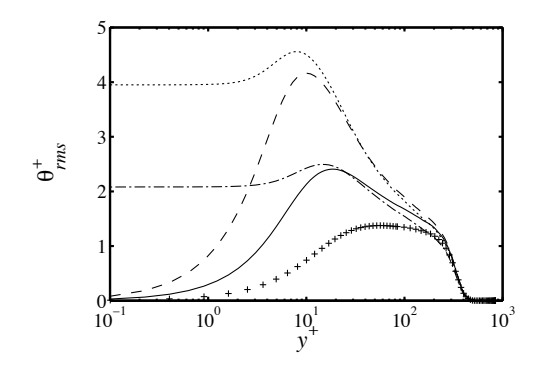


FIGURE 3.6. Profiles of the RMS values of the scalar fluctuation θ_{rms} at $Re_{\theta}=830.+\theta_{1}$ with Pr=0.2, —— θ_{2} with Pr=0.71, —— θ_{3} with Pr=0.71, —— θ_{4} with Pr=2.0, …… θ_{5} with Pr=2.0. Isoscalar wall: θ_{1} , θ_{2} and θ_{4} . Isoflux wall: θ_{3} and θ_{5} . A detailed discussion of the figure is found in Paper 1.

3.5. High-order statistics

The high-order moments of a quantity also contains important statistical information. Usually the skewness and flatness (kurtosis) factor of a statistically stationary variable a(x, y, z, t) are defined as

$$S(a) = \frac{\langle a'^3 \rangle}{\langle a'^2 \rangle^{\frac{3}{2}}} \tag{3.20}$$

and

$$F(a) = \frac{\langle a'^4 \rangle}{\langle a'^2 \rangle^2} \ . \tag{3.21}$$

where a(x,y,z,t) could be any quantity, such as velocity components, pressure, scalar concentration or their temporal/spatial derivative etc. For a quantity which has a Gaussian distribution, the skewness and flatness are 0 and 3, respectively. Departure from zero of the skewness indicates asymmetry of the fluctuations. Flatness factor larger than 3 is associated with a peaky signal with long tails which indicates rare events far away from the mean.

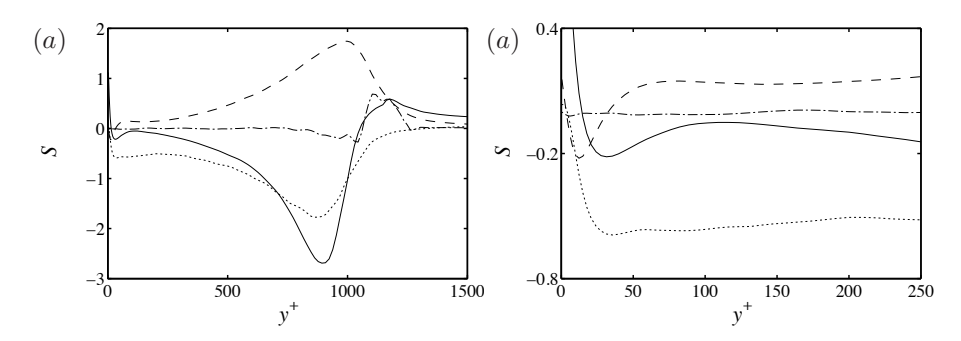


FIGURE 3.7. Skewness factor distributions of the velocity and pressure at $Re_{\theta} = 2500$. ——Streamwise velocity, ——Wallnormal velocity, ——Spanwise velocity, ——Pressure. (a) Skewness factor, (b) Zoom. The 99% boundary-layer thickness at $Re_{\theta} = 2500$ is about $y^+ \approx 840$. A detailed discussion of the figure is found in Paper 2.

3.5.1. High-order statistics for velocity field

The distribution of velocity components¹⁴ are shown in Figures 3.7 and 3.8. High values of both skewness and flatness near the wall¹⁵ and in the wake region indicate the intermittent nature in these regions, see e.g. Österlund &

 $^{^{14}}$ In channel flow, the spanwise component of the skewness should be zero since it reflects the geometrical symmetry of the solutions to NS equations, and usually used as an indication for convergence of the statistics (Kim *et al.* 1987).

¹⁵The large values of high-order statistics close to the wall should be accepted with some reservation, since both the denominator and the numerator of the skewness and flatness

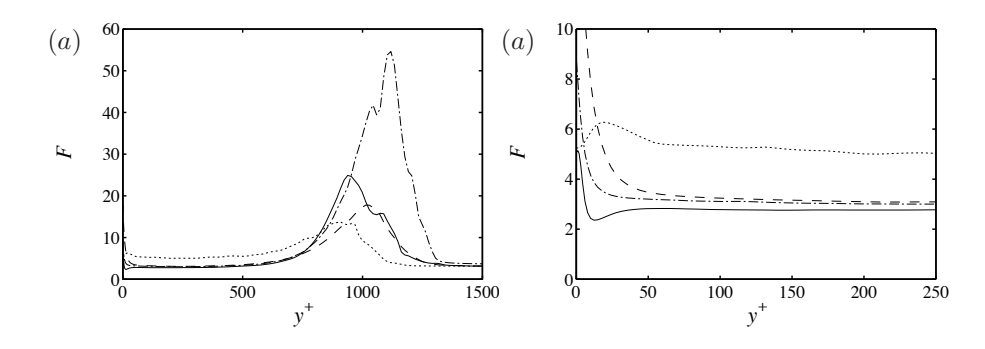


FIGURE 3.8. Flatness factor distributions of the velocity and pressure at $Re_{\theta} = 2500$. ——Streamwise velocity, ——Wallnormal velocity, ——Spanwise velocity, ——Pressure. (a) Flatness factor, (b) Zoom. The 99% boundary-layer thickness at $Re_{\theta} = 2500$ is about $y^+ \approx 840$. A detailed discussion of the figure is found in Paper 2.

Johansson (1999); Li et al. (2009). The Reynolds number effects are also strong in these regions, i.e. differences are noticeable in the viscous/buffer layer and much stronger in the outer region (Gad-el Hak and Bandyopadhyay 1994). High positive values of S_u in the viscous sublayer indicate that the region is dominated by positive fluctuations as a result of the sweep events which bring high-speed fluids from regions away from the wall. Further away from the wall as in the log region, the skewness factor remains only slightly different from a Gaussian distribution. In the outer region, the skewness is negative which is consistent with the arrival of the low-speed fluid coming from the near wall region by the ejection event (Gad-el Hak and Bandyopadhyay 1994). To be consistent with the streamwise component (since quadrant analysis shows that u' and v' are anti-correlated), the skewness of the wall-normal component is expected to be negative near the wall and positive in the outer region with nearly Gaussian distribution in the log region, and results show that this is indeed the case.

Earlier experiments of boundary layer flows by Andreopoulos et al. (1984) showed that for low Reynolds number (i.e. $Re_{\theta} = 3624$), the S_u changes the sign at about $y^+ \approx 15$ where the streamwise fluctuations peaks locate. At the same position, F_u reaches a minimum and S_v obtains its maximum positive value. As the Reynolds number increase, those positions continue to move towards the outer part of the flow, e.g. the S_u changes the sign at about $y^+ \approx 150$ when $Re_{\theta} = 15406$, and there seems no sign of reaching an asymptote which is an indication of the progressive spreading viscous effects to the outer part of the boundary layer (Gad-el Hak and Bandyopadhyay 1994).

factors become zero as the wall is approached, and any inaccuracy in its measurement (or computation) could be excessively amplified (Kim et al. 1987).

3.5.2. High-order statistics for scalar field

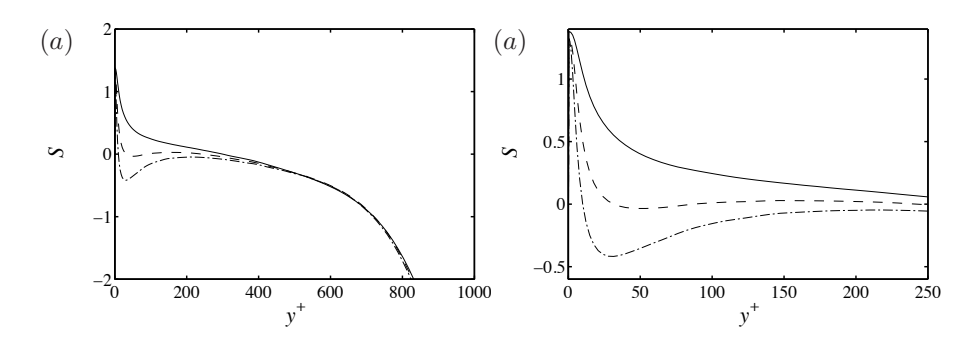


FIGURE 3.9. Skewness factor distributions of the scalar with isoscalar wall-boundary condition at $Re_{\theta}=2500$. — Pr=0.2, ——Pr=0.71, ——Pr=2.0. (a) Skewness factor, (b) Zoom. The 99% boundary-layer thickness at $Re_{\theta}=2500$ is about $y^+\approx 840$. A detailed discussion of the figure is found in Paper 2.

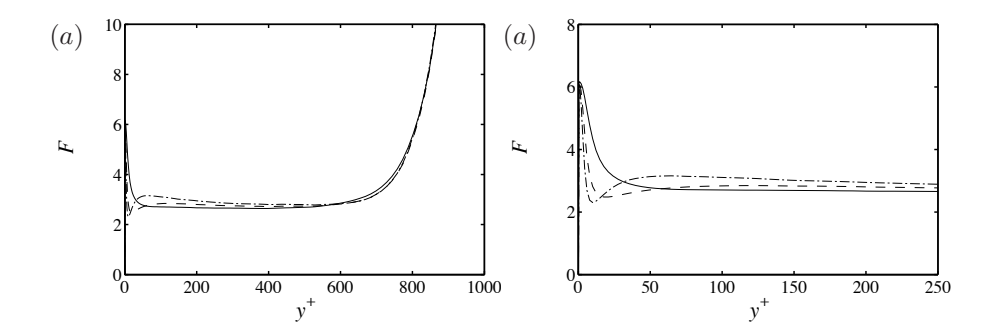


FIGURE 3.10. Flatness factor distributions of the scalar with isoscalar wall-boundary condition at $Re_{\theta} = 2500$. — Pr = 0.2, ——Pr = 0.71, ——Pr = 2.0. (a) Flatness factor, (b) Zoom. The 99% boundary-layer thickness at $Re_{\theta} = 2500$ is about $y^+ \approx 840$. A detailed discussion of the figure is found in Paper 2.

The distributions of the high-order statistics pertaining to the scalar fields as shown in Figures 3.9 and 3.10 look qualitatively the same as for the streamwise velocity. Within the sub-layer, $S(\theta)$ are positive which is consistent with the positive values of S(u) and see also previous experimental study by Antonia and Danh (1977). At $y^+ \approx 30$, $S(\theta)$ with Pr = 0.71 changes the sign. This wall-normal position is about twice as large as the one for the streamwise velocity and it becomes larger as Pr decreases. The wall-normal positions where

the minimum of F_{θ} are also different among the different Pr cases. The lower Prandtl number case has a profile similar to the profile of streamwise velocity component at much high Reynolds number, e.g. S_{θ} with Pr=0.2 changes the sign at a position about $y^+\approx 300$. These behaviours in the low Prandtl number case are thought to be due to the structural changes in the outer region. In addition, the maximum peak values of $S(\theta)$ and $F(\theta)$ near the boundary layer edge are much higher than those of the S(u) and F(u) which is also observed in previous experiments by Antonia and Danh (1977). Moreover, the wall values of both the $S(\theta)$ and $F(\theta)$ for the isoscalar boundary condition seem to be Prandtl number independent.

3.5.3. Influence of FST on high-order statistics

The influence of the free-stream turbulence on the high-order statistics is shown in Figure 3.11. With FST being present, the structures near the boundary layer edge are changed. The high peak near the boundary layer edge becomes less and less prominent indicating increased turbulent mixing of the free-stream and the flows inside the boundary layer. This loss of intermittency leads to the depression and vanishing of the wake region, see also the mean profiles as shown in Figures 3.3. The less prominent peak values of the high order statistics with increasing free-stream intensities are also observed in a recent experimental study by Sharp et al. (2009). However, for the high FST cases, the skewness factor becomes even positive as reported by Sharp et al. (2009) while for the present case it is still negative within the boundary layer.

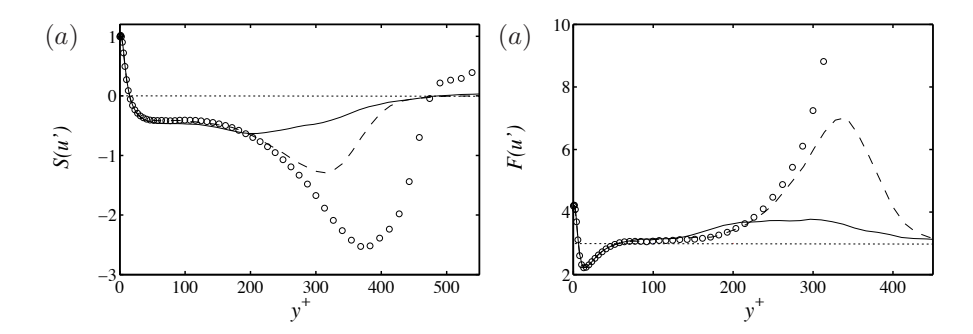


FIGURE 3.11. Skewness and flatness-factor distributions of the streamwise velocity at $Re_{\tau}=250$. ——Present LES results with inlet Tu=20% and L=5, ——Present LES results with inlet Tu=4.7% and L=5, o No FST case. (a) Skewness factor S(u'), (b) Flatness factor F(u'). The 99% boundary-layer thickness of the present data for the no FST case is about $y^+\approx 350$ at $Re_{\tau}=250$. A detailed discussion of the figure is found in Paper 4.

3.6. Coherent structures

Apart from the scaling of mean and fluctuating quantities, a lot of research efforts are put into the study of the turbulent structures. Even though wallbounded turbulence is characterised by chaotic and irregular motions, there are actually recurrent and well-organised features, i.e. coherent structures (coherent motions) present in the flow. In addition, it is believed that these structures are the building blocks for the turbulent field, and an understanding of these structures is of fundamental importance to improve our knowledge of the boundary-layer dynamics (Robinson 1991). Unfortunately, there is no consensus reached by the community on the exact definition of coherent structure. In general, coherent structure can be regarded as organised motions which are persistent in both space and time, and more important contribute to the transport of heat, mass and momentum significantly. The current view on the turbulent structures consists three principal element structures, namely the near-wall streaks (Kline et al. 1967), hairpin/horseshoe vortices (Theodorsen 1952) and large-scale motions (LSM) (Kim & Adrian 1999; del Álamo & Jiménez 2003; Abe et al. 2004; Hutchins & Marusic 2007; Schlatter et al. 2009).

It is very difficult to measure the organised motion partially due to that it is difficult to isolate them and subsequently average. Therefore, flow visualisation is usually used thanks to the advances in electronical and optical instrumentations and computer hardwares. There is no doubt that visualisation can play a vital role in improving our understanding of the complicated turbulent motions. However, sometimes the turbulent phenomena is too complex and even a flow visualisation does not translate immediately into "understanding" (Leal 2007). Furthermore, care has to be taken when using passive scalars (e.g. smoke or dye) for flow visualisation since the structures can be different in the scalar field and flow field due to missing pressure influences in the scalar field, see e.g. Guezennec et al. (1990); Bradshaw and Huang (1995). Nevertheless, visualisation using passive tracers has been extensively used for identifying new flow structures, improving our physical understanding and even become a new branch of research.

3.6.1. Near-wall streaks

The most widely studied structures in wall-bounded flow are the so-called near-wall streaks which are alternating high- (positive fluctuation) and low-speed (negative fluctuation) regions elongated in the streamwise direction. The importance of near-wall streaks was identified by Kline et al. (1967) who showed streaky structures near the wall in a water channel using tiny hydrogen bubbles released periodically from a thin platinum wire. These streaky structures have a spanwise spacing of about $\Delta z^+ \approx 100$, and a streamwise spacing $\Delta x^+ \approx 1000$ (Smith & Metzler 1983). However, recent simulations (Li et al. 2009; Schlatter et al. 2009) and experiments (Lin et al. 2008) reported a value around 120 for the spanwise spacing of the streaks. To further consider the spanwise organisation of the structures near the wall, one can calculate the spanwise two-point

correlations, see e.g. early studies by Deardorff (1970); Moin & Kim (1982). The spanwise two-point correlation coefficient of a statistically stationary variable a(x, y, z, t) is defined by

$$R_{aa}(x, y, \Delta z) = \frac{\langle a'(x, y, z, t)a'(x, y, z + \Delta z, t)\rangle}{\langle a'(x, y, z, t)^2\rangle}, \qquad (3.22)$$

where Δz is the spanwise separation. The spanwise two-point correlations for the three velocity components and pressure at $y^+ = 4.9$ are plotted in Figure 3.12. For each of the velocity correlations, a minimum is observed. The streamwise correlation R_{uu} becomes negative and reaches a minimum at $\Delta z^+ \approx 60$. The separation at which the minimum occurs is an estimate of the distance between a high speed streak and a low speed streak, so the mean spacing of streaks should be roughly twice this distance. The negative excursion attains its minimum at the wall-normal position where the u_{rms} has a maximum, i.e. $y^+ \approx 15$. The presence of the minimum of R_{vv} at $\Delta z^+ \approx 25$ is consistent with the numerical results by Kim et al. (1987) in turbulent channel. This separation is a measure of the mean diameter of the streamwise vortices in the near wall region. The minimum of R_{ww} appears at $\Delta z^+ \approx 60$ and indicates the existence of the counter-rotating vortex pairs. According to Moser & Moin (1984), the minimum of R_{ww} does not exist for $y^+ > 30$ and is more likely due to the splatting effect which can be caused by a single vortex. One thing to notice is that the spanwise two-point correlation coefficient of the pressure does not have the negative excursion which is also observed previously by Kim (1989). This indicates that the pressure fluctuation is a global quantity which correlate at even infinite separations. With increasing Reynolds number, the first minimum of R_{uu} , and R_{ww} weakens and gradually diminishing and meanwhile a second minimum starts to appear at large separation, i.e. $\Delta z = \mathcal{O}(\delta_{99})$ (Österlund 1999; Schlatter et al. 2010). On the contrary, R_{vv} seems to be Reynolds number independent, which is consistent with the previous results that the v fluctuations are essentially an inviscid phenomenon (Sreenivasan 1989). Note that the less pronounced first minimum does not indicate the absence of the near-wall streaks. It is due to the fact that at high Reynolds number, the contributions from the large-scale motions in the outer region have concealed the contributions from the streaks (Gupta et al. 1971; Österlund 1999; Abe et al. 2004), i.e. the small scales streaky structures are modulated by the larger outer structures (Mathis et al. 2009; Schlatter and Örlü 2010; Bernardini and Pirozzoli 2011). To recover the minimum at high Reynolds number, Österlund (1999) applied a high-pass filter to the signals before calculating the correlation coefficient. The cut-off wavelength was chosen to be the 99% boundary layer thickness such that structures which have a wavelength larger than the boundary layer thickness are damped. This filtering procedure produces a distribution of the correlation coefficient similar to those at low Reynolds numbers.

Similarly, the streaky structure also exist for scalar fields with the case of Pr = 0.71 being almost identical to the velocity structures, similar behaviours are also observed previously by Kim and Moin (1989); Bell and Ferziger (1993);

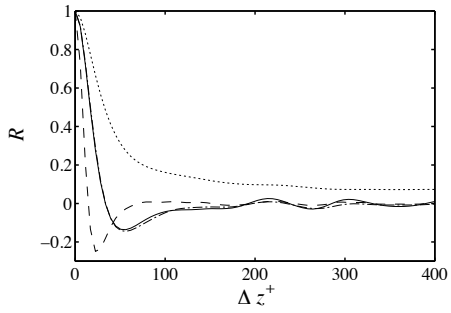


FIGURE 3.12. Spanwise two-point correlation coefficients of the velocity and pressure fluctuations at $y^+ = 4.9$ with $Re_{\theta} = 830$. R_{uu} , $--R_{vv}$, $--R_{ww}$, $--R_{vv}$, R_{pp} .

Kong et al. (2000). Kim and Moin (1989) reported that the correlation coefficient between the streamwise velocity and the scalar of Pr = 0.71 and 2.0 is as high as 0.95 in the wall region. Due to this high correlation, the spanwise spacing of the scalar streaks is also about 120 in wall units. The spanwise two-point correlations of the different scalars at $y^+ = 10$ are shown in Figure 3.13. It is seen that almost no difference exists between $R_{\theta\theta}$, Pr = 0.71and $R_{\theta\theta}$, Pr = 2.0 with isoscalar wall boundary condition. However, an obvious deviation of $R_{\theta\theta}$ at low Pr = 0.2 is found, see also similar behaviours in turbulent channel simulation by Kim and Moin (1989). It is noted that the distribution of $R_{\theta\theta}$, Pr = 0.2 is similar to R_{uu} at a much higher Reynolds number which is due to a dominance of outer-layer structures. On the contrary, the scalars of the isoflux boundary condition seem to be much more affected by the Prandtl number and have larger spanwise spacings than those of the isoscalar boundary condition. As expected, with increasing Reynolds number, the first minimum will become less prominent due to a larger-scale modulation as for the streamwise velocity component.

The spanwise streak spacing for both velocity and scalar fields varying with Reynolds numbers is shown in Figure 3.14. Apart from the general increase with increasing Reynolds number for all Prandtl number cases, the mean scalar streak spacings are larger for smaller Pr at the same Reynolds number.

The streaky structures are relatively quiescent most of the time. However, the low-speed fluid near the wall occasionally erupts violently into the outer region of the boundary layer (ejection motion). Kline et al. (1967) and Kim et al. (1971) were among the first to name this process as "bursting" which was later used by Wallace et al. (1972), Willmarth & Lu (1972) and Lu & Willmarth (1973) among others. During a bursting process, as described by Kim et al. (1971), the low-speed streaks were observed first to lift up slowly away from the wall, then start a growing oscillation and finally break up into more chaotic motion. The most probable wall-normal position is around $y^+ = 15$ where the turbulence intensity reaches maximum, see Figure 3.5 for more discussions.

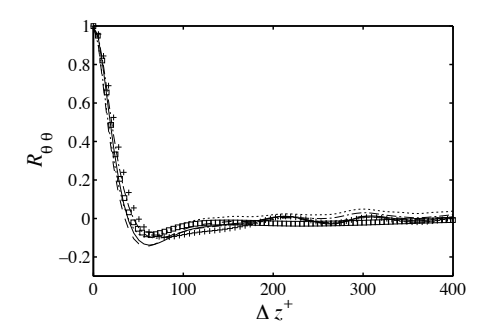


FIGURE 3.13. Spanwise two-point correlation coefficients of the scalar fluctuations at $y^+ = 9.8$ with $Re_{\theta} = 830$. $R_{\theta_1\theta_1}$, $--R_{\theta_2\theta_2}$, $+R_{\theta_3\theta_3}$, $--R_{\theta_4\theta_4}$, $--R_{\theta_5\theta_5}$. θ_1 with Pr = 0.2, θ_2 with Pr = 0.71, θ_3 with Pr = 0.71, θ_4 with Pr = 2.0, θ_5 with Pr = 2.0. Isoscalar wall: θ_1 , θ_2 and θ_4 . Isoflux wall: θ_3 and θ_5 .

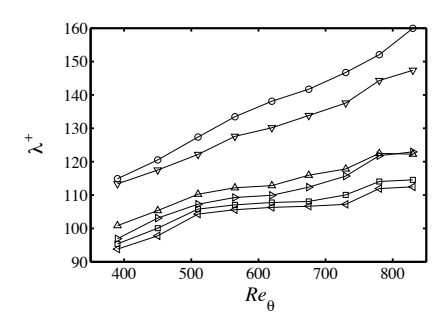


FIGURE 3.14. Streamwise variation of the mean spanwise streaks spacing at $y^+ \approx 7$. $\Box u$, $\circ \theta_1$, $\triangle \theta_2$, $\nabla \theta_3$, $\lhd \theta_4$, $\rhd \theta_5$. A detailed discussion of the figure is found in Paper 1.

Intermittently, the high-speed fluid also rushes in toward the wall at a shallow angle (sweep motion). Together with the ejection motion, these two events contribute to most of the production of the turbulence and are considered to be a self-sustained and quasi-cyclic sequence (Robinson 1991). Blackwelder & Kovasznay (1972) confirmed other observations that the disturbances associated with the bursting process extends to across the boundary layer.

Note that the position where the streaks break down $(y^+ \approx 15)$ is also the same position where the skewness factor of streamwise velocity changes the sign for low Reynolds number. As noted by Andreopoulos et al. (1984), this position continues to extend to the outer region of the boundary layer with increasing Reynolds number which indicates that changes in the velocity structure of the flow are likely to occur. However, there is no evidence deduced from the data

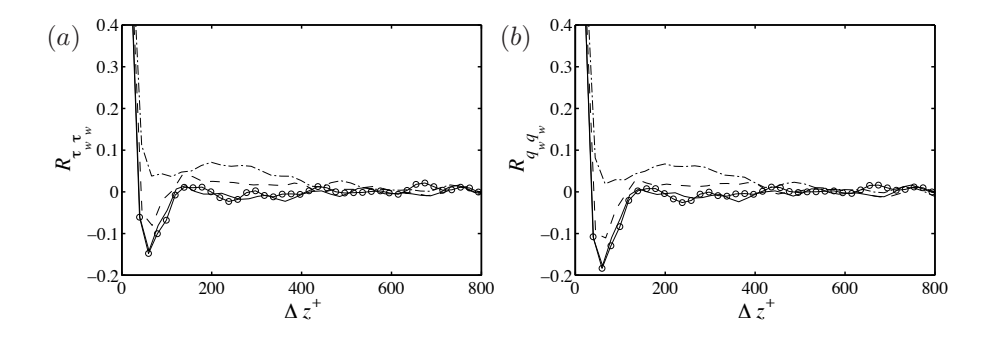


FIGURE 3.15. Spanwise two-point correlation of the wall shear stress $R_{\tau_w\tau_w}$ and the wall heat flux $R_{q_wq_w}$ at $Re_{\tau}=300.$ $-\circ-$ No FST Case, — L=2.5, — -Tu=40% at inlet, L=7.5, — -Tu=40% at inlet, L=15. (a) $R_{\tau_w\tau_w}$, (b) $R_{q_wq_w}$. A detailed discussion of the figure is found in Paper 4.

that the intermittent coherent flow structures, i.e. the near-wall streaks, have disappeared. According to Kline (1967), the skewness factor is associated with width of the streaks. By examining the results from DNS by Li *et al.* (2009) as shown in Figure 3.14, there is a trend for the spanwise spacing of the near-wall streaks to grow with increasing Reynolds number.

For the case with FST, the spanwise two-point correlation coefficient is "elevated" and this leads to the local positive maximum as shown in Figure 3.15. These plots are very similar to the ones presented by Schlatter $et\ al.$ (2009a) for a boundary layer with much higher Reynolds number, suggesting that the outer part of the boundary layer is changed due to the free stream turbulence.

3.6.2. Large-scale motions (LSM)

Besides the near-wall streaks, there are also structures existing in the outer region of the boundary layer (Kim & Adrian 1999; del Álamo & Jiménez 2003; Abe et al. 2004; Hutchins & Marusic 2007; Schlatter et al. 2009). These structures are related to the "inactive" motion by Townsend (1976) and usually scale with outer units, e.g. the channel height h or the boundary-layer thickness δ_{99} .

The spanwise premultiplied energy spectra pertaining to both velocity and scalar field is shown in Figure 3.16. A two-peak structure is usually observed assuming high enough Reynolds number, see Figure 3.16 (a) for the spectrum of streamwise velocity. These two peaks are associated with the near-wall streaks and the outer layer structures, respectively. The inner peak is consistently located at a wall-normal position about $y^+\approx 15$ which is also consistent with the channel flow simulation by del Álamo & Jiménez (2003), while the outer peak scales in outer units and locates at $y\approx 0.4\delta_{99}$ (Schlatter et al. 2010). Again as expected, the case for Pr=0.71 is similar to the spectrum of the

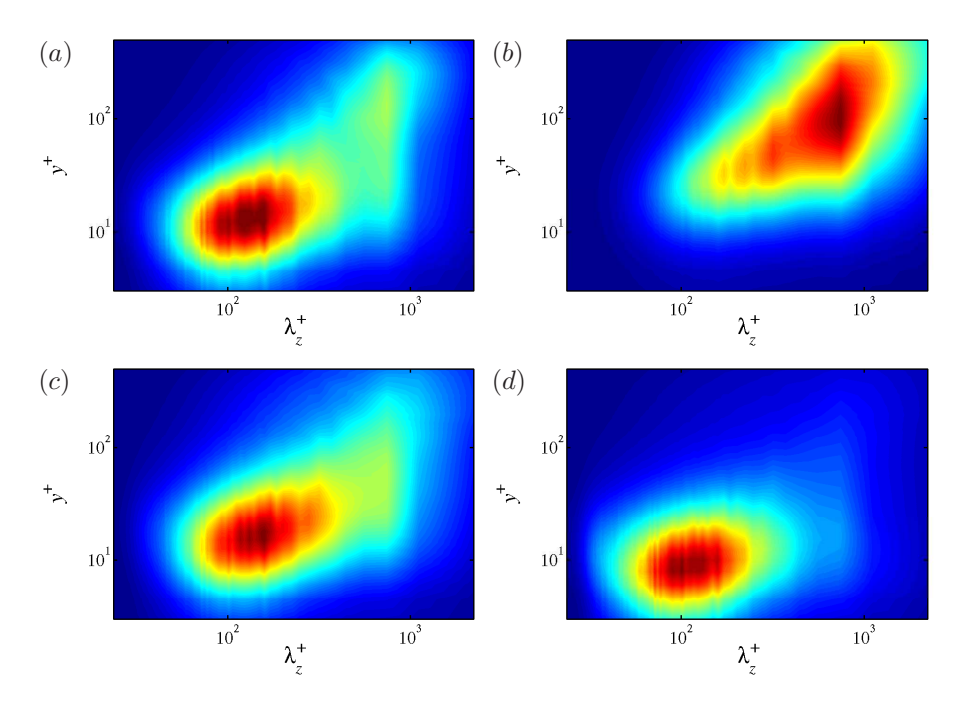


FIGURE 3.16. One-dimensional premultiplied spanwise spectra of the $k_z \Phi_{uu}(\lambda_z)/u_\tau^2$ and $k_z \Phi_{\theta\theta}(\lambda_z)/\theta_\tau^2$ at $Re_\theta = 2500$. (a) Spectrum of u; Spectrum of θ : (b) Pr = 0.2; (c) Pr = 0.71; (d) Pr = 2.0. A detailed discussion of the figure is found in Paper 3.

velocity. For case of Pr=0.2, a one-peak structure (only the outer peak) is observed indicating that the low Pr case is dominant by the larger scales in the outer region. On the other hand, the case for Pr=2.0 shows a two-peak structure, but with the outer peak being much weaker compared to the peak in the velocity spectrum at the same Reynolds number. It is expected that the outer peak will eventually vanish for certain high enough Prandtl number.

With the free-stream turbulence, the energy spectra and in particular the outer peaks are changed, see Figure 3.17. The inner peaks essentially are not changed while the wall-normal position of the outer peak moves from $\mathcal{O}(0.5\delta_{95})$ to $\mathcal{O}(\delta_{95})$. Meanwhile, the spanwise scale of the outer structures increase from $\mathcal{O}(1.2\delta_{95})$ to $\mathcal{O}(3.5\delta_{95})$ for a local turbulence intensity about 7%. The recent experimental study by Sharp *et al.* (2009) reported also such two-peak structures. Due to the difficulty to measure the spanwise scales in the experiments, they reported that the streamwise scale changes from $6\delta_{99}$ to $15\delta_{99}$ due to FST of about 10%.

Note that in experiments, VLSM or super-structures are identified, however many doubts are put on these giant structures. The first comes with problem

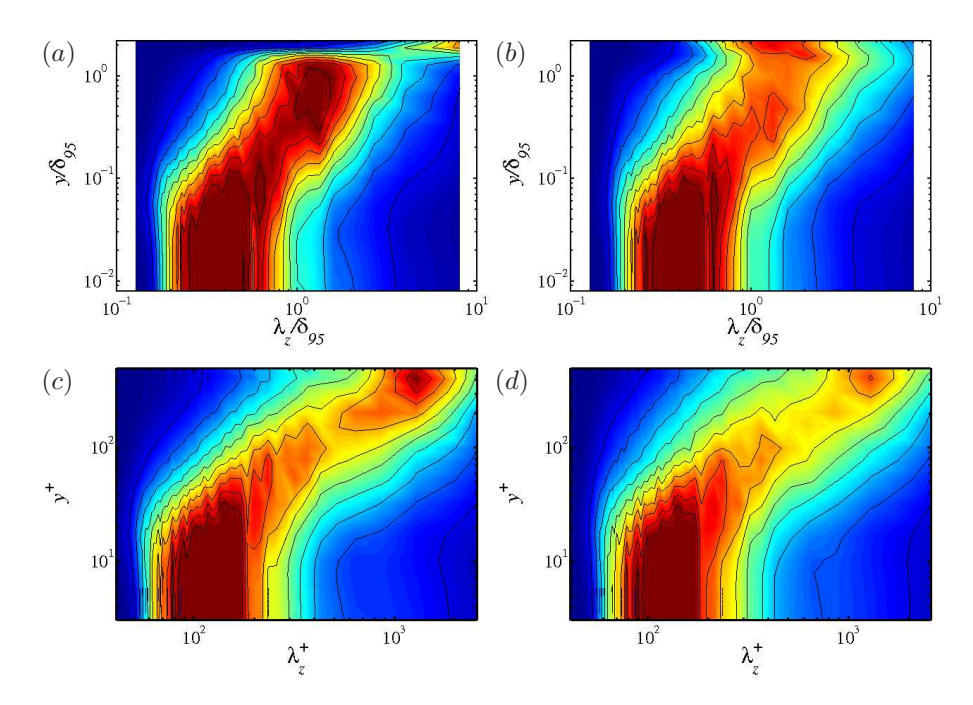


FIGURE 3.17. Premultiplied spanwise energy spectra of $\Phi_{uu}(\lambda_z)/u_{rms}^2$ and $\Phi_{\theta\theta}(\lambda_z)/\theta_{rms}^2$ with Pr=0.71 at $Re_{\theta}\approx 900$. (a) $\Phi_{uu}(\lambda_z)/u_{rms}^2$ with no FST at inlet, (b) $\Phi_{\theta\theta}(\lambda_z)/\theta_{rms}^2$ with no FST at inlet, (c) $\Phi_{uu}(\lambda_z)/u_{rms}^2$ with Tu=40% at inlet, (d) $\Phi_{\theta\theta}(\lambda_z)/\theta_{rms}^2$ with Tu=40% at inlet. A detailed discussion of the figure is found in Paper 4.

of the identification. At these length scales, e.g. low frequency fluctuations from the facility itself may have an important influence (Marusic $et\ al.\ 2010\ b$). Furthermore, the close lateral packing of structures might be interpreted as a single structure which leads to an overestimation of the length (Marusic $et\ al.\ 2010\ b$). Third, a considerable amount of data on VLSM is obtained from the temporal signals and to convert temporal spectra to streamwise ones, usually the Taylor's hypothesis is employed. However, the validity of Taylor's hypothesis remains an open question, and inappropriate usage will lead to inaccurate results, e.g. the recent challenges to the k_x^{-1} energy spectrum as pointed out in del Álamo and Jiménez (2009).

3.6.3. Hairpin vortices

Horseshoe/hairpin vortices were first polustrated by the aerodynamicist Theodorsen (1952), and they are commonly defined as an Ω -shaped vortical structure with two legs (streamwise vortices) connected via a raised spanwise-oriented head/arch. They reach up from the wall to transport fluid and produce

Reynolds shear stress. As the hairpin vortices are convected downstream, the legs elongate and become quasi-streamwise vortices which give birth to near-wall streaks. However, though being proposed as one of the primary structure of wall turbulence, the importance and even the presence of hairpin vortices have long been debated, see e.g. Cantwell (1981). Since the indirect evidence of the presence of hairpin vortices from a smoke visualisation by Head & Bandy-opadhyay (1981), a number of studies have postulated the existence of hairpin structures in turbulent shear flows, see e.g. Perry & Chong (1982); Adrian et al. (2000), however, no direct evidence of existence of hairpin vortices in fully turbulent flow has been shown.

Experimental technique is still not mature enough to provide the detailed information of the time evolution of the vortical structures, therefore DNS seems to be the ideal tool for this kind of study (Marusic et al. 2010b). By examining the DNS data of the turbulent boundary layer by Spalart (1988), Robinson (1991b) (after dividing the hairpin vortices into three parts: leg, neck and head) found that the majority of the hairpin vortices are only one-legged, and complete two-sided hairpin vortices are rarely observable in instantaneous realisations, similar observations are also made by Brooke & Hanratty (1993). Jeong et al. (1997) performed DNS simulation in turbulent channel flow and found there are no complete hairpin vortices in the ensemble-averaged structure. Additionally, in the study by Zhou et al. (1999), it is observed that the asymmetric hairpins, i.e. cane- or hook-like hairpin vortices with only one leg, are formed more readily in rapid succession and their streamwise separation is in better comparison with the experiments than the two-legged symmetric ones. However, recent DNS by Wu & Moin (2009) in a spatially developing turbulent boundary layer reported a predominance of hairpin vortices, but it can be argued that those hairpin vortices seen in the simulation by Wu & Moin (2009) are due to a post-transitional effects¹⁶. Further downstream where the flow is fully developed and far from the transitional region, no clear hairpin vortices are observable. However, some authors (Wu & Moin 2009; Gad-el Hak & Buschmann 2011) argue that the quasi-streamwise vortices 17 observed in the recent simulation by Schlatter & Örlü (2010) and earlier simulations e.g. Schoppa & Hussain (2002); Spalart (1988) are mainly due to the streamwise periodic boundary condition employed in those simulations which leads to the distortion of the vortical structures. However, this is most probably not true since in the simulation by Schlatter & Örlü (2010), the inflow is laminar, i.e. Blasius profile, and does not contain any vortical structures.

 $^{^{16}}$ The Reynolds number in the simulation reached by Wu & Moin (2009) is too low to be free from transitional effects, i.e. the flow is not fully turbulent. It is not surprising that one can observe a predominance of hairpin vortices. What is more surprising was how quickly this view was adopted by the research community as an example of a fully turbulent boundary layer.

 $^{^{17}\}mathrm{The}$ "one-legged freak" as named in Gad-el Hak & Buschmann (2011).

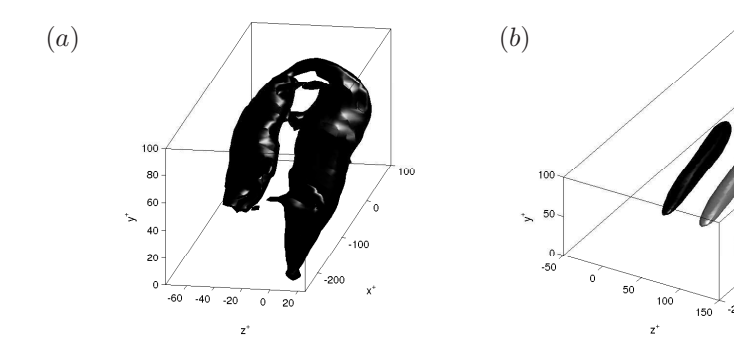


FIGURE 3.18. Averaged educed structure. (a) In the early transitional region ($Re_{\theta} \approx 200 \sim 300$) over 14 clear hairpin structures. Isocontour level of $\lambda_2^+ = -0.0035$, calculated based on shear stress at $Re_{\theta} = 650$. The total number of educed vortices in the same region is 189. (b) In the turbulent region at contour level $\lambda_2^+ = -0.003$. Black: turbulent boundary layer at $Re_{\theta} = 4200$, grey: turbulent boundary layer at $Re_{\theta} = 2500$, white: turbulent channel at $Re_{\tau} = 590$. A detailed discussion of the figure is found in Paper 9.

The educed averaged structure from the present data is shown in Figure 3.18. In the early transitional region as shown in Figure 3.18 (a), the averaged structure is a hairpin vortex which has a clear head, neck and two legs. Whereas in the fully turbulent region as shown in Figure 3.18 (b), the averaged structure is nothing but a quasi-streamwise vortex, i.e. no head neither neck, which is similar to that is found in turbulent channel flow (Jeong et al. 1997). In addition, Robinson (1991b) also concluded that streamwise vortices populate the inner region of the boundary layer and strong asymmetries are the rule, rather than the exception which dismissed the existence of hairpin vortices which feature a symmetric pattern. The eduction scheme used here for identifying streamwise vortices is similar to what is that used by Jeong et al. (1997) which is based on the λ_2 criterion Jeong & Hussain (1995)¹⁸.

3.6.4. Inner/outer interactions

Even though the near-wall cycle seems to be self-sustained, it is believed that the outer structures have at least a modulating influence on the near-wall events (Robinson 1991). This has been observed both in simulation and experiments, see e.g. Hutchins & Marusic (2007b); Schlatter et al. (2009). One such example is shown in Figure 3.19 (a) where the spanwise two-point correlation of the wall-shear stress τ_w is shown as a function of Reynolds number. Except for the

¹⁸Other methods for identify vortex are e.g. low-pressure region which coincides roughly with the vortex core (Robinson 1991b), Q criterion by Chong *et al.* (1990). It is thought that both λ_2 and Q criterion give qualitatively the same results.

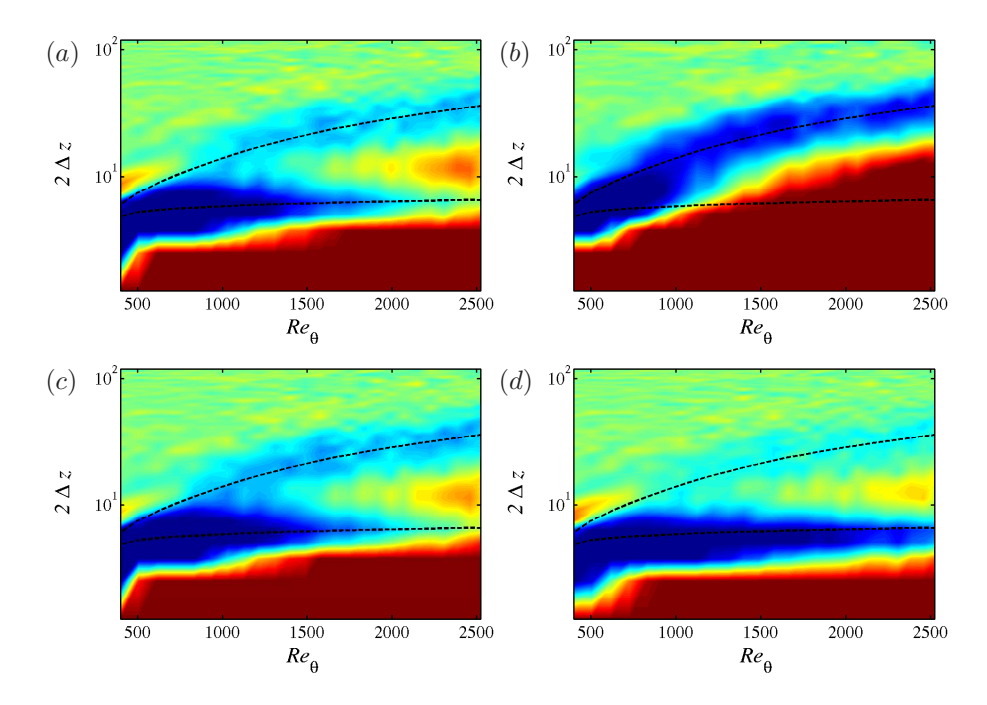


FIGURE 3.19. Spanwise two-point correlation of the wall scalar flux $R_{q_wq_w}$. (a) Pr=0.2; (b) Pr=2.0. Colour bar is [-0.6:0.6], --0.85 δ_{99} and 120 plus units. A detailed discussion of the figure is found in Paper 3.

near-wall peak at $2\Delta z^+ \approx 120$ (dash line) showing the existence of the streaks, a second peak (solid line) is clearly visible for $Re_{\theta} > 1500$ which indicates the footprints of the large-scale structure onto the fluctuating wall-shear stress. Compared to the distribution of the wall shear stress, the wall scalar flux with Pr = 0.71 is similar as expected. For the other two cases, i.e. Pr = 0.2 and 2.0, the distributions are clearly different from the wall-shear stress. For the lower Prandtl numbers, a much stronger outer peak, i.e. footprint of the dominant larger scales can be observed while the inner peak is completely missing. For the higher Pr case, the inner peak is dominant with outer peak barely visible. These results suggest that the inner and outer structures of the velocity/scalar field are not dependent on each other, i.e. they can self-sustain independently.

To further quantify the influence of the large scale energy-containing motions on the small scales, i.e. amplitude modulation, Mathis et al. (2009) employed the Hilbert transformation to small-scale fluctuating velocity signals after filtering in spectral space. It is conjectured that a nonlinear amplitude modulation indeed takes place of the small scale by the large scales motions in the log region. Though the natural approach would be to use a two-point correlation coefficient for studying the modulation influence, however, due to

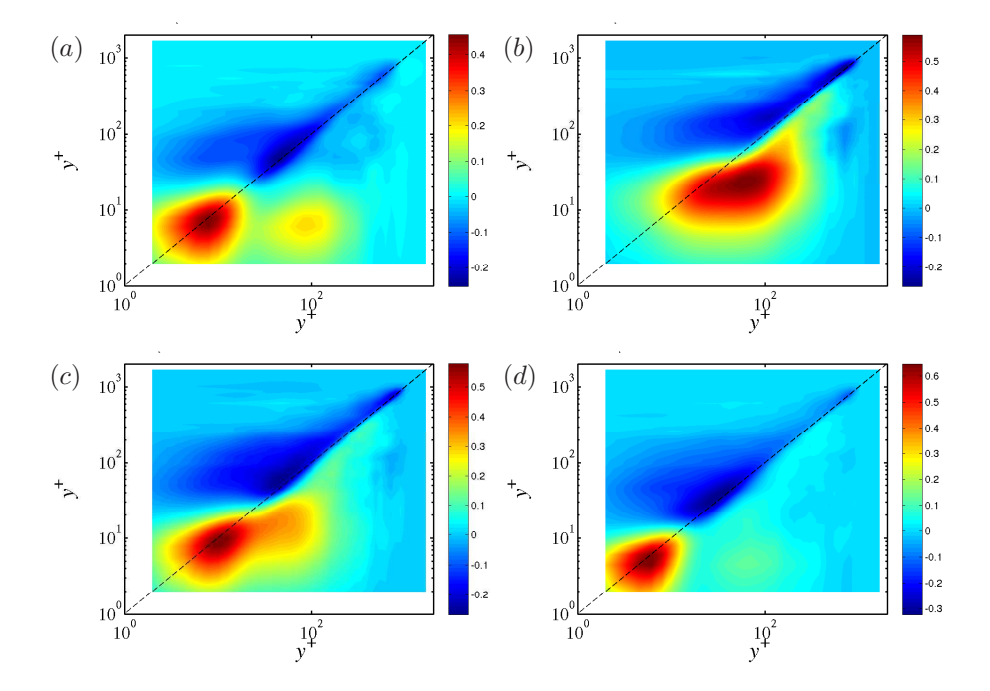


FIGURE 3.20. Two-point amplitude modulation covariance C^{2p} map at $Re_{\theta} = 2520$. (a) u, (b) θ with Pr = 0.2, (c) θ with Pr = 0.71, (d) θ with Pr = 2.0. A detailed discussion of the figure is found in Paper 3.

experimental difficulties in systematically performing two-point synchronised measurements, Mathis et al. (2009) considered the single-point correlation coefficient which provides reasonable estimate for a two-point correlation coefficient. Later, a note of caution concerning the interpretation of the amplitude-modulation correlation coefficient is made by Schlatter and Örlü (2010) in which they demonstrated that the correlation coefficient used to quantify the amplitude modulation is proportional to the skewness of the original signal irrespective of any modulation. Hence, it is not sufficient to unambiguously detect or quantify the large scale amplitude modulation on the small scales. Recently, the analysis of Mathis et al. (2009) is extended by Bernardini and Pirozzoli (2011) using again the two-point amplitude modulation correlation coefficient. They showed that this new two-point correlation does not appear to be proportional to the skewness of the original signal and therefore it provides a refined quantification of the amplitude modulation effects and truly reflects the top-down interaction.

Here the method suggested by Bernardini and Pirozzoli (2011) is chosen to study the amplitude modulation of the large scales onto the small scales as shown in Figure 3.20. Following the notation in Bernardini and Pirozzoli

(2011), the modulating influence of an wall-normal position at y_1 on another position y_2 is quantified by the covariance $C^{2p}(y_1, y_2) = \langle u_L(y_1)u_{EL}(y_2)\rangle$. u_L the the large scale component of the raw signal after a spanwise filter with cutoff wavelength $\lambda_z = 0.4\delta_{99}$. The spanwise filter wavelength is chosen according to approximately the wavelength which separates the inner and outer peak in the energy spectrum. Note that a wavelength of $\lambda_z = 0.5\delta_{99}$ is chosen by Bernardini and Pirozzoli (2011), however, the effect of varying the filter width has no qualitative effects on the results. $u_{EL}(y_2)$ is the low-pass filtered envelope of the small-scale component of the raw signal. For more details of the decoupling procedure, one should refer to original work by Mathis et al. (2009).

The resulting map for the streamwise velocity component as shown in Figure 3.20 (a) is consistent with the results by Bernardini and Pirozzoli (2011), i.e. a strong positive peak is observed lying on the diagonal in the left corner and a distinct second weaker positive peak emerges next to the dominant one. This second peak located at $y^+ \approx (100,8)$, will increase in strength with Reynolds number and represents the signature of the large-scale amplitude modulation on the small scales. The results pertaining to the scalars fields are shown in Figure 3.20 (b) – (d). As expected, the correlation map of Pr = 0.71 is similar to that of the streamwise velocity. The second peak in the map of the higher Prandtl number, Pr = 2.0, is much weaker, almost invisible, which indicates a weak large-scale modulation. This is in agreement with the spectra shown in Figure 3.16 (d). On the contrary, the low Prandtl case Pr = 0.2, due to dominant outer structures, the correlation map only shows this one peak which indicates the strong influence of the amplitude modulation.

3.7. Ongoing work

TABLE 3.1. List of resolution for the ongoing LES (calculated without dealiasing i.e. in spectral space; add a factor of 1.5 in the two wall-parallel direction to obtain the resolution in physical space). δ_0^* is the displacement thickness at the inlet.

box dimension	grid resolution	Reynolds number	
$13500\delta_0^* \times 400\delta_0^* \times 540\delta_0^*$	$9216 \times 513 \times 768$ $\Delta x^{+} = 25.5, \Delta z^{+} = 10.9$ $\Delta y^{+} = 0.12 - 14.2$	$Re_{\theta} = 188-8400$	

A new series of simulation of spatially developing turbulent boudnary layers via LES is ongoing at the moment. The sub-grid scale (SGS) stresses are modelled by the ADM-RT model (Schlatter *et al.* 2004) which is shown to be accurate in transitional and turbulent flow at a low cost (Schlatter *et al.* 2010). The ongoing work is a similar study as the previous one by Schlatter *et al.* (2010), i.e. employing the same numerical methods, grid resolution, SGS model, etc, but reaching a higher Reynolds number at $Re_{\theta} = 8400$. The grid

information is shown in Table 3.1. These Reynolds numbers are clearly the highest to be reached via well-resolved transient numerical simulations. At this Reynolds number, a first approach to an asymptotic state of the mean velocity and thus the emergence of a true "overlap" region can be expected. Some prelimenary results are shown here to illustrate the quality of the expected results. The highest Reynolds number obtained is about $Re_{\theta} = 8400$ which is twice the one reached by the previous work (Schlatter et al. 2010). The numerical setup is similar to the previous study by Schlatter et al. (2010) and a total number of 10 bilion grid points is required. In Figure 3.21 (a), the downstream evolution of the skin-friction coefficient is compared with the previous DNS by Schlatter & Örlü (2010), empirical relation by Nagib et al. (2007) and experimental data by Örlü (2009), and the agreement is fairly good especially at higher Reynolds numbers. The mean velocity profile and the RMS of the fluctuations are shown in Figures 3.21 (b) and (c). Again the agreement with the previous DNS and experimental data is exellent at higher Reynolds numbers; Potential sources of small differences at lower Reynolds numbers are currently under investigation. For the u_{rms} , the Reynolds number dependence of the peak value is clearly visible, i.e. an increasing peak with increasing Reynolds number. In Figure 3.21 (d), the log-law indicator function $\Xi = y^{+} \frac{\mathrm{d}\langle u \rangle^{+}}{\mathrm{d}y^{+}}$ for velocity field is shown. Monkewitz et al. (2007) proposed a functional form for Ξ up to the logarithmic region, featuring a maximum at $y^+ \approx 10$ and a local minimum around $y^+ \approx 70$. After the minimum, the indicator function is supposed to asymptote to $1/\kappa$ in the log-region at sufficiently high Reynolds number. The highest Reynolds number reached in the present LES data is still on the lower end to develop an asymptotical logarithmic region with the proposed $\kappa = 0.38$ by (Österlund et al. 2000), the log-law indicator function closely follows the correlation developed by Monkewitz et al. (2007) and just reached about the plateau before increasing again in the wake region.

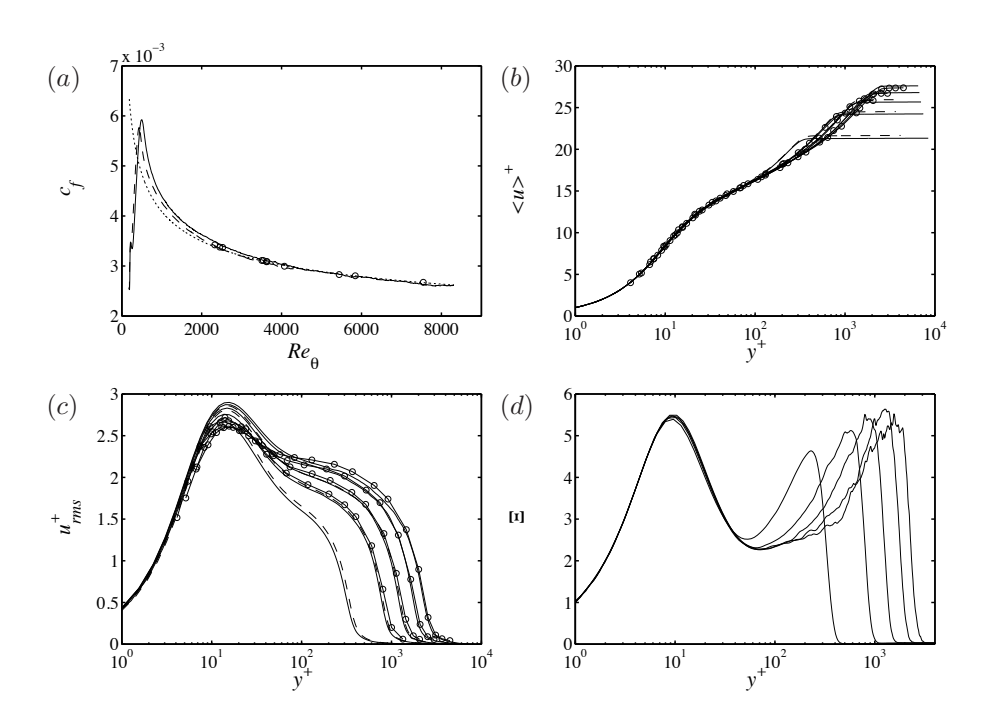


FIGURE 3.21. Preliminary results for the ongoing LES upto $Re_{\theta} = 8000$. — LES at $Re_{\theta} = 1000, 2500, 4000, 5844, 7545,$ ——DNS at $Re_{\theta} = 1000, 2500, 4000, \circ$ experimental data by Örlü (2009) at $Re_{\theta} = 2526, 4070, 5844, 7545, \cdots$ correlation by Nagib et al. (2007) $2(\frac{1}{0.384}ln(Re_{\theta}) + 4.127)^{-2}$. (a) c_f , (b) $\langle u \rangle$, (c) u_{rms} , (d) Ξ .

CHAPTER 4

Conclusions and outlook

"There is always an easy solution to every human problem – neat, plausible, and wrong."

- H. L. Mencken (1880 - 1956)

"You can always count on the Americans to do the right thing after they've tried everything else."

- Sir Winston S. Churchill (1874 - 1965)

In the present thesis, spatially evolving turbulent boundary layers together with passive scalars are investigated numerically. The parallelised research code together with the large-scale computer system make the study of wall turbulence at numerically very high Reynolds numbers possible.

The basic flow statistics and energy budgets pertaining to both flow and scalar fields are in close agreement with available high quality experimental and DNS data in literature at comparable Reynolds numbers. Furthermore, the good agreement at high Reynolds number $Re_{\theta} > 2000$ indicates that the results are insensitive to the details of the experimental and numerical setup, e.g. the surface roughness, tripping device, streamwise pressure gradients, boundary conditions. By analysing the spanwise and temporal spectra, a two-peak structure is merged. The inner peak reflects the existence of the near-wall streaks, while the outer peak indicates the presence of the larger-scale motions. Furthermore, the large-scale structure is found to be about $0.85\delta_{99}$ in width and persists for about $10\delta_{99}/U_{\infty}$ time units. It is found that a nonlinear amplitude modulation indeed takes place of the small scale by the large scales motions in the log region. Concerning the vortical structures in the flow field, it is found that no hairpin like structures exist in the averaged field in the nearwall region of the turbulent boundary layer, instead, only the quasi-streamwise vortex survives. This is consistent with previous results in turbulent channel flow, which again reflects the similarities in the near-wall region for both types of flow geometry.

For the results pertaining to scalar field, the mean scalar profiles are independent of the different boundary conditions whereas the effects on the scalar variances and high-order statistics are obvious in the near-wall region. The

scalar (Pr = 0.71) with isoscalar boundary condition is highly correlated with the streamwise velocity component in the near-wall region. However, near the boundary-layer edge, only a mild correlation between these two quantities was observed. The Prandtl number effects are clearly shown via the energy spectra and the two-point correlations. There are much more prominent outer-layer structures for scalar fields with lower Pr, while for higher Pr, only the spectral peaks pertaining to small scales are observable. Similar to the velocity field, the amplitude modulation of the outer structures on the small scales close to the wall also exists for the scalar field.

As an extension to the non-canonical case, the influences of the free-stream turbulence is considered. With the presence of free-stream turbulence, a more prominent depression of the wake region can be observed with increasing turbulence intensity for both the mean velocity and temperature profiles. As much as 30% increases of both the skin-friction coefficient and the Stanton number are found for a local turbulence intensity of 7%. The temperature field seems to be more affected by the presence of the free-stream turbulence which is shown by the increasing Reynolds analogy factor with increasing turbulence intensity. By employing the spanwise premultiplied energy spectra, it is found that the original two-peak structure in the calm free stream case is altered. The inner peak stays the same while a new peak emerges at approximately the height of the boundary layer thickness with a spanwise scale of about $\mathcal{O}(3 \sim 4\delta_{95})$. The outer peak originally located in the overlap region in the no-FST case vanishes or at least becomes much less dominant. It is believed that these newly formed large-scale structures due to the free-stream turbulence penetrate through the boundary layer down to the wall and cause the observed increase of both skin friction and heat transfer on the wall. In addition, it is suggested that a turbulent boundary layer at moderate Reynolds number under the influence of free-stream turbulence appears similar to a boundary layer at higher Reynolds number without FST. Detailed analysis on the statistics obtained from high-Reynolds-number simulations and at moderate Reynolds number with FST could be interesting as also suggested by Sharp et al. (2009).

An extension of the present work is to simulate such canonical flows at even higher Reynolds numbers since most engineering applications happen at very high Reynolds numbers, so there is always a need for well-resolved simulations at high Reynolds number. With the present increasing speed of the computer power, by the middle of 21 century, it is expected that to simulate the wing of an airplane will be possible. A series simulations via LES is already ongoing. The Reynolds number is twice as much as the previous DNS study by Schlatter & Örlü (2010), reaching a Reynolds number $Re_{\theta} = 8400$. The preliminary results are in good agreement with the previous simulations.

For the free-stream case, the future simulation should consider fewer configurations, but with increased numerical resolution to further quantitatively study the various effects of FST. To critically compare with the experiments, the length scales used in the simulation should be further increased, and this

in turn will require a large number of grid points and very large computational domain to comfortably accommodate the large scale structures present in the free stream.

Other possible extensions include considering the effects of streamline curvature and buoyancy in turbulence. Ealier studies showed that there is a qualitatively analogy between the flows over curved boundaries and flows with buoyancy. It is definitely interesting to study the buoyancy and curvature effects on the structural changes in turbulent shear flows, and possible influences on heat transfer problems.

Acknowledgements

"A good friend is someone you can talk about many things; The better ones are those even you don't talk anything, both of you won't feel embarrassing"

- anonymous

"Sometimes you see beautiful people with no brains. Sometimes you have ugly people who are intelligent, like scientists"

- José Mourinho

First, I would like to thank Dr. Philipp Schlatter and Prof. Dan Henningson, as my supervisors, for accepting me as a PhD student and sharing their knowledge/experiences in fluid mechanics, numerical simulations and many other things in life. The financial support by Swedish Research Council (Vetenskapsrådet) for the PhD project and computer time provided by Swedish National Infrastructure for Computing (SNIC) is greatly acknowledged, as well as the the travel stipends from "Erik Petersohns Minne".

As the main supervisor, I greatly appreciated the incredible and persistent patience of Dr. Philipp Schlatter with me. *Danke sehr!* As everyone else in the group, I am surely impressed by your experiences and knowledge in numerics. Actually, I am more astonished by your coding skills which I guess not everyone knows. For example, I will never manage to figure out how to use commands like MPI_UB by myself.

I would also like to thank Prof. Dan S. Henningson as my main supervisor for the first three years. *Tack så mycket!* I really appreciated your enthusiasm, encouragement, support and especially the sense of humour.

Many thanks to Prof. She who made my short visit in Beijing University very pleasant. It is very interesting to see how the research work is done at another group and how they view the problem from a different perspective.

I am also grateful to the family of von Bahr for their hospitality. To celebrate Christmas with you makes me feel like being at home and I really appreciate it. Moreover, I like the food very much, especially the home-made köttbullar.

During the PhD, I do not only learn a lot about turbulence and numerical simulations but I also enjoyed the very nice atmosphere in our group and the department which is maybe more important. As a "product" made in China, and made by Chinese, plus my inactive/passive personality, it is a difficult for me to go abroad. But it turns out that staying in Sweden and doing a PhD in Dan's group is one of the few right decisions I have ever made. Needless to say, such a nice atmosphere is due to the presence of nice people: Ardeshir, Luca, Espen, Yohann, Flavio, Gataneo, Mattias, Stefan, Shervin, Milos, Francesco, George, Ruth, Azad, Iman, Lailai, Joy, Armin, Nima, Reza, Sasan. Colleagues from other groups at Mechanics should not be forgotten: Arne, Hanno, Nicholas, Erik, Geert, Gunnar, Andreas, Enrico, Florian, Marit, Werner, Linus, Peter, Zeinab, Amin, Liang, Andreas, Krishnagoud, Robert, Ruoli, Feng, Yue, Stevin. I shall also thank those sitting in the lab: Henrik, Fredrik, Ramis, Bengt, Outi, Thomas, Gabriele, Karl, Robert, Mathias. I am also grateful to the non-academic staff: Carolina, Heide, Malin, Nina, Karina, Pär, Arne and Bubba.

Here I would like to spend a little bit more text on the colleagues who I know a little bit more. One can think it as my own taste about people, which might be completely off from the real person, so one should not take it too seriously.

Starting from the Antonios and Onofrio, maybe because exposed in the sun too much in the early years, you are quite "hot", technically speaking like an active scalar. For Antonios: you are self-confident (even though I do not see where your self-confidence comes from), optimistic (maybe a little bit too much). For Onofrio, you are more like "vesuvio under an ice-sheet". Next comes the Germans (Lars-Uve und David). I had some impressions about German people from movies or books, and these images I had in mind are very well reflected on you two guys, for example never say no to beer, meticulous, patriotic. However, the fact that you are quite funny and like to make jokes makes me know something new about Germans. For the Johan, you are relatively "cold" compared to the other two "hot" ones in our office, technically speaking like a passive scalar². I know you are one of those people who likes to make everyting in order, however, I happen to be the one on the opposite. For your tolerence and understanding throughout these years, I really appreciate it. In summary, it is very nice and lucky for me to know you guys. Puss och Kram!

感谢亲戚朋友多年来对我的关怀与帮助,以及爸爸妈妈一直以来对我的溺爱!

¹I do NOT mean they are attractive, not for me at least.

²You know, I like passive scalars.

Bibliography

- ABE, H. & KAWAMURA, H. 2002 A study of turbulence thermal structure in a channel flow through DNS up to $Re_{\tau}=640$ with Pr=0.025 and 0.71. In *Advances in Turbulence IX* (ed. I. P. Castro, P. E. Hancock & T. G. Thomas), pp. 399–402. CIMNE, Barcelona, Spain.
- ABE, H., KAWAMURA, H. & CHOI, H. 2004a Very large-scale structures and their effects on the wall shear-stress fluctuations in a turbulent channel flow up to $Re_{\tau}=640$. ASME J. Fluids Engng. 126 (5), 835–843.
- ABE, H., KAWAMURA, H. & MATSUO, Y. 2001 Direct numerical simulation of a fully developed turbulent channel flow with respect to the Reynolds number dependence. ASME J. Fluids Engng. 123 (2), 382–393.
- ABE, H., KAWAMURA, H. & MATSUO, Y. 2004b Surface heat-flux fluctuations in a turbulent channel flow up to $Re_{\tau}=1020$ with Pr=0.025 and 0.71. Int. J. Heat Fluid Flow 25 (3), 404–419.
- Adrian, R. J. 1982 Comment on "A note on Poisson's equation for pressure in a turbulent flow". *Phys. Fluids* **25** (3), 577–577.
- Adrian, R. J., Meinhart, C. D. & Tomkins, C. D. 2000 Vortex organization in the outer region of the turbulent boundary layer. *J. Fluid Mech.* **422**, 1–54.
- DEL ÁLAMO, J. C. & JIMÉNEZ, J. 2003 Spectra of the very large anisotropic scales in turbulent channels. *Phys. Fluids* **15** (6), L41–L44.
- DEL ÁLAMO, J. C. & JIMÉNEZ, J. 2009 Estimation of turbulent convection velocities and corrections to Taylor's approximation. *J. Fluid Mech.* **640**, 5–26.
- DEL ÁLAMO, J. C., JIMÉNEZ, J., ZANDONADE, P. & MOSER, R. D. 2004 Scaling of the energy spectra of turbulent channels. *J. Fluid Mech.* **500**, 135–144.
- Alfredsson, P. H., Johansson, A. V., Haritonidis, J. H. & Eckelmann, H. 1988 The fluctuating wall-shear stress and the velocity field in the viscous sublayer. *Phys. Fluids* **31** (5), 1026–1033.
- ALVELIUS, K. & SKOTE, M. 2000 The performance of a spectral simulation code for turbulence on parallel computers with distributed memory. *Tech. Rep* TRITA-MEK 2000:17. KTH Mechanics, Stockholm, Sweden.
- Anderson, J. D. 2005 Ludwig Prandtl's Boundary Layer. *Physics Today* **58** (12), 42–48.
- Andreopoulos, J., Durst, F., Zaric, Z. & Jovanovic, J. 1984 Influence of Reynolds number on characteristics of turbulent wall boundary layers. *Exps. Fluids* 2, 7–16.

- ANTONIA, R. A. & DANH, H. Q. 1977 Structure of temperature fluctuations in a turbulent boundary layer. *Phys. Fluids* **20** (7), 1050–1057.
- ANTONIA, R. A. & KIM, J. 1991 Turbulent Prandtl number in the near-wall region of a turbulent channel flow. *Int. J. Heat Mass Transfer* **34** (7), 1905–1908.
- Antonia, R. A. & Kim, J. 1994 Low-Reynolds-number effects on near-wall turbulence. J. Fluid Mech. 276, 61–80.
- Antonia, R. A., Krishnamoorthy, L. V. & Fulachier, L. 1988 Correlation between the longitudinal velocity fluctuation and temperature fluctuation in the near-wall region of a turbulent boundary layer. *Int. J. Heat Mass Transfer* **31** (4), 723–730.
- ARAYA, G. 2008 Numerical heat transfer analysis in turbulent wall bounded flows. PhD thesis, Rensselaer Polytechnic Institute, Troy, New York, U.S.A.
- Barenblatt, G. I. 1993 Scaling laws for fully developed turbulent shear flows. Part 1. Basic hypotheses and analysis. *J. Fluid Mech.* **248**, 513–520.
- BARENBLATT, G. I., CHORIN, A. J., HALD, O. H. & PROSTOKISHIN, V. M. 1997a Structure of the zero-pressure-gradient turbulent boundary layer. *Proc. Natl. Acad. Sci. U.S.A.* **94**, 7817–7819.
- BARENBLATT, G. I., CHORIN, A. J. & PROSTOKISHIN, V. M. 1997b Scaling laws for fully developed turbulent flow in pipes: discussion of experimental data. *Proc. Natl. Acad. Sci. U.S.A.* **94**, 773–776.
- BARENBLATT, G. I. & PROSTOKISHIN, V. M. 1993 Scaling laws for fully developed turbulent shear flows. Part 2. Processing of experimental data. *J. Fluid Mech.* **248**, 521–529.
- BATCHELOR, G. K. 1959 Small-scale variation of convected quantities like temperature in turbulent fluid: Part 1. General discussion and the case of small conductivity. *J. Fluid Mech.* 5 (01), 113–133.
- Bell, D. M. & Ferziger, J. H. 1993 Turbulent boundary layer DNS with passive scalars. In *Near-Wall Turbulent Flows* (ed. R. M. C. So, C. G. Speziale & B. E. Launder), pp. 327–366. Elsevier, Amsterdam, The Netherlands.
- Bergant, R. & Tiselj, I. 2007 Near-wall passive scalar transport at high Prandtl numbers. *Phys. Fluids* **19** (6), 065105.
- Bernardini, M. & Pirozzoli, S. 2011 Inner/outer layer interactions in turbulent boundary layers: a refined measure for the large-scale amplitude modulation mechanism. *Phys. Fluids* **23** (6), 061701.
- Bertolotti, F. P., Herbert, T. & Spalart, P. R. 1992 Linear and nonlinear stability of the Blasius boundary layer. *J. Fluid Mech.* **242**, 441–474.
- BEVILAQUA, P. M. & LYKOUDIS, P. S. 1978 Turbulence memory in self-preserving wakes. J. Fluid Mech. 89 (03), 589–606.
- BIRD, R. B., STEWART, W. E. & LIGHTFOOT, E. N. 2002 Transport Phenomena, 2nd edn. John Wiley & Sons, New York, U.S.A.
- BLACKWELDER, R. F. & KOVASZNAY, L. S. G. 1972 Large-scale motion of a turbulent boundary layer during relaminarization. *J. Fluid Mech.* **53** (01), 61–83.
- Blackwell, B. F., Kays, W. M. & Moffat, R. J. 1972 The turbulent boundary layer on a porous plate: an experimental study of the heat transfer behavior with adverse pressure gradients. *Tech. Rep* Report HMT-16. Thermosciences Division, Department of Mechanical Engineering, Stanford University, C.A., U.S.A.
- Blair, M. F. 1983a Influence of free-stream turbulence on turbulent boundary layer

- heat transfer and mean profile development, Part I Experimental data. ASME J. Heat Transfer 105, 33–40.
- Blair, M. F. 1983b Influence of free-stream turbulence on turbulent boundary layer heat transfer and mean profile development, Part II Analysis of results. ASME J. Heat Transfer 105, 41–47.
- Boussinesq, J. 1877 Théorie de l'écoulement Tourbillant. Mem. Présentés par Divers Savants Acad. Sci. Inst. Fr. 23, 46–50.
- Bradshaw, P. 1967 'inactive' motion and pressure fluctuations in turbulent boundary layers. J. Fluid Mech. 30 (02), 241–258.
- Bradshaw, P. 1972 The understanding and prediction of turbulent flow. *Aero. J.* **76**, 403–418.
- Bradshaw, P. 1974 Effect of free-stream turbulence on turbulent shear layers. *Tech. Rep* Aero Report 74-10. Imperial College of Science and Technology, Department of Aeronautics, London, U.K.
- Bradshaw, P. 1976 Introduction. In *Topics in Applied Physics. Volume 12. Turbulence* (ed. P. Bradshaw), pp. 1–44. Springer-Verlag, Berlin, Germany.
- Bradshaw, P. 1996 Turbulence modeling with application to turbomachinery. *Progress in Aerospace Sciences* **32** (6), 575–624.
- Bradshaw, P. 1997 Understanding and prediction of turbulent flow–1996. *Int. J. Heat Fluid Flow* 18 (1), 45–54.
- Bradshaw, P. & Huang, G. P. 1995 The law of the wall in turbulent flow. *Proc. Roy. Soc. Lond. Ser. A* **451** (1941), 165–188.
- Bradshaw, P. & Koh, Y. M. 1981 A note on Poisson's equation for pressure in a turbulent flow. *Phys. Fluids* **24** (4), 777.
- Brandt, L., Schlatter, P. & Henningson, D. S. 2004 Transition in boundary layers subject to free-stream turbulence. *J. Fluid Mech.* **517**, 167–198.
- BRICTEUX, L., DUPONCHEEL, M. & WINCKELMANS, G. 2009 A multiscale subgrid model for both free vortex flows and wall-bounded flows. *Phys. Fluids* **21** (10), 105102.
- BROOKE, J. W. & HANRATTY, T. J. 1993 Origin of turbulence producing eddies in a channel flow. *Phys. Fluids A* **5** (4), 1011–1022.
- Buschmann, M. H. & Gad-el Hak, M. 2007 Recent developments in scaling of wall-bounded flows. *Progress in Aerospace Sciences* **42** (5-6), 419–467.
- Buschmann, M. H. & Gad-el Hak, M. 2010 Normal and cross-flow Reynolds stresses: differences between confined and semi-confined flows. *Exps. Fluids* 49, 213–223.
- Calmet, I. & Magnaudet, J. 1997 Large-eddy simulation of high-schmidt number mass transfer in a turbulent channel flow. *Phys. Fluids* **9** (2), 438–455.
- Cantwell, B. J. 1981 Organized motion in turbulent flow. *Ann. Rev. Fluid Mech.* 13 (1), 457–515.
- CANUTO, C., HUSSAINI, M. Y., QUARTERONI, A. & ZANG, T. A. 1988 Spectral Methods in Fluid Dynamics. Springer, Berlin, Germany.
- CEBECI, T. & Bradshaw, P. 1984 Physical and Computational Aspects of Convective Heat Transfer. Springer, Berlin, Germany.
- Cenedese, A., Romano, G. P. & Antonia, R. A. 1998 A comment on the "linear" law of the wall for fully developed turbulent channel flow. *Exps. Fluids* **25**, 165–170.

- Chauhan, K. A., Monkewitz, P. A. & Nagib, H. M. 2009 Criteria for assessing experiments in zero pressure gradient boundary layers. *Fluid Dyn. Res.* **41** (2), 021404
- Chen, C. H. P. & Blackwelder, R. F. 1978 Large-scale motion in a turbulent boundary layer: a study using temperature contamination. *J. Fluid Mech.* 89 (01), 1–31.
- Chevalier, M., Schlatter, P., Lundbladh, A. & Henningson, D. S. 2007 A pseudo-spectral solver for incompressible boundary layer flows. *Tech. Rep* TRITA-MEK 2007:07. KTH Mechanics, Stockholm, Sweden.
- Choi, H. & Moin, P. 1994 Effects of the computational time step on numerical solutions of turbulent flow. J. Comp. Phys. 113 (1), 1–4.
- Chong, M. S., Perry, A. E. & Cantwell, B. J. 1990 A general classification of three-dimensional flow fields. *Phys. Fluids A* **2** (5), 765–777.
- CHOU, P. Y. & CHOU, R. L. 1995 50 years of turbulence research in China. Ann. Rev. Fluid Mech. 27 (1), 1–16.
- CIMBALA, J. M., NAGIB, H. M. & ROSHKO, A. 1988 Large structure in the far wakes of two-dimensional bluff bodies. *J. Fluid Mech.* **190**, 265–298.
- CLAUSER, F. H. 1956 The turbulent boundary layer. Adv. Appl. Mech. 4, 1–51.
- COLBRUN, A. P. 1933 A method of correlating forced convection heat transfer data and a comparison with fluid friction. Trans. Am. Inst. Chem. Eng. 29, 174–210.
- COLEMAN, G. N. & SANDBERG, R. D. 2010 A primer on direct numerical simulation of turbulence- methods, procedures and guidelines. *Tech. Rep* AFM-09/01a. Aerodynamics & Flight Mechanics Research Group, School of Engineering Sciences, University of Southampton, Southampton, U.K.
- CORRSIN, S. 1952 Heat transfer in isotropic turbulence. J. Appl. Phys. 23 (1), 113–118.
- CORRSIN, S. & KISTLER, A. L. 1954 Free-stream boundaries of turbulent flows. Tech. Rep NACA-TR-1244. NASA, U.S.A.
- COURANT, R., FRIEDERICHS, K. & LEWY, H. 1928 Über die partiellen Differenzengleichungen der mathematischen Physik. *Mathematische Annalen* **100** (1), 32–74.
- Crank, J. & Nicolson, P. 1947 A practical method for numerical evaluation of solutions of partial differential equations of the heat-conduction type. *Proc. Camb. Phil. Soc.* 43 (1), 50–67.
- Daly, B. J. & Harlow, F. H. 1970 Transport equations in turbulence. *Phys. Fluids* 13 (11), 2634–2649.
- DE GRAAFF, D. B. & EATON, J. K. 2000 Reynolds-number scaling of the flat-plate turbulent boundary layer. J. Fluid Mech. 422, 319–346.
- Deardorff, J. W. 1970 A numerical study of three-dimensional turbulent channel flow at large Reynolds numbers. J. Fluid Mech. 41 (2), 453–480.
- DIMOTAKIS, P. E. 2005 Turbulent mixing. Ann. Rev. Fluid Mech. 37, 329–356.
- Durst, F., Jovanovic, J. & Kanevce, L. 1987 Probability density distribution in turbulent wall boundary-layer flows. In *Turbulent Shear Flows 5* (ed. F. Durst, B. E. Launder, J. L. Lumley, F. W. Schmidt & J. H. Whitelaw), pp. 197–220. Springer-Verlag, Berlin, Germany.
- Erm, L. P. & Joubert, P. N. 1991 Low-reynolds-number turbulent boundary layers. J. Fluid Mech. 230, 1–44.

- FARABEE, T. M. & CASARELLA, M. J. 1991 Spectral features of wall pressure fluctuations beneath turbulent boundary layers. *Phys. Fluids* **3**, 2410–2420.
- Fernholz, H. H. & Finley, P. J. 1996 The incompressible zero-pressure-gradient turbulent boundary layer: an assessment of the data. *Progress in Aerospace Sciences* **32** (4), 245–311.
- Ferrante, A. & Elghobashi, S. 2005 Rreynolds number effect on drag reduction in a microbubble-laden spatially developing turbulent boundary layer. *J. Fluid Mech.* **543**, 93–106.
- FLORES, O. & JIMÉNEZ, J. 2006 Effect of wall-boundary disturbances on turbulent channel flows. J. Fluid Mech. 566, 357–376.
- FRISCH, U. & ORSZAG, S. A. 1990 Turbulence: challenges for theory and experiment. *Physics Today* **43** (1), 24–32.
- FRÖHLICH, J. & RODI, W. 2002 Introduction to large-eddy simulation of turbulent flows. In *Closure Strategies for Turbulent and Transitional Flows* (ed. B. E. Launder & N. D. Sandham), pp. 267–298. Cambridge University Press, Cambridge, U.K.
- GEORGE, W. K. 2007 Is there a universal log law for turbulent wall-bounded flows?. *Proc. Roy. Soc. Lond. Ser. A* **365** (1852), 789–806.
- George, W. K. & Castillo, L. 1997 Zero-pressure-gradient turbulent boundary layer. ASME Appl. Mech. Rev. 50 (12), 689–729.
- George, W. K. & Davidson, L. 2004 Role of initial conditions in establishing asymptotic flow behaviour. AIAA J. 42 (3), 438–446.
- GERMANO, M., PIOMELLI, U., MOIN, P. & CABOT, W. H. 1991 A dynamic subgrid-scale eddy viscosity model. *Phys. Fluids A* **3** (7), 1760–1765.
- GEURTS, B. J. 1999 Balancing errors in LES. In *Direct and Large-Eddy Simulation III* (ed. N. D. Sandham, P. R. Voke & L. Kleiser), pp. 1–12. Springer-Verlag, Berlin, Germany.
- GEURTS, B. J. & LEONARD, A. 2002 Is LES ready for complex flows? In *Closure Strategies for Turbulent and Transitional Flows* (ed. B. E. Launder & N. D. Sandham), pp. 720–739. Cambridge University Press, Cambridge, U.K.
- Goldschmidt, V. W., Young, M. F. & Ott, E. S. 1981 Turbulent convective velocities (broadband and wavenumber dependent) in a plane jet. *J. Fluid Mech.* **105**, 327–345.
- Grant, H. L., Stewart, R. W. & Moilliet, A. 1962 Turbulence spectra from a tidal channel. *J. Fluid Mech.* 12 (02), 241–268.
- GROSCH, C. E. & SALWEN, H. 1978 The continuous spectrum of the Orr-Sommerfeld equation. Part 1. The spectrum and the eigenfunctions. *J. Fluid Mech.* 87 (1), 33–54.
- Guala, M., Hommema, S. E. & Adrian, R. J. 2006 Large-scale and very-large-scale motions in turbulent pipe flow. *J. Fluid Mech.* **554**, 521–542.
- Guezennec, Y., Stretch, D. & Kim, J. 1990 The structure of turbulent channel flow with passive scalar transport. In *Studying Turbulence Using Numerical Simulation Databases III*, pp. 127–138.
- Gupta, A. K., Laufer, J. & Kaplan, R. E. 1971 Spatial structure in the viscous sublayer. *J. Fluid Mech.* **50**, 493–512.
- Gad-el Hak, M. & Bandyopadhyay, P. R. 1994 Reynolds number effects in wall-bounded turbulent flows. *AME Appl. Mech. Rev.* 47 (8), 307–365.

- Gad-el Hak, M. & Buschmann, M. 2011 Turbulent boundary layers: is the wall falling or merely wobbling?. *Acta Mechanica* 218, 309–318.
- HANCOCK, P. E. 1978 Effect of free-stream turbulence on turbulent boundary layers. PhD thesis, Imperial College of Science and Technology, London, U.K.
- HANCOCK, P. E. & BRADSHAW, P. 1983 The effect of free-stream turbulence on turbulent boundary layers. ASME J. Fluids Engng. 105, 284–289.
- HANCOCK, P. E. & BRADSHAW, P. 1989 Turbulence structure of a boundary layer beneath a turbulent free stream. *J. Fluid Mech.* **205**, 45–76.
- HATTORI, H., HOURA, T. & NAGANO, Y. 2007 Direct numerical simulation of stable and unstable turbulent thermal boundary layers. *Int. J. Heat Fluid Flow* **28** (6), 1262 1271.
- Head, M. R. & Bandyopadhyay, P. 1981 New aspects of turbulent boundary-layer structure. *J. Fluid Mech.* **107**, 297–338.
- Hetsroni, G., Kowalewski, T. A., Hu, B. & Mosyak, A. 2001 Tracking of coherent thermal structures on a heated wall by means of infrared thermography. *Exps. Fluids* **30** (3), 286–294.
- Hetsroni, G., Tiselj, I., Bergant, R., Mosyak, A. & Pogrebnyak, E. 2004 Convection velocity of temperature fluctuations in a turbulent flume. *ASME J. Heat Transfer* **126**, 843–838.
- HISHIDA, M. & NAGANO, Y. 1979 Structure of turbulent velocity and temperature fluctuations in fully developed pipe flow. ASME J. Heat Transfer 101, 15–22.
- HOFFMANN, P. H. & PERRY, A. E. 1979 The development of turbulent thermal layers on flat plates. *Int. J. Heat Mass Transfer* **22** (1), 39–46.
- Honkan, A. & Andreopoulos, Y. 1997 Vorticity, strain-rate and dissipation characteristics in the near-wall region of turbulent boundary layers. *J. Fluid Mech.* **350**, 29–96.
- HOURA, T. & NAGANO, Y. 2006 Effects of adverse pressure gradient on heat transfer mechanism in thermal boundary layer. *Int. J. Heat Fluid Flow* **27** (5), 967–976.
- HOYAS, S. & JIMÉNEZ, J. 2006 Scaling of the velocity fluctuations in turbulent channels up to $Re_{\tau}=2003$. Phys. Fluids 18 (1), 011702.
- HULTMARK, M., BAILEY, S. C. C. & SMITS, A. J. 2010 Scaling of near-wall turbulence in pipe flow. J. Fluid Mech. 649, 103–113.
- HUTCHINS, N. & MARUSIC, I. 2007a Evidence of very long meandering features in the logarithmic region of turbulent boundary layers. J. Fluid Mech. 579, 1–28.
- HUTCHINS, N. & MARUSIC, I. 2007b Large-scale influences in near-wall turbulence. Proc. Roy. Soc. Lond. Ser. A 365, 647–664.
- Hutchins, N., Nickels, T. B., Marusic, I. & Chong, M. S. 2009 Hot-wire spatial resolution issues in wall-bounded turbulence. *J. Fluid Mech.* **635**, 103–136.
- IRITANI, Y., KASAGI, N. & HIRATA, M. 1985 Heat transfer mechanism and associated turbulence structure in a near wall region of a turbulent boundary layer. In *Turbulent Shear Flows 4* (ed. L. J. S. Bradburry, F. Durst, B. E. Launder, F. W. Schmidt & J. H. Whitelaw), pp. 223–234. Springer-Verlag, Berlin, Germany.
- Jacobs, R. G. & Durbin, P. A. 2000 Bypass transition phenomena studies by computer simulation. *Tech. Rep* TF-77. Stanford University, U.S.A.
- Jacobs, R. G. & Durbin, P. A. 2001 Simulations of bypass transition. *J. Fluid Mech.* 428, 185–212.

- Jeong, J. & Hussain, F. 1995 On the identification of a vortex. J. Fluid Mech. 285, 69–94
- Jeong, J., Hussain, F., Schoppa, W. & Kim, J. 1997 Coherent structures near the wall in a turbulent channel flow. *J. Fluid Mech.* **332**, 185–214.
- JIMÉNEZ, J. 2003 Computing high-Reynolds-number turbulence: will simulations ever replace experiments?. J. Turbulence 4 (22), 1–14.
- JIMÉNEZ, J. & HOYAS, S. 2008 Turbulent fluctuations above the buffer layer of wall-bounded flows. J. Fluid Mech. 611, 215–236.
- JIMÉNEZ, J., HOYAS, S., SIMENS, M. P. & MIZUNO, Y. 2010 Turbulent boundary layers and channels at moderate Reynolds numbers. J. Fluid Mech. 657, 335– 360.
- JIMÉNEZ, J. & PINELLI, A. 1999 The autonomous cycle of near-wall turbulence. J. Fluid Mech. $\bf 389$, $\bf 335-\bf 359$.
- JIMÉNEZ, J., SIMENS, M. P., HOYAS, S. & MIZUNO, Y. 2008 Entry length requirements for direct simulations of turbulent boundary layers. Tech. Rep Annual Research Briefs 2008. CTR, U.S.A.
- JOHANSSON, A. V. & ALFREDSSON, P. H. 1983 Effects of imperfect spatial resolution on measurements of wall-bounded turbulent shear flows. J. Fluid Mech. 137, 409–421.
- KACHANOV, Y. S. 1994 Physical mechanisms of laminar-boundary-layer transition. Annu. Rev. Fluid Mech. 26, 411–482.
- KADER, B. A. 1981 Temperature and concentration profiles in fully turbulent boundary layers. Int. J. Heat Mass Transfer 24 (9), 1541–1544.
- VON KÁRMÁN 1939 The analogy between fluid friction and heat transfer. *Trans.* ASME **61**, 705–710.
- Karniadakis, G. & Sherwin, S. 2005 Spectral/hp element methods for computational fluid dynamics. Oxford University Press, Oxford, U.K.
- Kasagi, N. & Iida, O. 1999 Progress in direct numerical simulation of turbulent heat transfer. In *Proceedings of the 5th ASME/JSME Joint Thermal Engineering Conference, San Diego, U.S.A.*.
- KASAGI, N., KURODA, A. & HIRATA, M. 1989 Numerical investigation of near-wall turbulent heat transfer taking into account the unsteady heat conduction in the solid wall. ASME J. Heat Transfer 111 (2), 385–392.
- Kasagi, N. & Ohtsubo, Y. 1993 Direct numerical simulation of low Prandtl number thermal fluid in a turbulent channel flow. In *Turbulent Shear Flows 8* (ed. F. Durst), pp. 97–119. Springer-Verlag, Berlin, Germany.
- Kasagi, N., Tomita, Y. & Kuroda, A. 1992 Direct numerical simulation of passive scalar field in a turbulent channel flow. ASME J. Heat Transfer 114 (3), 598–606.
- KAWAMURA, H., ABE, H. & MATSUO, Y. 1999 DNS of turbulent heat transfer in channel flow with respect to Reynolds and Prandtl number effects. *Int. J. Heat Fluid Flow* **20** (3), 196–207.
- KAWAMURA, H., ABE, H. & MATSUO, Y. 2004 Very large-scale structures observed in DNS of turbulent channel flow with passive scalar transport. In *Proceedings of the Fifteenth Australasian Fluid Mechanics Conference* (ed. M. Behnia, W. Lin & G. D. McBain). The University of Sydney, Australia, 2004.
- KAWAMURA, H., OHSAKA, K., ABE, H. & YAMAMOTO, K. 1998 DNS of turbulent

- heat transfer in channel flow with low to medium-high Prandtl number fluid. *Int. J. Heat Fluid Flow* **19** (5), 482–491.
- KAYS, W. M. 1994 Turbulent Prandtl number Where are we?. ASME J. Heat Transfer 116, 284–295.
- KAYS, W. M. & CRAWFORD, M. E. 1993 Convective Heat and Mass Transfer, 3rd edn. McGraw-Hill, New York, U.S.A.
- Khujadze, G. & Oberlack, M. 2004 DNS and scaling laws from new symmetry groups of ZPG turbulent boundary layer flow. *Theoret. Comput. Fluid Dynamics* 18, 391–411.
- KIM, H. T., KLINE, S. J. & REYNOLDS, W. C. 1971 The production of turbulence near a smooth wall in a turbulent boundary layer. *J. Fluid Mech.* **50**, 133–160.
- KIM, J. 1989 On the structure of pressure fluctuations in simulated turbulent channel flow. J. Fluid Mech. 205, 421–451.
- Kim, J. & Hussain, F. 1993 Propagation velocity of perturbations in turbulent channel flow. *Phys. Fluids A* 5 (3), 695–706.
- Kim, J. & Moin, P. 1989 Transport of passive scalars in a turbulent channel flow. In *Turbulent Shear Flows 6* (ed. J.-C. André, J. Cousteix, F. Durst, B. E. Launder & F. W. Schmidt), pp. 85–96. Springer-Verlag, Berlin, Germany.
- Kim, J., Moin, P. & Moser, R. 1987 Turbulence statistics in fully developed channel flow at low Reynolds number. *J. Fluid Mech.* 177, 133–166.
- Kim, K. C. & Adrian, R. J. 1999 Very large-scale motion in the outer layer. *Phys. Fluids* 11 (2), 417–422.
- KLEBANOFF, P. S. 1954 Characteristics in a boundary layer with zero pressure gradient. *Tech. Rep* NACA-TN-3178. NASA, U.S.A.
- KLINE, S. J. 1967 Observed structural features in turbulent and transitional boundary layers. In *Fluid Mechanics of Internal Flow* (ed. G. Sovran), pp. 27–79. Elsevier, Amsterdam, The Netherlands.
- KLINE, S. J., REYNOLDS, W. C., SCHRAUB, F. A. & RUNSTADLER, P. W. 1967 The structure of turbulent boundary layers. *J. Fluid Mech.* **30**, 741–773.
- Kolmogorov, A. N. 1941 Local structure of turbulence in incompressible viscous liquid at high reynolds number. *Dokl. Nauk. SSSR* **30**, 299–303.
- Komminaho, J. & Skote, M. 2002 Reynolds stress budgets in Couette and boundary layer flows. Flow, Turbulence Combust. 68 (2), 167–192.
- Kondjoyan, A., Péneau, F. & Boisson, H. C. 2002 Effect of high free stream turbulence on heat transfer between plates and air flows: A review of existing experimental results. *Int. J. Therm. Sci.* 41 (1), 1–16.
- Kong, H., Choi, H. & Lee, J. S. 2000 Direct numerical simulation of turbulent thermal boundary layers. *Phys. Fluids* **12** (10), 2555–2568.
- KRISHNAMOORTHY, L. V. & ANTONIA, R. A. 1987 Temperature-dissipation measurements in a turbulent boundary layer. J. Fluid Mech. 176, 265–281.
- Krogstad, P.-A., Kaspersen, J. H. & Rimestad, S. 1998 Convection velocities in a turbulent boundary layer. *Phys. Fluids* **10** (4), 949–957.
- Kunkel, G. J. & Marusic, I. 2006 Study of the near-wall-turbulent region of the high-Reynolds-number boundary layer using an atmospheric flow. *J. Fluid Mech.* **548**, 375–402.
- Laadhari, F. 2007 Reynolds number effect on the dissipation function in wall-bounded flows. *Phys. Fluids* **19** (3), 038101.

- Landau, L. D. 1944 On the problem of turbulence. *Doklady Akademii Nauk SSSR* 44, 339–342.
- Leal, L. G. 2007 Advanced Transport Phenomena: Fluid Mechanics and Convective Transport. Cambridge University Press, Cambridge, U.K.
- LEE, J. H. & SUNG, H. J. 2011 Direct numerical simulation of a turbulent boundary layer up to $Re_{\theta} = 2500$. Int. J. Heat Fluid Flow 32 (1), 1–10.
- LeHew, J., Guala, M. & McKeon, B. J. 2010 A study of convection velocities in a zero pressure gradient turbulent boundary layer. In 40th AIAA Fluid Dynamics Conference and Exhibit, 28 June 1 July 2010, Chicago, Illiois, U.S.A..
- Lenaers, P., Li, Q., Brethouwer, G., Schlatter, P. & Örlü, R. 2011 Negative streamwise velocities and other rare events near the wall in turbulent flows. In *Advances in Turbulence XIII*. 12-15 September 2011, Warsaw, Poland.
- Leonard, A. 1974 Energy cascade in large eddy simulation of turbulent fluid flows. *Adv. Geophys.* **18** (A), 237–248.
- Li, Q., Schlatter, P., Brandt, L. & Henningson, D. S. 2009 DNS of a spatially developing turbulent boundary layer with passive scalar transport. *Int. J. Heat Fluid Flow* **30** (5), 916–929.
- LI, Q., Schlatter, P. & Henningson, D. S. 2008 Spectral simulations of wall-bounded flows on massively parallel computers. *Tech. Rep.* KTH Mechanics, Stockholm, Sweden.
- LI, Q., SCHLATTER, P. & HENNINGSON, D. S. 2010a Comparison of SGS models for passive scalar mixing in turbulent channel flows. In *Direct and Large-Eddy Simulation VIII*. Springer-Verlag, Berlin, Germany.
- LI, Q., SCHLATTER, P. & HENNINGSON, D. S. 2010b Simulations of heat transfer in a boundary layer subject to free-stream turbulence. J. Turbulence 11 (45), 1–33.
- LIGRANI, P. M. & BRADSHAW, P. 1987 Spatial resolution and measurement of turbulence in the viscous subl ayer using subminiature hot-wire probes. *Experiments in Fluids* 5, 407–417.
- LILLY, D. K. 1992 A proposed modification of the Germano subgrid-scale closure method. *Phys. Fluids A* 4 (3), 633–635.
- LIN, J., LAVAL, J. P., FOUCAUT, J. M. & STANISLAS, M. 2008 Quantitative characterization of coherent structures in the buffer layer of near-wall turbulence. Part 1: streaks. *Exp. Fluids* **45**, 999–1013.
- LU, S. S. & WILLMARTH, W. W. 1973 Measurements of the structure of the Reynolds stress in a turbulent boundary layer. J. Fluid Mech. 60, 481–511.
- Lugt, H. J. 1979 The dilemma of defining a vortex. In *Recent Development in Theo*retical and Experimental Fluid Mechan ics, pp. 309–321. Springer-Verlag, Berlin, Germany.
- Lund, T. S., Wu, X. & Squires, K. D. 1998 Generation of turbulent inflow data for spatially-developing boundary layer simulations. *J. Comp. Phys.* **140** (2), 233–258.
- L'VOV, V. S., PROCACCIA, I. & RUDENKO, O. 2008 Universal model of finite Reynolds number turbulent flow in channels and pipes. *Phys. Lett. Rev.* **100** (5), 054504.
- Maciejewski, P. K. & Moffat, R. J. 1992a Heat transfer with very high free-stream turbulence. I: Experimental data. ASME J. Heat Transfer 114 (4), 827–833.

- MACIEJEWSKI, P. K. & MOFFAT, R. J. 1992b Heat transfer with very high free-stream turbulence. II: Analysis of results. ASME J. Heat Transfer 114 (4), 834–839.
- Maday, Y. & Patera, A. T. 1989 Spectral element methods for the incompressible Navier-Stokes equations. In *State-of-the-art surveys on computational mechanics*, *ASME*, *New York* (ed. A. K. Noor & J. T. Oden), pp. 71–143.
- Malik, M. R., Zang, T. A. & Hussaini, M. Y. 1985 A spectral collocation method for the Navier-Stokes equations. J. Comp. Phys. 61 (1), 64–88.
- Marusic, I. 2009 Unravelling turbulence near walls. J. Fluid Mech. 630, 1-4.
- Marusic, I. & Kunkel, G. J. 2003 Streamwise turbulence intensity formulation for flat-plate boundary layers. *Phys. Fluids* **15** (8), 2461–2464.
- MARUSIC, I., MATHIS, R. & HUTCHINS, N. 2010a High Reynolds number effects in wall turbulence. Int. J. Heat Fluid Flow 31 (3), 418–428.
- MARUSIC, I., MCKEON, B. J., MONKEWITZ, P. A., NAGIB, H. M., SMITS, A. J. & SREENIVASAN, K. R. 2010b Wall-bounded turbulent flows at high Reynolds numbers: Recent advances and key issues. *Phys. Fluids* **22** (6), 065103.
- Mathis, R., Hutchins, N. & Marusic, I. 2009 Large-scale amplitude modulation of the small-scale structures in turbulent boundary layers. *J. Fluid Mech.* **628**, 311–337.
- Meneveau, C. 1994 Statistics of turbulence subgrid-scale stresses: Necessary conditions and experimental tests. *Phys. Fluids* 6 (2), 815–833.
- METZGER, M. M. & KLEWICKI, J. C. 2001 A comparative study of near-wall turbulence in high and low Reynolds number boundary layers. *Phys. Fluids*.
- MILLIKAN, C. M. 1938 A critical discussion of turbulent flows in channels and circular tubes. In *Proceedings of the 5th International Congress on Applied Mechanics*, *Cambridge*, *M.A.*, *U.S.A*. (ed. J. P. Den Hartog & H. Peters), pp. 386–392. Wiley, New York, U.S.A.
- MOCHIZUKI, S. & NIEUWSTADT, F. T. M. 1996 Reynolds-number-dependence of the maximum in the streamwise velocity fluctuations in wall turbulence. *Exps. Fluids* 21, 218–226.
- Moin, P. & Kim, J. 1982 Numerical investigation of turbulent channel flow. *J. Fluid Mech.* 118, 341–377.
- Moin, P. & Kim, J. 1997 Tackling turbulence with supercomputers. *Scientific American* **276** (1), 62–68.
- Moin, P., Squires, K., Cabot, W. & Lee, S. 1991 A dynamic subgrid-scale model for compressible turbulence and scalar transport. *Phys. Fluids A* **3** (11), 2746–2757.
- Monkewitz, P. A., Chauhan, K. A. & Nagib, H. M. 2007 Self-consistent high-Reynolds-number asymptotics for zero-pressure-gradient turbulent boundary layers. *Phys. Fluids* **19** (11), 115101.
- Monkewitz, P. A., Chauhan, K. A. & Nagib, H. M. 2008 Comparison of mean flow similarity laws in zero pressure gradient turbulent boundary layers. *Phys. Fluids* **20** (105102), 1–16.
- MORKOVIN, M. V. 1964 Effects of compressibility on turbulent flows. In *Mechanics of Turbulence: Colloque International sur la Mecanique de la turbulence, Marseille, France, 1961* (ed. A. J. Favre), pp. 367–380. Gordon and Breach.
- Moser, R. D., Kim, J. & Mansour, N. N. 1999 Direct numerical simulation of turbulent channel flow up to $Re_{\tau} = 590$. Phys. Fluids 11 (4), 943–945.

- Moser, R. D. & Moin, P. 1984 Direct numerical simulation of curved turbulent channel flow. *Tech. Rep.* NASA TM-85974. NASA, U.S.A.
- Mosyak, A., Pogrebnyak, E. & Hetsroni, G. 2001 Effect of constant heat flux boundary condition on wall temperature fluctuations. *ASME J. Heat Transfer* 123 (2), 213–218.
- Murlis, J., Tsai, H. M. & Bradshaw, P. 1982 The structure of turbulent boundary layers at low Reynolds numbers. *J. Fluid Mech.* **122**, 13–56.
- NA, Y. & HANRATTY, T. J. 2000 Limiting behavior of turbulent scalar transport close to a wall. *Int. J. Heat Mass Transfer* **43** (10), 1749–1758.
- NAGANO, Y. & TAGAWA, M. 1988 Statistical characteristics of wall turbulence with a passive scalar. *J. Fluid Mech.* **196**, 157–185.
- NAGANO, Y. & TAGAWA, M. 1995 Coherent motions and heat transfer in a wall turbulent shear flow. J. Fluid Mech. 305, 127–157.
- NAGIB, H. M. & CHAUHAN, K. A. 2008 Variations of von Kármán coefficient in canonical flows. *Phys. Fluids* **20** (10), 101518.
- NAGIB, H. M., CHAUHAN, K. A. & MONKEWITZ, P. A. 2007 Approach to an asymptotic state for zero pressure gradient turbulent boundary layers. *Proc. Roy. Soc. Lond. Ser. A* **365**, 755–770.
- NAVIER, C. L. M. H. 1823 Mémoire sur les lois du mouvement des fluides. *Mem. Acad. Sci. Inst. Fr.* **6**, 389–440.
- NICKELS, T. B. 2004 Inner scaling for wall-bounded flows subject to large pressure gradients. *J. Fluid Mech.* 1, 217–239.
- NORDSTRÖM, J., NORDIN, N. & HENNINGSON, D. S. 1999 The fringe region technique and the Fourier method used in the Direct Numerical Simulation of spatially evolving viscous flows. SIAM J. Sci. Comp. 20 (4), 1365–1393.
- Ohlsson, J., Schlatter, P., Fischer, P. F. & Henningson, D. S. 2010 Direct numerical simulation of separated flow in a three-dimensional diffuser. *J. Fluid Mech.* **650**, 307–318.
- ÖRLÜ, R. 2009 Experimental studies in jet flows and zero pressure-gradient turbulent boundary layers. PhD thesis, Department of Mechanics, KTH, Stockholm, Sweden.
- ÖRLÜ, R. & ALFREDSSON, P. H. 2011 On spatial resolution issues related to time-averaged quantities using hot-wire anemometry. *Experiments in Fluids* **49**, 101–110.
- Örlü, R. & Schlatter, P. 2011 On the fluctuating wall-shear stress in zero pressure-gradient turbulent boundary layer flows. *Phys. Fluids* **23** (2), 021704.
- ÖSTERLUND, J. M. 1999 Experimental studies of zero pressure-gradient turbulent boundary layer flow. PhD thesis, Department of Mechanics, KTH, Stockholm, Sweden.
- ÖSTERLUND, J. M. & JOHANSSON, A. V. 1999 Turbulence statistics of zero pressuregradient turbulent boundary layers. *Tech. Rep.* KTH Mechanics, Stockholm, Sweden.
- ÖSTERLUND, J. M., JOHANSSON, A. V., NAGIB, H. M. & HITES, M. H. 1999 Wall shear stress measurements in high Reynolds number boundary layers from two facilities. In 30th AIAA Fluid Dynamics Conference, Norfolk, V.A., U.S.A..
- ÖSTERLUND, J. M., JOHANSSON, A. V., NAGIB, H. M. & HITES, M. H. 2000 A note on the overlap region in turbulent boundary layers. *Phys. Fluids* **12** (1), 1–4.

- Ovchinnikov, V., Choudhari, M. M. & Piomelli, U. 2008 Numerical simulations of boundary-layer bypass transition due to high-amplitude free-stream turbulence. *J. Fluid Mech.* **613**, 135–169.
- Patera, A. T. 1984 A spectral element method for fluid dynamics laminar flow in a channel expansion. *J. Comp. Phys.* **54**, 468–488.
- PECK, B. & SIGURDSON, L. 1994 The three-dimensional vortex structure of an impacting water drop. *Phys. Fluids* 6 (2), 564–576.
- PÉNEAU, F., BOISSON, H. C. & DJILALI, D. 2000 Large eddy simulation of the influence of high free-stream turbulence on a spatially evolving boundary layer. *Int. J. Heat Fluid Flow* **21** (5), 640–647.
- PÉNEAU, F., BOISSON, H. C., KONDJOYAN, A. & DJILALI, D. 2004 Structure of a flat plate boundary layer subjected to free-stream turbulence. *Int. J. Comput. Fluid Dynamics* 18 (2), 175–188.
- PÉNEAU, F., LEGENDRE, D., MAGNAUDET, J. & BOISSON, H. C. 1999 Large eddy simulation of a spatially growing boundary layer using a dynamic mixed subgrid-scale model. In *Direct and Large-Eddy Simulation III* (ed. N. D. Sandham, P. R. Voke & L. Kleiser), pp. 99–110. Springer-Verlag, Berlin, Germany.
- Perry, A. E. & Chong, M. S. 1982 On the mechanism of wall turbulence. J. Fluid Mech. 119, 173–217.
- Perry, A. E. & Hoffmann, P. H. 1976 An experimental study of turbulent convective heat transfer from a flat plate. J. Fluid Mech. 77, 355–368.
- Perry, A. E., Marusic, I. & Jones, M. B. 2002 On the streamwise evolution of turbulent boundary layers in arbitrary pressure gradients. *J. Fluid Mech.* 461, 61–91.
- PIOMELLI, U. 2001 Large-eddy and direct simulation of turbulent flows. In CFD2001 9e conférence annuelle de la société Canadienne de CFD. Kitchener, Ontario, Canada.
- PIOMELLI, U. & BALARAS, E. 2002 Wall-layer models for large-eddy simulations. Ann. Rev. Fluid Mech. 34, 349–374.
- PIOMELLI, U., MOIN, P. & FERZIGER, J. H. 1988 Model consistency in large eddy simulation of turbulent channel flows. *Phys. Fluids* **31** (7), 1884–1891.
- Pope, S. B. 2000 Turbulent Flows. Cambridge University Press, Cambridge, U.K.
- Prandtl, L. 1904 über Flüssigkeitsbewegung bei sehr kleiner Reibung. In Verhandlungen des dritten internationalen Mathematiker Kongresses in Heidelberg, 1904 (ed. A. Krazer), pp. 484–491. Teubner, Leipzig, Germany.
- PRANDTL, L. 1910 Eine Beziehung zwischen Wärmeaustausch und Strömungswiderstand der Flüssigkeiten. Phyz. Z. 11, 1072–1078.
- PRANDTL, L. 1925 Bericht über Untersuchungen zur ausgebildeten Turbulenz. Z. Angew. Math. Mech. $\bf 5$, 136–139.
- Prandtl, L. 1932 Zur turbulenten Strömung in Rohren und längs Platten. Ergebnisse der Aerodynamischen Versuchsanstalt zu Göttingen 4, 18–29.
- PURTELL, L. P., KLEBANOFF, P. S. & BUCKLEY, F. T. 1981 Turbulent boundary layer at low Reynolds number. *Phys. Fluids* **24** (5), 802–811.
- Quadrio, M. & Luchini, P. 2003 Integral space—time scales in turbulent wall flows. *Phys. Fluids* **15** (8), 2219–2227.
- RANNIE, W. D. 1956 Heat transfer in turbulent shear flow. J. Aero. Sci. 23 (5), 485–489.

- REDJEM-SAAD, L., OULD-ROUISS, M. & LAURIAT, G. 2007 Direct numerical simulation of turbulent heat transfer in pipe flows: Effect of Prandtl number. *Int. J. Heat Fluid Flow* **28** (5), 847–861.
- REYNOLDS, A. J. 1975 The prediction of turbulent Prandtl and Schmidt numbers. *Int. J. Heat Mass Transfer* **18**, 1055–1069.
- REYNOLDS, O. 1874 On the extent and action of the heating surface for steam boilers. Proc. Literary and Philosophical Society of Manchester, U.K. 14, 7–12.
- REYNOLDS, O. 1883 An experimental investigation of the circumstances which determine whether the motion of water in parallel channels shall be direct or sinuous and of the law of resistance in parallel channels. *Philos. Trans. R. Soc.* 174, 935–982.
- REYNOLDS, O. 1895 On the dynamical theory of incompressible viscous fluids and the determination of the criterion. *Philos. Trans. R. Soc.* 186, 123–164.
- RICHARDSON, L. F. 1922 Weather Prediction by Numerical Process. Cambridge University Press, Cambridge, U.K.
- ROACH, P. E. & BRIERLEY, D. H. 1992 The influence of a turbulent freestream on zero pressure gradient transitional boundary layer development, part I: Test cases T3A and T3B. In *Numerical Simulation of Unsteady Flows and Transition to Turbulence, ERCOFTAC*, pp. 319–347. Cambridge University Press, Cambridge, U.K.
- ROBINSON, S. K. 1991a Coherent motions in the turbulent boundary layer. Ann. Rev. Fluid Mech. 23, 601–639.
- ROBINSON, S. K. 1991b The kinematics of turbulent boundary layer structure. *Tech. Rep* NASA TM-103859. NASA, U.S.A.
- ROGERS, M., MOIN, P. & REYNOLDS, W. 1986 The structure and modeling of the hydrodynamic and passive scalar fields in homogeneous turbulent shear flow. *Tech. Rep* TF-25. Stanford University, U.S.A.
- RÜEDI, J.-D., NAGIB, H. M., ÖSTERLUND, J. M. & MONKEWITZ, P. A. 2003 Evaluation of three techniques for wall-shear stress measurements in three-dimensional flows. *Exp. Fluids* **35**, 389–396.
- SAGAUT, P. 2005 Large Eddy Simulation for Incompressible Flows, An Introduction, 3rd edn. Springer, Berlin, Germany.
- Samimy, M., Breuer, K. S., Leal, L. G. & Steen, P. H. 2003 An Gallery of Fluid Motion. Cambridge University Press, Cambridge, U.K.
- SANDHAM, N. D. 2002 Introduction to direct numerical simulation. In *Closure Strate-gies for Turbulent and Transitional Flows* (ed. B. E. Launder & N. D. Sandham), pp. 248–266. Cambridge University Press, Cambridge, U.K.
- Schewe, G. 1983 On the structure and resolution of wall-pressure fluctuations associated with turbulent boundary-layer flow. *J. Fluid Mech.* **134**, 311–328.
- Schlatter, P. 2001 Direct numerical simulation of laminar-turbulent transition in boundary layer subject to free-stream turbulence. Master's thesis, Institute of Fluid Dynamics, ETH, Zürich, Switzerland.
- Schlatter, P. 2005 Large-eddy simulation of transition and turbulence in wall-bounded shear flow. PhD thesis, ETH Zürich, Switzerland.
- Schlatter, P. & Brandt, L. 2008 DNS of three-dimensional turbulent boundary layers. In *Direct and Large-Eddy Simulation VII*. To appear.
- SCHLATTER, P., BRANDT, L., BRUHN, T. & HENNINGSON, D. S. 2006a Dynamic

- high-pass filtered eddy-viscosity models for LES of turbulent boundary layers. In *Bulletin American Physical Society*, , vol. 51, p. 213.
- Schlatter, P., de Lange, H. C. & Brandt, L. 2007a The effect of free-stream turbulence on the growth and breakdown of Tollmien-Schlichting waves. In $Advances\ in\ Turbulence\ XI$ (ed. J. M. L. M. Palma & A. Silva Lopes), pp. 179–181. Springer, Berlin, Germany.
- Schlatter, P., de Lange, H. C. & Brandt, L. 2007b Numerical study of the stabilisation of Tollmien-Schlichting waves by finite amplitude streaks. In *Turbulence and Shear Flow Phenomena 5, August 2007, Munich, Germany* (ed. R. Friedrich, N. A. Adams, J. K. Eaton, J. A. C. Humphrey, N. Kasagi & M. A. Leschziner), pp. 849–854.
- SCHLATTER, P., LI, Q., BRETHOUWER, G., JOHANSSON, A. V. & HENNINGSON, D. S. 2009a Towards large-eddy simulations of high-Reynolds number turbulent boundary layers. In *TSFP-6*, *June 2009*, *Seoul, Korea* (ed. N. Kasagi, J. K. Eaton, R. Friedrich, J. A. C. Humphrey, A. V. Johansson & H. J. Sung), , vol. I, pp. 271–276.
- Schlatter, P., Li, Q., Brethouwer, G., Johansson, A. V. & Henningson, D. S. 2010a Simulations of spatially evolving turbulent boundary layers up to $Re_{\theta}=4300.$ Int. J. Heat Fluid Flow **31** (3), 251–261.
- Schlatter, P., Li, Q., Brethouwer, G., Johansson, A. V. & Henningson, D. S. 2010b Structure of a turbulent boundary layer studied by DNS. In *Direct and Large-Eddy Simulation VIII*.
- Schlatter, P. & Örlü, R. 2010a Assessment of direct numerical simulation data of turbulent boundary layers. J. Fluid Mech. 659, 116–126.
- Schlatter, P. & Örlü, R. 2010b Quantifying the interaction between large and small scales in wall-bounded turbulent flows: a note of caution. *Phys. Fluids* **22** (5), 051704.
- Schlatter, P., Örlü, R., Li, Q., Brethouwer, G., Fransson, J. H. M., Johansson, A. V., Alfredsson, P. H. & Henningson, D. S. 2009b Turbulent boundary layers up to $Re_{\theta}=2500$ studied through numerical simulation and experiments. *Phys. Fluids* **21** (5), 051702.
- Schlatter, P., Stolz, S. & Kleiser, L. 2004 LES of transitional flows using the approximate deconvolution model. *Int. J. Heat Fluid Flow* **25** (3), 549–558.
- Schlatter, P., Stolz, S. & Kleiser, L. 2005 Evaluation of high-pass filtered eddyviscosity models for large-eddy simulation of turbulent flows. *J. Turbulence* **6** (5), 1–21.
- Schlatter, P., Stolz, S. & Kleiser, L. 2006b LES of spatial transition in plane channel flow. J. Turbulence 7 (33), 1–24.
- Schlichting, H. 1987 Boundary Layer Theory, 7th edn. McGraw-Hill, New York, U.S.A.
- Schoppa, W. & Hussain, F. 2002 Coherent structure generation in near-wall turbulence. J. Fluid Mech. 453, 57–108.
- Schwertfirm, F. & Manhart, M. 2007 DNS of passive scalar transport in turbulent channel flow at high Schmidt numbers. *Int. J. Heat Fluid Flow* **28** (6), 1204–1214.
- SEGALINI, A., ÖRLÜ, R., SCHLATTER, P., ALFREDSSON, P. H., RÜEDI, J.-D. & TALAMELLI, A. 2011 A method to estimate turbulence intensity and transverse

- Taylor microscale in turbulent flows from spatially averaged hot-wire data. Experiments in Fluids pp. 1–8.
- SHARP, N. S., NEUSCAMMAN, S. & WARHAFT, Z. 2009 Effects of large-scale free stream turbulence on a turbulent boundary layer. *Phys. Fluids* **21** (9), 095105.
- SIMONICH, J. C. & BRADSHAW, P. 1978 Effect of free-stream turbulence on heat transfer through a turbulent boundary layer. ASME J. Heat Transfer 100 (4), 671–677.
- SKOTE, M., HENNINGSON, D. S. & HENKES, R. A. W. M. 1998 Direct numerical simulation of self-similar turbulent boundary layers in adverse pressure gradients. Flow, Turbulence Combust. 60, 47–85.
- SMITH, C. R. & METZLER, S. P. 1983 The characteristics of low-speed streaks in the near-wall region of a turbulent boundary layer. J. Fluid Mech. 129, 27–54.
- SMITS, A. J. & WOOD, D. H. 1985 The response of turbulent boundary layers to sudden perturbations. *Ann. Rev. Fluid Mech.* 17 (1), 321–358.
- SPALART, P. R. 1988 Direct simulation of a turbulent boundary layer up to $Re_{\theta} = 1410$. J. Fluid Mech. 187, 61–98.
- Spalart, P. R. 2009 Detached-eddy simulation. Ann. Rev. Fluid Mech. 41 (1), 181–202.
- SPALART, P. R. 2011 The law of the wall. Indications from DNS, and opinion. In Progress in Wall Turbulence: Understanding and Modelling (ed. M. Stanislas, J. Jiménez & I. Marusic), pp. 9–20. Springer-Verlag, Berlin, Germany.
- SPALART, P. R. & WATMUFF, J. H. 1993 Experimental and numerical study of a turbulent boundary layer with pressure gradients. J. Fluid Mech. 249.
- Sreenivasan, K. R. 1989 The turbulent boundary layer. In *Frontiers in Experimental Fluid Mechanics* (ed. M. Gad-el Hak), pp. 159–209. Springer-Verlag, Berlin, Germany.
- Stokes, G. G. 1845 On the theories of the internal friction of fluids in motion, and of the equilibrium and motion of elastic solids. *Trans. Camb. Phil. Soc.* 8 (22), 287–305.
- Stolz, S. & Adams, N. A. 1999 An approximate deconvolution procedure for large-eddy simulation. *Phys. Fluids* **11** (7), 1699–1701.
- Stolz, S., Adams, N. A. & Kleiser, L. 2001 An approximate deconvolution model for large-eddy simulation with application to incompressible wall-bounded flows. *Phys. Fluids* **13** (4), 997–1015.
- Subramanian, C. S. & Antonia, R. A. 1981 Effect of Reynolds number on a slightly heated turbulent boundary layer. *Int. J. Heat Mass Transfer* **24** (11), 1833–1846.
- SWIFT, J. 1733 On Poetry. A Rhapsody .
- Taylor, G. I. 1919 Conditions at the surface of a hot body exposed to the wind. Tech. Rep 272. Rep. Memo. Advis. Comm. Aweonaut. London.
- Teitel, M. & Antonia, R. A. 1993 Heat transfer in fully developed turbulent channel flow: Comparison between experiment and direct numerical simulations. *Int. J. Heat Mass Transfer* **36** (6), 1701–1706.
- Tennekes, H. & Lumley, J. L. 1972 A First Course in Turbulence. The MIT Press, Cambridge, U.S.A.
- THEODORSEN, T. 1952 Mechanism of turbulence. In Proc. 2nd Midwestern Conference

- on Fluid Mechanics, March 17-19, Ohio State Univ., Columbus, Ohio, U.S.A., pp. 1-19.
- THOLE, K. A. & BOGARD, D. G. 1996 High freestream turbulence effects on turbulent boundary layers. ASME J. Fluids Engng. 118 (2), 276–284.
- THOMAS, N. H. & HANCOCK, P. E. 1977 Grid turbulence near a moving wall. *J. Fluid Mech.* 82, 481–496.
- Tiselj, I., Bergant, R., Mavko, B., Bajsić, I. & Hetsroni, G. 2001 DNS of turbulent heat transfer in channel flow with heat conduction in the solid wall. *ASME J. Heat Transfer* **123**, 849–857.
- Tiselj, I., Horvat, A., Mavko, B., , Pogrebnyak, E., Mosyak, A. & Hetsroni, G. 2004 Wall properties and heat transfer in near-wall turbulent flow. *Numer. Heat Transfer, Part A* 46, 717–729.
- Tohdoh, K., Iwamoto, K. & Kawamura, H. 2008 Direct numerical simulation of passive scalar transport in a turbulent boundary layer. In *Proceedings of the 7th International ERCOFTAC Symposium on Engineering Turbulence Modelling and Measurements, Limassol, Cyprus, 2008*, pp. 169–174.
- Townsend, A. A. 1976 The Structure of Turbulent Shear Flow, 2nd edn. Cambridge University Press, Cambridge, U.K.
- TREFETHEN, L. N. 1996 Finite Difference and Spectral Methods for Ordinary and Partial Differential Equations. unpublished text, available on line.
- TSINOBER, A. 2009 An Informal Conceptual Introduction to Turbulence, 2nd edn. Springer-Verlag, Berlin, Germany.
- Tsuji, Y., Fransson, J. H. M., Alfredsson, P. H. & Johansson, A. V. 2007 Pressure statistics and their scaling in high-Reynolds-number turbulent boundary layer. *J. Fluid Mech.* **585**, 1–40.
- VREMAN, B., GEURTS, B. & KUERTEN, H. 1995 A priori test of large eddy simulation of the compressible plane mixing layer. *Journal of Engineering and Mathematics* **29** (4), 299–327.
- Wallace, J. M., Eckelmann, H. & Brodkey, R. S. 1972 The wall region in turbulent shear flow. *J. Fluid Mech.* **54**, 39–48.
- WARHAFT, Z. & LUMLEY, J. L. 1978 An experimental study of the decay of temperature fluctuations in grid-generated turbulence. *J. Fluid Mech.* 88, 659–685.
- White, F. M. 2006 Viscous Fluid Flow, 3rd edn. McGraw-Hill, New York, U.S.A.
- Wikström, P. 1998 Measurements, direct numerical simulation and modeling of passive scalar transport in turbulent flows. PhD thesis, Department of Mechanics, KTH, Stockholm, Sweden.
- WILLMARTH, W. W. & Lu, S. S. 1972 Structures of the Reynolds stress near the wall. J. Fluid Mech. 55, 65–92.
- WINCKELMANS, G. S., JEANMART, H. & CARATI, D. 2002 On the comparison of turbulence intensities from large-eddy simulation with those from experiment or direct numerical simulation. *Phys. Fluids* 14 (5), 1809–1811.
- WOOD, D. H. 1980 A reattaching, turbulent, thin shear layer. PhD thesis, Department of Aeronautics, Imperial College, London, U.K.
- Wu, X. & Moin, P. 2008 A direct numerical simulation study on the mean velocity characteristics in turbulent pipe flow. *J. Fluid Mech.* **608**, 81–112.
- Wu, X. & Moin, P. 2009 Direct numerical simulation of turbulence in a nominally zero-pressure-gradient flat-plate boundary layer. J. Fluid Mech. 630, 5–41.

- Wu, X. & Moin, P. 2010 Transitional and turbulent boundary layer with heat transfer. *Phys. Fluids* **22** (8), 085105.
- You, D. & Moin, P. 2007 A dynamic global-coefficient subgrid-scale eddy-viscosity model for large-eddy simulation in complex geometries. *Phys. Fluids* **19** (6), 065110.
- You, D. & Moin, P. 2009 A dynamic global-coefficient subgrid-scale model for large-eddy simulation of turbulent scalar transport in complex geometries. *Phys. Fluids* **21** (4), 045109.
- Zanoun, E.-S., Durst, F. & Nagib, H. 2003 Evaluating the law of the wall in two-dimensional fully developed turbulent channel flows. *Phys. Fluids* **15** (10), 3079–3089.
- Zhou, J., Adrian, R. J., Balachandar, S. & Kendall, T. M. 1999 Mechanisms for generating coherent packets of hairpin vortices in channel flow. *J. Fluid Mech.* **387**, 353–396.
- Zhou, Y. & Antonia, R. A. 1995 Memory effects in a turbulent plane wake. Exps. Fluids $\bf 19$ (2), 112–120.

Part II

Papers

 $"I'm\ gonna\ make\ him\ an\ offer\ he\ can't\ refuse"$

- The Godfather (1972)